Geochemical Modelling of CO_2 Storage

Özgür Gündoğan

Submitted for the degree of Doctor of Philosophy

Heriot-Watt University

Institute of Petroleum Engineering

June 2011

ABSTRACT

The injection of CO_2 into the reservoir acidifies the brine, which in turn drives mineral dissolution and precipitation processes. This thesis explores how far geochemical modelling can be applied to evaluate the CO_2-brine-rock interactions during CO_2 storage in North Sea saline formations.

First, modelling requirements and the capabilities and limitations of the numerical codes used in this study (PHREEQC, GEM, TOUGHREACT and MoReS) were identified. Solubility of CO_2 in brine by different models at conditions relevant to CO_2 storage was compared. Batch modelling of three sandstone core samples from target CO_2 storage formations was performed to compare the numerical codes and assess mineral trapping capacity of the formations. Finally, reactive transport modelling of Rannoch formation at reservoir scale was studied. The simulation results of GEM and MoReS were compared.

It was shown that current codes can model geochemical reactions with acceptable simplifications and the choice of simulator is not critical for the model predictions. It was demonstrated how thermodynamic data and activity models can affect the modelling results. It was also found that the models are sensitive to relative mineral composition, grid discretization, permeability models, and kinetic parameters. Mineral trapping is comparable to solubility trapping in Rannoch formation.

ACKNOWLEDGMENTS

This research was funded by Scottish Research Development Grant, Heriot-Watt University and CO_2GEONET.

The following software providers are greatly acknowledged: United States Geological Survey for providing PHREEQC, Lawrence Berkeley National Laboratory for providing TOUGHREACT, Computer Modeling Group for providing GEM and supporting software, Schlumberger for providing ECLIPSE300 and Shell International Exploration and Production for providing MoReS.

This thesis is the combined efforts of a number of people.

I thank my supervisor, mentor and teacher Prof. Eric Mackay. Without him this thesis would have never been completed. I thank him for the support at all fronts and for his patience. He was always beyond the call of duty. He is, in every sense of the term, the best person anyone could ever wish to work with. I will miss him wherever I go.

I thank Dr. Min Jin for the continuous support and for sharing his technical knowledge, but also for listening me, especially when Murphy ruled my world. At times during my PhD I felt that he was the only person who understood my problems. He also deserves much credit for the geological model used in this thesis. I hope our friendship will last forever.

I thank Dr. Lingli Wei who I met quite late during the course of this study, but whose interest encouraged the final development of this work. I thank him for allowing me to attend the MoReS course and to make my time at Shell useful, interesting and pleasant. I am grateful for the technical support he provided on MoReS models and sharing his professional opinion. I also thank him for running the most of the MoReS simulations on the clusters of Shell Research Laboratories. He is an inspiration and a fantastic discussion friend.

I thank David Parkhurst for giving technical support on PHREEQC and for comments on some parts of the thesis.

I thank Computer Modelling Group and David Hicks for technical support.

I thank the unsung heroes of IPE. All the administrative and support staff, thank you.

I thank my former supervisor Prof. Ugo Bilardo who oriented me towards CO_2 storage and Dr. Fatosh Gozalpour who gave me the chance to start my PhD.

I shared long working hours with Alastair Reid. I thank him for being a fantastic office mate.

Finally, I thank my husband Antonio Bucci for his suggestions and criticisms, and for creating the intellectually stimulating environment at home.

TABLE OF CONTENTS

LIST OF MINERALS

Albite	$NaAlSi_3O_8$
Analcime	$NaAlSi_2O_6.H_2O$
Anhydrite	$CaSO_4$
Ankerite	$CaFe(CO_3)_2$
Annite	$KFe_3(AlSi_3)O_{10}(OH)_2$
Anorthite	$CaAl_2Si_2O_8$
Calcite	$CaCO_3$
Chalcedony	SiO_2
Clinochlore-14A	$MgAl_2Si_3O_{10}(OH)_8$
Daphnite-14A	$Fe_5Al_2Si_3O_{10}(OH)_8$
Dawsonite	$NaAl(CO_3)(OH)_2$
Dolomite	$CaMg(CO_3)_2$
Enstatite	$MgSiO_3$
Fayalite	Fe_2SiO_4
Forsferite	Mg_2SiO_4
Gibbsite	$Al(OH)_3$
Illite	$K_{0.6}Mg_{0.25}Al_{2.3}Si_{3.5}O_{10}(OH)_2$
Kaolinite	$Al_2Si_2O_5(OH)_4$
K-feldspar	$KAlSi_3O_8$
Magnesite	$MgCO_3$
Montmorillonite	$(Ca_{0.5}Na)_{0.33}(Al_{1.67}Mg_{0.33})Si_4O_{10}(OH)_2$
Muscovite	$KAl_2(AlSi_3)O_{10}(OH)_2$
Olivine	$(MgFe)_2SiO_4$
Quartz	SiO_2
Serpentine	$Mg_3Si_2O_5(OH)_4$
Siderite	$FeCO_3$

CHAPTER 1

INTRODUCTION

While the international scientific and political community debates climate change because of the relative uncertainties, the reduction of anthropogenic CO_2 emissions is taken as a precautionary measure. The system of emission allowances introduced by the Kyoto Protocol and the resulting market attribute a monetary value to negative environmental impacts. Thus a system that determines costs, prices and profits for the operating enterprises in the energy sector has been introduced. Therefore the reduction of CO_2 emissions is not seen as a choice, but rather as essential.

The Intergovernmental Panel on Climate Change (IPCC, 2005) considers carbon capture and storage (CCS) in the portfolio of mitigation options for stabilizing atmospheric greenhouse gases. In 2009 the European Council adopted a directive to enable environmentally-safe CCS (2009/31/EC). The directive outlines the regulatory framework for the commission, member states and potential CCS operators. It specifies the characterisation and assessment criteria to determine the suitability of a geological formation for use as a storage site. According to these criteria, characterisation of the dynamic storage behaviour requires, among other things, consideration of the reactive

processes and development of an insight into changes in formation fluid chemistry and subsequent reactions, and use of reactive transport modelling to assess these processes.

Depleted oil and gas reservoirs, saline aquifers and coal seams are possible storage formations. Geological storage of CO_2 uses similar technologies as used by the oil and gas industry, and commercial scale projects underway, such as Sleipner (Torp and Gale, 2004), Weyburn (Preston et al., 2005) and In Salah (Wright, 2007), demonstrate that it is a feasible mitigation option. However, for the development of this technology worldwide on large scale we should guarantee the long term containment of CO_2 and storage security, which depends mainly on the physical and geochemical trapping mechanisms.

1.1 Problem statement

Injection of large quantities of CO_2 involves complex coupled physical and chemical processes such as multiphase flow, solute transport, mineral dissolution and precipitation. Injected CO_2 can dissolve in or mix with the formation fluid, react with reservoir rock and well materials. Geochemical modelling has an important role in understanding these processes. Experimental studies to investigate these processes are very few and limited regarding time, space and reservoir conditions. Due to the large spatial and temporal scales it is difficult to investigate the geochemical processes by experimental studies and field observations. Numerical modelling is an important tool to extend the experimental results and predict the behaviour of CO_2 in the reservoir storage.

There are questions that need to be investigated related to four main aspects of CO_2 storage (geochemical trapping, injectivity, well integrity and caprock integrity):

- How much CO_2 can be trapped geochemically?
- Can CO_2 alter the caprock and leak to the surface?
- Can CO_2 alter the wellbore and leak to the surface?
- Can CO_2 alter the formation around the wellbore and affect the injectivity?

These questions can be partly answered by geochemical modelling.

We can consider geochemical modelling applications of CO_2 storage in two broad areas with different time and space scales: injectivity and long term containment of CO_2. Long term containment can be divided into three main categories: trapping of CO_2, well integrity and caprock integrity (Figure 1.1).

1.1.1. Trapping of CO_2

CO_2 is trapped by two principal mechanisms: hydrogeological and geochemical retention (Gunter et al., 2004). The trapping mechanisms depend on three main factors: fluid properties, geochemical properties and geological variables. The timescales of different trapping mechanisms are different from one another.

1. Hydrogeological trapping: This is the main form of trapping during the injection period. There are two types of hydrogeological trapping. The first type is structural/stratigraphical trapping. The CO_2 is trapped as a free phase in physically sealed formations (reservoirs). The second type is hydrodynamic trapping. In this case, once CO_2 is injected into a deep saline aquifer with slow groundwater flow rates, it displaces the brine and migrates vertically towards the surface under buoyancy forces. When it reaches the top of the formation it continues to flow as a single phase. At the front of the CO_2 plume, CO_2 continues to displace water in a drainage process, while at the tail water displaces CO_2 in an imbibition process (Juanes et al., 2006). Since water is the wetting phase it exists as films on the rock surface. When imbibition takes place the films of water thickens and snaps off the pore throats. This leads to trapping of disconnected bubbles of the gas in the interstices of the pores and as a result CO_2 is trapped as a residual phase.
2. Geochemical trapping: As a consequence of geochemical interactions with formation water and the rock, CO_2 is trapped in three ways. The first type is solubility trapping, when CO_2 dissolves in brine:

$$CO_2 + H_2O = H_2CO_3$$

Not only is dissolved CO_2 no more a free phase and cannot flow upwards due to buoyancy forces, but also, the dissolved CO_2 increases the density of the brine,

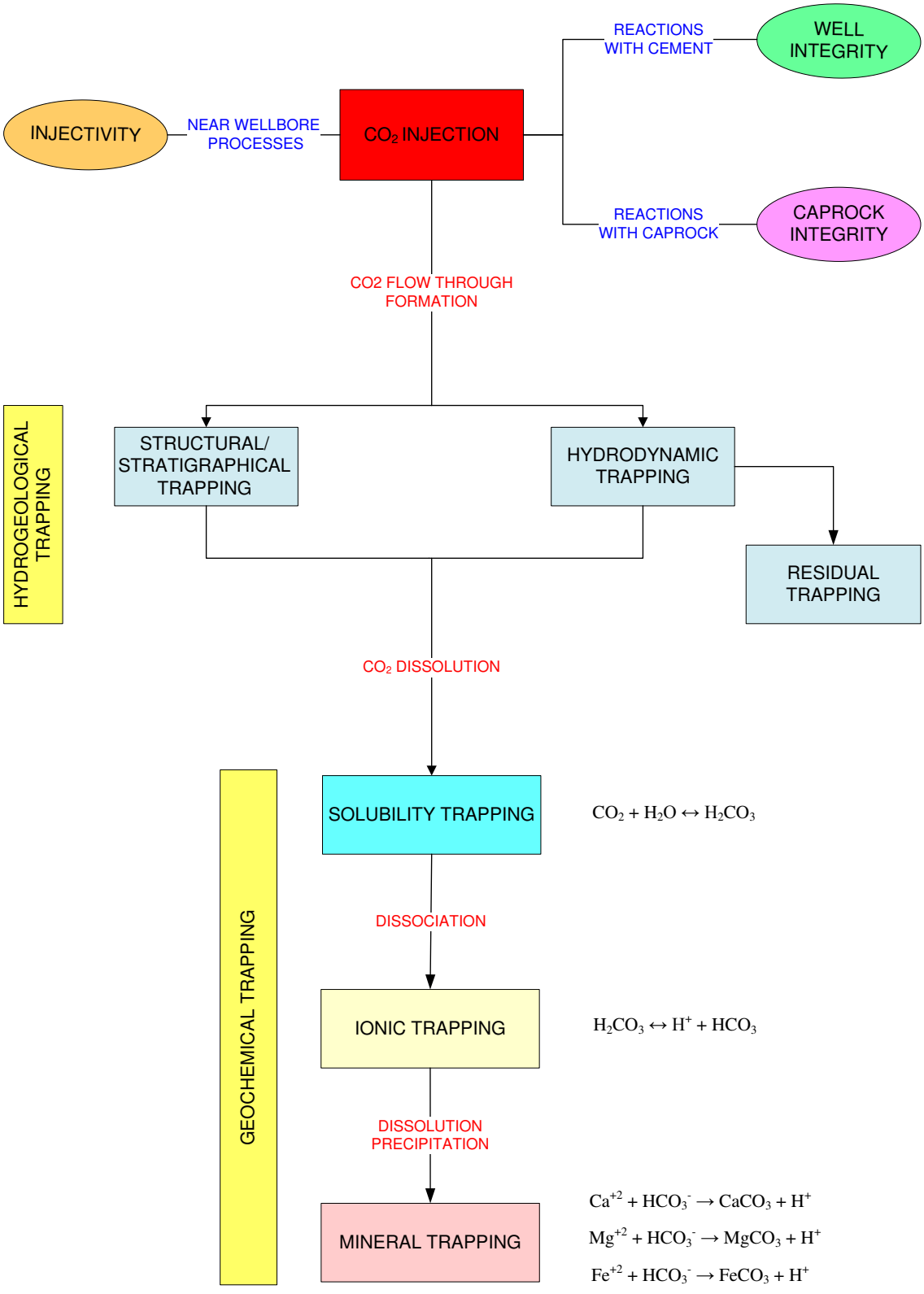

Figure 1.1 Geochemical reactions involved in CO_2 storage at different stages

and so brine with dissolved CO_2 moves downward. This leads to convective mixing with the unsaturated brine deeper in the formation. Another mechanism that contributes to the dissolution is the diffusion of dissolved CO_2 in the brine, but this is a slower mechanism than convective mixing. Hence the time needed to dissolve the entire CO_2 depends strongly on the vertical permeability of the formation. CO_2 solubility increases with pressure, and it decreases with temperature and brine salinity. This is the main trapping mechanism for a period of tens to hundreds of years following injection.

The second type of geochemical trapping is ionic trapping. When CO_2 dissolves in brine it forms a weak acid:

$$H_2CO_3 = H^+ + HCO_3^-$$

and reacts with the minerals and forms bicarbonate or carbonate ions. For example calcite dissolution can be represented as:

$$CaCO_3 + CO_2 + H_2O \rightarrow Ca^{2+} + 2HCO_3^-$$

Reaction with carbonate minerals is rapid, but is slow in the case of silicate minerals. These ions can continue to react with calcium, magnesium and iron from silicate minerals, and carbonate minerals precipitate. This is mineral trapping. For example, the dissolution of anorthite:

$$2H^+ + CaAl_2Si_2O_8 + H_2O \rightarrow Ca^{2+} + Al_2Si_2O_5(OH)_4$$

is followed by the precipitation of calcite:

$$Ca^{2+} + HCO_3^- \rightarrow CaCO_3 + H^+$$

Factors effecting the dissolution and precipitation of minerals are pressure, temperature, pH, mineral and brine composition and rock-brine interface. The dependence of solubility, ionic and mineral trapping of CO_2 on the chemical characteristics of the host formation water at equilibrium is shown in Figure 1.2. The pH is governed by the solubility of CO_2 and the neutralizing capacity of the

brine and the rock minerals. pH will be buffered faster in carbonate reservoir than siliciclastic reservoirs. Silicate minerals work as proton sinks consuming H^+ and neutralizing the acidity, and hence have more potential for mineral trapping than carbonate minerals. Mineral trapping is the most secure form of trapping, but the slowest.

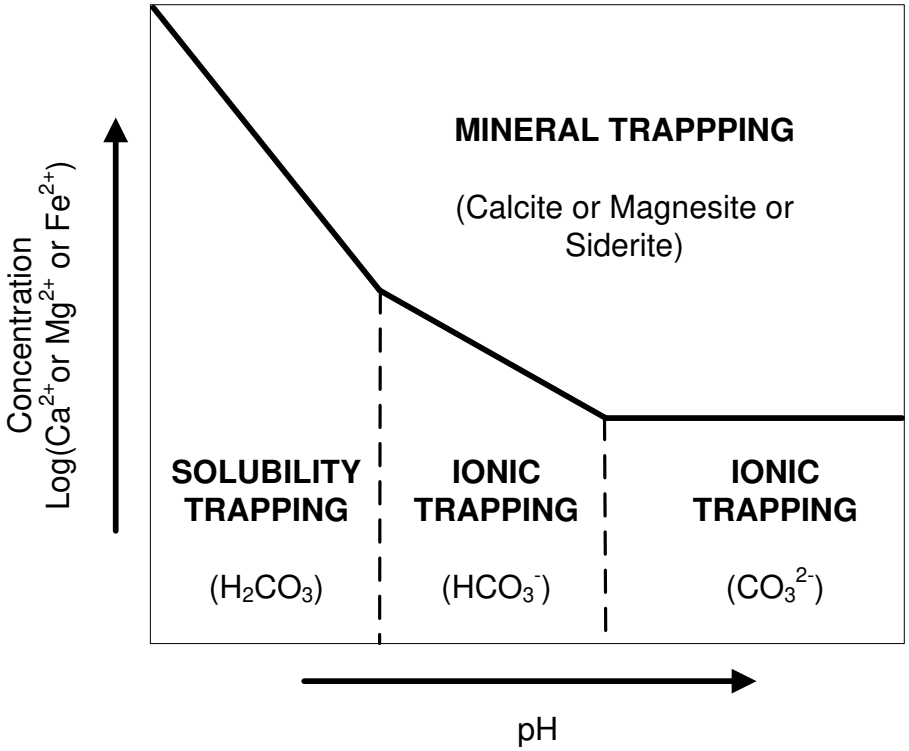

Figure 1.2 Dependence of solubility, ionic and mineral trapping of CO_2 on the chemical characteristics of the host formation water at equilibrium. The phase boundary along which carbonate minerals would precipitate is indicated by solid lines (after Gunter et al., 2004)

1.1.2. Well integrity (reactions with well completions)

In a typical well completion cement is used as a seal between steel casing and formation rock. Corrosion of casing and alteration of cement by reactions induced by CO_2 can lead to CO_2 migration paths to surface. Well completions are designed for life of tens of years and their integrity for much longer time (thousands of years) is uncertain. Hence the modelling of cement alteration is important to minimise the risk of leakage through the well and to ensure the long term containment of CO_2.

Cements are mixtures containing hydrated calcium silicate and calcium aluminosilicate and are highly alkaline (Rochelle et al., 2004). Carbonation is the main process that

causes the deterioration of cement. Dissolved CO_2 reacts with the hydrated calcium silicate and the calcium hydroxide forming calcium carbonate and calcium bicarbonate migrating out of the cement (Cailly et al., 2005). This process increases the porosity and permeability. On the other hand a CO_2 ganglion has a high solvent capacity and could transport a wide variety of components from the reservoir that could alter the cement.

1.1.3. Caprock integrity

Reactions with the caprock are important because any alteration of sealing capacity can lead to migration of CO_2. Caprock integrity is particularly important during the early years of storage as the hydrogeological trapping is the main trapping mechanism during this period.

When the buoyant CO_2 moves upwards and reaches the caprock it may dissolve in the formation water of the caprock and, because of the concentration gradient, may diffuse into the caprock. This will cause acidification of the water and hence both dissolution and precipitation can take place, which may cause impairment or enhancement of the seal. In the beginning the acidic water of the caprock increases the permeability and forms a path for migration. Then the leaking fluid could further increase the permeability and enhance the leakage. If the CO_2 saturated reservoir brine becomes rich in divalent cations due to the dissolution of reservoir rock minerals, once the brine diffuses into the caprock, carbonates can precipitate due to the higher pH of caprock brine and lower partial pressure of CO_2. The precipitation of the carbonates enhances the sealing capacity of the caprock (Rochelle et al, 2004; Gaus et al., 2005).

1.1.4. Geochemical impacts on injectivity (near wellbore processes)

The purpose of geochemical modelling of the near wellbore is to understand how the CO_2 displacement changes near the wellbore zone and to ensure sufficient injectivity that the planned amount of CO_2 can be injected during the injection period.

Depending on the formation rock, composition of the fluids and thermodynamic conditions, chemical dissolution and precipitation processes can occur near the wellbore region, and this can lead to increased or decreased injectivity. Around the wellbore the flow rate varies by orders of magnitude. This is particularly important as the dissolution

depends on the injection flow rate and different flow rates result in different dissolution patterns (Cailly et al., 2005). The dissolution potential of the system with two phases flowing simultaneously is different in two ways from a case where water saturated in CO_2 is the only mobile phase. Firstly, in the case of two phases there is an unlimited source of acidity, while in the single phase scenario acidity is spent whilst the dissolution proceeds. At low rates acid is spent locally and forms a compact dissolution pattern. When the flow rate increases acid is not spent completely and acidity is transported further and forms a wormhole pattern. At very high flow rates, because of the filtration of high acidity from the walls of the wormholes, the dissolution pattern becomes uniform. Secondly, in multiphase flow, the brine has limited access to the pore surface because of the non-wetting CO_2 phase which impacts the dissolution and precipitation processes. High flow rates can limit the permeability reduction near the wellbore, displacing the geochemical equilibrium area of precipitation far from the well (Egermann et al., 2005).

Drying is another phenomenon induced by the injection. Injected dry gas vaporizes the water near the wellbore (André et al., 2007). Vaporization concentrates the solids in the brine. When sufficiently concentrated, minerals will precipitate, leading to permeability reduction around the wellbore. Due to its abundance in formation brines, sodium chloride will be the principal precipitate to deposit due to vaporization. Because the saturation front initially displaces away from the well very quickly, the mass of precipitate that can deposit by this mechanism is generally small. However, when the brine salinity is high and the capillary-driven imbibition is strong the salt precipitation could be high enough to block the pores (Alkan et al., 2010). In situations where it causes concern, a low salinity or freshwater brine preflush may be considered to precede the CO_2 injection.

1.2 Motivation and Objectives

For the reasons given above geochemical modelling is essential for the applications of CO_2 storage. Geochemical models are needed to predict the effects of CO_2 injection underground. These predictions are important for decision making processes for the applicability of CO_2 storage in a particular reservoir, for the capacity calculations and

injection designs. Although some North Sea reservoirs are candidates for CO_2 storage, there are few geochemical modelling studies on North Sea formations.

Computer codes such as PHREEQC, GEM and TOUGHREACT are widely used to simulate these reactive processes (Gaus et al., 2005; Audigane et al., 2007; Wigand et al., 2008; Xu et al., 2005; Thibeau et al, 2007; Cantucci et al., 2009). Emerging codes, such as MoReS (Wei, 2010) in which the PHREEQC code is recently incorporated, have been applied to CO_2 storage studies. To build confidence in numerical simulations the intercomparison of the codes is essential. Lawrence Berkeley National Laboratory (LBNL) (Pruess et al., 2004) coordinated a benchmark study of several numerical codes including GEM and TOUGHREACT, but these codes were not compared from the geochemical point of view. Before this work was undertaken, a comparison of the three codes had not been carried out.

There are a number of CO_2 solubility models that can be applied to CO_2 storage. The most accurate ones are the standalone models (Duan and Sun, 2003; Akinfiev and Diamond 2010). These models are not implemented in numerical models due to their complexity. So far there has been no direct comparison of these models with the solubility models used by the numerical codes.

The objectives of this thesis are the following:

- Identify the model requirements of geochemical modelling of CO_2 storage
- Identify the criteria for code selection and the strength and weaknesses of the codes used in this thesis
- Compare the CO_2 solubility models
- Compare the PHREEQC, GEM and TOUGHREACT codes
- Evaluate the typical reservoir formations of the North Sea
- Evaluate a generic North Sea reservoir.

1.3 Thesis Outline

Chapter 1 contains the introductory background addressing the reasons for geochemical modelling of CO_2 storage, the motivation, the objectives of the thesis and thesis outline.

Chapter 2 reviews the most relevant literature on geochemical modelling of CO_2 storage. It is divided into three categories: numerical evidence, experimental evidence and natural analogues.

Chapter 3 gives the theoretical fundamentals behind geochemical modelling. The main parameters are described. The requirements of geochemical modelling in the context of CO_2 storage are discussed. The criteria for the code selection are given. The strength and weaknesses of the codes are identified.

Chapter 4 gives the theoretical bases of the CO_2 solubility models. CO_2 solubility models are reviewed. The fugacity calculations with different equations of state are evaluated. CO_2 solubility models are compared and their application to CO_2 storage is discussed.

Chapter 5 compares the PHREEQC, GEM and TOUGHREACT codes by applying them to the batch models of selected North Sea core samples. The main reactions for these formations are also identified.

Chapter 6 evaluates a realistic 3D heterogeneous reservoir by GEM and MoReS. The formation type studied is Rannoch formation.

Chapter 7 summarises the conclusions of this research and gives recommendations for the future work.

1.4 References

Alkan, H., Cinar, Y. and Ulker, E., 2010, Impact of Capillary Pressure, Salinity and In situ Conditions on CO_2 Injection into Saline Aquifers, Transport in Porous Media, 84(3): 799-819.

Akinfiev, N.N. and Diamond, L.W., 2010, Thermodynamic model of aqueous CO_2-H_2O-NaCl solutions from -22 to 100° C and from 0.1 to 100 MPa, Fluid Phase Equilibria, 295(1): 104-124.

André, L., Audigane, P., Azaroual, M. and Menjoz, A., 2007, Numerical modeling of fluid-rock chemical interactions at the supercritical CO_2-liquid interface during CO_2 injection into a carbonate reservoir, the Dogger aquifer (Paris Basin, France), Energy Conversion and Management, 48(6): 1782.

Audigane, P., Oldenburg, C.M., van der Meer, B., Geel, K., Lions, J., Gaus, I., Robelin, C., Durst, P. and Xu, T., 2007, Geochemical modelling of the CO_2 injection into a methane gas reservoir at the K12-B field, North Sea, Special Publication of AAPG on Geological Storage of CO_2.

Cailly, B., Le Thiez, P., Egermann, P., Audibert, A., Vidal-Gilbert, S., Longaygue, X., 2005, Geological storage of CO_2: A state-of-the-art of injection processes and technologies, Oil and Gas Science and Technology - Review IFP, 60(3): 517-525.

Cantucci, B., Montegrossi, G., Vaselli, O., Tassi, F., Quattrocchi, F., Perkins, E.H., 2009, Geochemical modeling of CO_2 storage in deep reservoirs: The Weyburn Project (Canada) case study, Chemical Geology, 265(1-2): 181-197.

Duan, Z. and Sun, R., 2003, An improved model calculating CO_2 solubility in pure water and aqueous NaCl solutions from 273 to 533 K and from 0 to 2000 bar, Chemical Geology, 193(3-4): 257.

EC, 2009, Directive 2009/31/EC of the European Parliament and of the Council of 23 April 2009, Official Journal of the European Union, 5 June 2009.

Egermann, P., Bazin, B. and Vizika, O., 2005, An experimental investigation of reaction-transport phenomena during CO_2 injection, SPE 93674

Gaus, I., Azaroual, M. and Czernichowski Lauriol, I., 2005, Reactive transport modelling of the impact of CO_2 injection on the clayey caprock at Sleipner (North Sea), Chemical Geology, 217(3-4): 319-337.

Gunter, W.D., Bachu S., Benson S., 2004, The role of hydrogeological and geochemical trapping in sedimentary basins for secure geological storage of carbon dioxide. In: Baines, S.J. and Worden, R.H (eds) Geological Storage of Carbon Dioxide, Geological Society, London, Special publications, 233: 129-145.

IPCC, 2005, IPCC Special Report on Carbon Dioxide Capture and Storage, Cambridge University Press, Cambridge, United Kingdom, New York, NY, USA.

Juanes, R., Spiteri E. J., Orr, F. M. Jr., and Blunt M. J., 2006, Impact of relative permeability hysteresis on geological CO_2 storage, Water Resources Res., 42.

Preston, C. Monea M., Jazrawi W., Brown K., Whittaker S., White D., Law D., Chalaturnyk R. and B. Rostron, 2005, IEA GHG Weyburn CO_2 monitoring and storage project, Fuel Processing Technology, 86(14-15): 1547-1568.

Pruess, K., García J., Kovscek T., Oldenburg C., Rutqvist J., Steefel C. and Xu T., 2004, Code intercomparison builds confidence in numerical simulation models for geologic disposal of CO_2, Energy, 29(9-10): 1431-1444.

Rochelle, C.A., Czernichowski-Lauriol, I., Milodowski, A.E., 2004, The impact of chemical reactions in CO_2 storage in geologic formations: a brief review. In: Baines, S.J. and Worden, R.H (eds) Geological Storage of Carbon Dioxide, Geological Society, London, Special publications, 233: 87–106.

Thibeau, S., Nghiem, L. and Ohkuma, H., 2007, A Modeling study of the role of selected minerals in enhancing CO_2 mineralization during CO_2 aquifer storage, SPE Annual Technical Conference and Exhibition, Anaheim, California, USA, SPE 109739.

Torp, T.A. and Gale, J., 2004, Demonstrating storage of CO_2 in geological reservoirs: The Sleipner and SACS projects, Energy, 29(9-10): 1361-1369.

Wei, L., 2010, Rigorous Water Chemistry Modelling in reservoir simulations for waterflood and EOR Studies, Abu Dhabi International Petroleum Exhibition and Conference, SPE 138037.

Wigand, M., Carey, J.W., Schütt, H., Spangenberg, E. and Erzinger, J., 2008, Geochemical effects of CO_2 sequestration in sandstones under simulated in situ conditions of deep saline aquifers, Applied Geochemistry, 23(9): 2735.

Wright, I.W., 2007, Three years CO_2 geological storage at In Salah, International Petroleum Technology Conference, Dubai, UAE, SPE 11326-MS.

Xu, T., Apps, J.A. and Pruess, K., 2005, Mineral sequestration of carbon dioxide in a sandstone-shale system, Chemical Geology, 217: 295-318.

CHAPTER 2

EVIDENCE OF CO_2 - BRINE - ROCK INTERACTIONS

The main objective of this chapter is to review the literature and provide evidence of CO_2-brine-rock interactions relevant to CO_2 storage. The chapter is divided into three sections: numerical evidence, experimental evidence and natural analogues.

2.1 Numerical evidence

Numerical studies of CO_2-brine-rock interactions relevant to CO_2 storage are divided into two categories: batch models and reactive transport models. Most of these studies addressed the short term and long term assessment of the sandstones and carbonates as these rock types are the most likely candidates for CO_2 storage. There are also few studies on caprocks that assess the sealing capacity. Reviewed literature is listed in Table 2.1.

Table2.1 Numerical models of CO_2-brine-rock interactions

Rock	Simulator	Dimension	T (°C)	P (bar)	Dissolution	Precipitation	Reference
Carbonate (Dogger) Sandstone (North Sea)	CO2ROCK CATCO2	0D	78	160	Albite Illite	K-feldspar Calcite Quartz Kaolinite	Czernichowski-Lauriol et al. (1996)
Glauconitic Sandstone Carbonate (Nisku)	PATHARC	0D	54	130	Annite Albite K-feldspar Kaolinite Calcite	Siderite Muscovite Quartz	Gunter et al. (2000)
Sandstone (Sleipner)	NUFT	2D	37	90-110	K-feldspar Mg-chlorite	Dawsonite Carbonates Muscovite Kaolinite Silica	Johnson et al. (2004)
Serpentinite (Gruppo di Voltri)	EQ3/6	0D	60	250	Serpentine	Magnesite Silica	Cipolli et al. (2004)
Glauconitic Sandstone (Alberta basin) Gulf Coast sediment Dunite	TOUGHREACT	0D	54	260	Glauconite Oligoclase Kaolinite Calcite Illite Na-smectite Clinochlore 14A Daphnite-14A Forsterite Fayalite	Illite K-feldspar Siderite Ankerite Dawsonite Calcite Magnesite	Xu et al. (2004)

Table 2.1 Continued

Rock	Simulator	Dimension	T (°C)	P (bar)	Dissolution	Precipitation	Reference
Sandstone / Shale (Gulf Coast)	TOUGHREACT	1D radial	75	200	Chlorite Oligoclase	Ankerite Dawsonite Siderite Na-smectite	Xu et al. (2005, 2007)
Shale (Sleipner)	PHREEQC	1D	37	100	Albite Anorthite	Calcite Kaolinite Dawsonite	Gaus et al. (2005)
Sandstone (Haizume)	EQ3/6	0D	50	110	Plagioclase Feldspar	Calcite Dawsonite Dolomite Muscovite Kaolinite Quartz	Zwingmann et al. (2005)
Sandstone (Frio)	CRUNCH	1D	64	100	Plagioclase	Calcite Magnesite Dawsonite	Knauss et al. (2005)
Sandstone	GEM	2D	45	118	Kaolinite Illite	Carbonates	Calabrese et al. (2005)
Sandstone	GEM	2D 3D	60	156	Anorthite	Calcite	Ozah et al. (2005)
Sandstone (Rose Sun)	Geochemist's Workbench	0D	54	220	Albite K-feldspar Glauconite	Siderite Dawsonite	Zerai et al. (2006)
Carbonate-rich shale	TOUGHREACT	1D, 2D	45	105	Calcite Illite Chlorite	Carbonates Na-smectite Quartz	Gherardi et al. (2007)

Table 2.1 Continued

Rock	Simulator	Dimension	T (°C)	P (bar)	Dissolution	Precipitation	Reference
Sandstone /Shale (Sleipner)	TOUGHREACT	2D radial	37	100	Chlorite Albite Muscovite Calcite	Dawsonite Carbonates K-feldspar Kaolinite Chalcedony	Audigane et al. (2007)
Sandstone (Sleipner)	GEM	3D	~33	~95	Anorthite Illite Annite	Carbonates Kaolinite Chalcedony	Thibeau et al. (2007)
Carbonate (Dogger)	TOUGHREACT	1D	75	180	Carbonate	Calcite Siderite	Andrè et al. (2007, 2010)
Carbonate (Rousse)	CHESS GEM	0D 3D	?	100	Chlorite Montmorillonite	Siderite Quartz Kaolinite	Thibeau et al. (2009)
Sandstone (Weyburn)	PHREEQC	0D	62	150	K-feldspar Kaolinite	Dawsonite Chalcedony Muscovite	Cantucci et al. (2009)
Sandstone	GEM	3D	?	?	Albite Anorthite Enstatite	Calcite Kaolinite Quartz	Okamoto et al. (2009)
Sandstone Carbonate	TOUGHREACT	1D	70	?	Feldspar	Ankerite Dawsonite	Xiao et al. (2009)
Sandstone (Songliao basin)	TOUGHREACT	2D	50	120	Chlorite Plagioclase Oligoclase	Ankerite Dawsonite	Zhang et al. (2009)
Sandstone (Frio)	TOUGHREACT	1D radial	59	150	Calcite	Ankerite Dawsonite	Xu et al. (2010)

2.1.1. Reaction paths, long term containment and trapping capacity

Different researchers have attempted to model CO_2 storage in Sleipner as it is the first CO_2 storage project in an aquifer. Although the simulation results are significantly different among these studies mainly due to the different conceptualization of the models, such as the mineral selection, they identified the possible mineralization paths as summarized below.

Johnson et al. (2004) modelled the CO_2 storage at Sleipner using the reactive transport simulator NUFT (Nitao, 1998). The model is a 2D model and contains 4000 variably sized grid cells. The simulations revealed that 80-85% of CO_2 remains as free gas, 15-20% dissolves in brine and less than 1% precipitates as carbonates after 20 years. The following trapping mechanisms were identified:

$$K\text{-}feldspar + Na^+ + CO_2(aq) + H_2O \rightarrow Dawsonite + 3Silica + K^+$$

$$M^{2+} + CO_2(aq) + H_2O \rightarrow MCO_3 + 2H^+$$

$$K\text{-}feldspar + 2.5Mg\text{-}chlorite + 12.5CO_2(aq) \rightarrow Muscovite + 1.5Kaolinite + 12.5Magnesite + 4.5Silica + 6H_2O$$

Audigane et al. (2007) performed simulations for the study of the long term storage of CO_2 at Sleipner using TOUGHREACT. The authors used a batch model and a 2D vertical radial geometry with a layered system of permeable sands and semi permeable shales. Simulations were run for a period of 10000 years. The three main reactions identified in the shale by batch models were the following:

$$Chlorite + Calcite + 5CO_2 \rightarrow 2.5Siderite + 2.5Dolomite + Kaolinite + Chalcedony + 2H_2O$$

$$Albite + CO_2 + H_2O \rightarrow Dawsonite + Chalcedony$$

$$Muscovite + 2Chalcedony + H_2O \rightarrow K\text{-}feldspar + Kaolinite$$

Reactivity of sand is slightly different with more limited albite and chlorite dissolution. The alteration of muscovite to K-feldspar is also limited. The dawsonite was formed by the reaction:

$$2Na^+ + Kaolinite + 2CO_2 + H_2O \rightarrow 2Dawsonite + 2Chalcedony + 2H^+$$

2D modelling showed that a gas bubble accumulates under the caprock in the beginning, but after 6000 years it dissolves completely. It predicted similar reactivity as in the batch model. At the end of the simulation 5% of injected CO_2 is trapped by minerals and the remaining 95% by solubility. The sensitivity analysis demonstrated that the residual gas saturation has an impact on the spreading and dissolution of CO_2, and lower grid resolution underestimates the CO_2 dissolution rate. However, both have minor impact on the long term storage predictions.

Thibeau et al. (2007) investigated three CO_2 mineralization pathways in the Utsira aquifer using GEM. The three pathways considered were the following:

$$Anorthite + 2H_2O + CO_2 \rightarrow Calcite + Kaolinite$$

$$4Illite + Calcite + CO_2 + 4H_2O + 2.4H^+ \rightarrow Dolomite + 2.4K^+ + 4.8Chalcedony + 4.6Kaolinite$$

$$Annite + 3CO_2 + H^+ \rightarrow K^+ + 0.5H_2O + 3Siderite + 2Chalcedony + 0.5Kaolinite$$

Initially the reservoir behaves as a carbonate reservoir due to the fast kinetics of carbonates. After 10000 years almost all CO_2 is mineralized and the maximum porosity change is below 0.25%. The authors found that illite has limited CO_2 mineralization potential compared to anorthite and annite.

Czernichowski-Lauriol et al. (1996) studied two formations, the Dogger aquifer formation in Paris and a typical North Sea sandstone. The Dogger formation was represented by calcite and disordered dolomite at 78°C and 160 bar. The North Sea sandstone was represented by quartz, K-feldspar, Na-feldspar, calcite, kaolinite and illite at 98°C and 250 bar. The simulations were both run in batch mode using the CO2ROCK simulator. The simulations showed that CO_2 solubility is enhanced in sandstone formations due to the buffering capacity of silicate minerals. For the sandstone formations reactive transport modelling was also performed using the CATCO2 code (the chemistry module was still CO2ROCK). However no reaction kinetics was considered. They observed albite and illite precipitation, and if all the minerals were in excess, K-feldspar, calcite, quartz and kaolinite would precipitate. The porosity increased from 14.1% to 14.3% after 38 years. If a realistic composition were used they would have observed significant differences. First albite and then illite would completely dissolve. Consequently, complex transition zones would form: a forward

zone with K-feldspar and kaolinite dissolution and illite precipitation; a backward zone with illite dissolution and K-feldspar and kaolinite precipitation.

Gunter et al. (2000) modelled CO_2 injection into Nisku (carbonate) aquifer and glauconitic sandstone aquifer using the PATHARC geochemical modelling code. The simulations were run at 54°C and 130 bar. The annite was used as proxy for glauconite in the simulations. In the Nisku aquifer, equilibrium was reached very quickly and small amounts of siderite and calcite dissolved and dolomite precipitated. In a glauconitic sandstone aquifer equilibrium was reached within hundreds of years. All CO_2 was trapped as siderite due to the annite dissolution which can be expressed as:

$$3Annite + 11CO_2 \rightarrow Muscovite + 9Siderite + 6Quartz + H_2O + 2K^+ + 2HCO_3^-$$

Albite, K-feldspar and kaolinite also dissolved and muscovite precipitated.

Xu et al. (2004) investigated the mineral sequestration of CO_2 in glauconitic sandstone from the Alberta basin, from a Gulf Coast formation and from dunite (olivine rock). The formations were modelled by batch models at 54°C and 260 bar using TOUGHREACT. In the glauconitic sandstone complete dissolution of glauconite, oligoclase, kaolinite and calcite was observed. Illite, K-feldspar, siderite and ankerite precipitated. In the Gulf Coast formation kaolinite, K-feldspar, Na-smectite and oligoclase dissolved completely. Clinochlore-14A and daphnite-14A also dissolved. Illite, siderite, calcite, dawsonite and ankerite precipitated. In the dunite simulation, forsterite and fayalite dissolved, and as a consequence magnesite and siderite precipitated. The simulations revealed that dunite, glauconite and chlorite (clinochlore-14A and daphnite-14A) have sequestration potential. The simulations also showed that mineral trapping can be comparable with, or larger than, solubility trapping. Later Xu et al (2005, 2007) studied the mineral sequestration of CO_2 in a sandstone-shale system for a Gulf Coast aquifer. The simulations showed that the greatest amount of CO_2 sequestration occurs in the sandstone due to the higher content of chlorite and oligoclase in sandstone. CO_2 is trapped as ankerite and dawsonite.

Cipolli et al. (2004) modelled the CO_2 injection into the serpentinites of the Gruppo di Voltri in Italy at 60°C and 250 bar using the geochemical modelling code EQ3/6. For

each mole of serpentine, 3 moles of magnesite are precipitated, which can be expressed as

$$MgSi_2O_5(OH)_4 + 3CO_2 \rightarrow 3MgCO_3 + 2SiO_2 + 2H_2O$$

However the implementation of CO_2 storage is limited due to the progressive reduction of porosity from 19% to 0%.

Zwingmann et al. (2005) evaluated the CO_2 sequestration potential of the Haizume formation in Japan, also using the geochemical modelling code EQ3/6. The formation is composed of quartz, plagioclase, feldspar, pyroxene and clays, and it is at 50°C and 110 bar. Precipitation of calcite, dawsonite, dolomite, muscovite, kaolinite and quartz was predicted. The trapping potential of CO_2 in minerals is 18.8 mol/kgH_2O in 200000 years.

Calabrese et al. (2005) studied the CO_2 injection into a depleted gas reservoir in Northern Italy using GEM. A homogeneous 2D model with 5000 grid blocks was used. Quartz, illite, kaolinite, calcite and dolomite were modelled. After 1000 years only around 1% of injected CO_2 is trapped as carbonates. The change in porosity is less than 1%.

Ozah et al. (2005) modelled the mineral reactions by GEM for a 10000 year period. 2D and 3D models with 64000 and 32000 grid blocks respectively were used. Calcite, anorthite, kaolinite, siderite and glauconite were modelled. Significant calcite precipitation due to anorthite dissolution was observed. Only 4% and 5% of CO_2 is mineralized for the 2D and 3D case respectively.

Zerai et al. (2006) presented the results of equilibrium, path-of-reaction and kinetic modelling of CO_2-brine-mineral reactions in the Rose Sun Sandstone aquifer, Ohio, USA. Simulations were run using Geochemist's Workbench under no flow conditions. Dissolution of albite, K-feldspar and glauconite, and precipitation of siderite and dawsonite were observed. Simulations indicated that the fugacity of CO_2, brine-to-rock ratio, initial brine composition and kinetic rates influence the mineral precipitation and dissolution. Siderite is more stable than dawsonite at lower CO_2 fugacities. Increasing brine-to-rock ratio has a similar effect as increasing CO_2 fugacity.

Okamoto et al. (2009) performed a sensitivity study in order to investigate the effect of the reactive surface area and magnesium containing minerals on CO_2 storage over 1000 years using GEM. The simulations predicted that the start of mineralization is six times longer if the reactive surface area is reduced by a factor of 10, and if magnesium containing mineral (enstatite) were included in the model more calcite precipitates.

Thibeau et al. (2009) modelled CO_2 injection into a depleted gas reservoir, Rousse in France, using GEM. Rousse is a dolomitic (84-98% dolomite) reservoir at 4200 m depth. Simulations predicted the dissolution of iron-rich chlorite and consecutive precipitation of siderite. After 1000 years 70% of the injected CO_2 is mineralized and the porosity reduced from 3% to 2.95%.

Xiao et al. (2009) performed 1D simulations of CO_2 injection and co-injection of CO_2 with H_2S and SO_2 in siliciclastic and carbonate reservoirs for a period of 10000 years using TOUGHREACT. The simulations gave similar results for pure CO_2 and the mixture of CO_2 and H_2S injection cases. The results of the co-injection of CO_2 with SO_2 are significantly different due to very low pH. In siliciclastic reservoirs the main CO_2 trapping is in the form of ankerite and dawsonite, as much as 80 kg/m^3 in feldspar rich reservoirs. The minerals are formed far from the injection wells and are unlikely to cause injection problems.

Zhang et al. (2009) modelled the CO_2 storage in Songliao basin sandstone using TOUGHREACT. A homogeneous 2D model was used. The formation is composed of quartz, illite, chlorite, calcite, plagioclase and K-feldspar. The simulations indicated the mineralization of CO_2 mainly in ankerite only after 1000 years and it reaches maximum 8 kg/m^3 after 10000 years. The slow precipitation is due to the small reactive surface area for chlorite used by the authors. If oligoclase (containing both Na and Ca) were used, instead of albite (containing only Na), as proxy for plagioclase the mineralization of CO_2 increases significantly up to 55 kg/m^3 due to dawsonite precipitation.

The literature review indicated that several formations around the world were modelled and CO_2 trapping capacity is very variable ranging from no trapping to complete trapping depending on the formation. Minerals that supply divalent cations by dissolution have more potential for mineral trapping. Hence, sandstones have more

potential than carbonates to trap CO_2 in mineral forms. However the studies also revealed that some formations have high trapping capacity but they are not suitable for CO_2 storage due to the progressive reduction of porosity.

The studies are mostly batch models or 1D models, which do not take into account the transport effects. Several codes were used, but the only four 3D models were all modelled using GEM. Thermodynamic data used during modelling were not usually reported but the models are very dependent to these data. Although the formations modelled were widespread only one formation from the North Sea was modelled. Moreover due to the different conceptualization of the formation different results were obtained by different authors.

2.1.2. Modelling of field observations

Cantucci et al. (2009) modelled the Weyburn CO_2 injection project using PHREEQC. The simulations ran for 100 years at 62°C and 150 bar. They predicted calcite, K-feldspar and kaolinite dissolution, and chalcedony, dawsonite and muscovite precipitation. The model was validated against the fluid samples taken in the first three years of injection. The calculated composition showed a good match for the majority of the species, with the exception of Ca^{2+}, Mg^{2+} and K^{+}. The authors concluded that the differences are likely due to the complexation effect of carboxylic acid and the overestimation of the K-feldspar kinetic reaction rate.

Xu et al. (2010) modelled the water chemistry changes induced by CO_2 injection at the Frio-I brine pilot in the US gulf coast. 1600 tons of CO_2 were injected into a highly permeable sandstone at 59°C and circa 150 bar. Frio formation is fine grained quartz and feldspar sandstone with minor amounts of illite and calcite. Water samples were taken before, during and after the injection. The samples revealed a sharp drop of pH, a significant increase in HCO_3^- and dissolved Fe. There are also increases in other metals such as Zn and Pb. A 1D radial reactive transport simulation with 226 grid blocks of 1000 years duration was performed using TOUGHREACT. The changes in the water samples were reproduced well in the model. For the long term simulation, during the first 10 years the mineral trapping is negative due to the calcite dissolution. Mineral

trapping starts after 100 years due to ankerite and dawsonite precipitation and it is estimated that the CO_2 in free phase would disappear after 500 years.

2.1.3. Caprock

Gaus et al. (2005) modelled the impacts of CO_2 injection on the caprock at Sleipner via a 1D model using the PHREEQC code. The results showed that after 15000 years the section of the caprock exposed to the geochemical reactions is the reservoir - caprock interface, where there is a slight decrease of porosity (<3%), which enhances the sealing, while in the rest of the caprock there is a negligible change in porosity. Johnson et al. (2004) also modelled the Sleipner caprock, and according to their simulation results porosity and permeability reduction is much greater, 8% and 22% respectively in 20 years of simulation. The differences between the two models are due to the different mineralogies adapted for the caprock. Although the extent of permeability reduction is different in the two studies, they both indicate that the mineralization, even if it is slight, has a significant impact on the integrity of the caprock.

Gherardi et al. (2007) investigated the alteration of the caprock by CO_2 injection in a depleted gas reservoir in Italy. 1D and 2D simulations were carried out using TOUGHREACT. The carbonate-rich shale caprock consists of 33% by volume of calcite and dolomite, 47% by volume of silicate clay minerals (muscovite, Na-smectite, chlorite, kaolinite and illite) and 20% by volume of quartz. Two scenarios, sealed caprock and fractured caprock, were considered. The simulations indicated that the geochemical changes in the caprock are mainly controlled by the reactions involving calcite dissolution and precipitation. In a fractured caprock, where advective transport dominates, CO_2 migrates through the caprock and consequently porosity increases due to the calcite dissolution. In a sealed caprock, where aqueous diffusion dominates, calcite precipitates due to the increase of calcium concentrations, and consequently porosity decreases.

2.1.4. Near well region

One of the concerns during CO_2 injection is the effect of the geochemical processes that take place around the wellbore, which can induce injectivity changes.

André et al. (2007) applied TOUGHREACT to model the evolution of the geochemical reactivity in the near well region of the Dogger aquifer. The formation consists mainly of carbonates (85%), with some aluminosilicates and illite. Two injection cases were considered: injection of CO_2 saturated water and injection of pure supercritical CO_2. In the first case, the results showed strong carbonate dissolution with a porosity increase of up to 90% 10 m around the injection well after an injection period of 10 years. Further from the well, between 15 m and 50 m, siderite and calcite precipitated. However, porosity still increased due to dolomite dissolution. In the second case, a supercritical CO_2 bubble formed 5 meters around the well surrounded by a two-phase zone between 5 and 650 m. As there is no significant geochemical reactivity between supercritical CO_2 and rock, the global reactivity is much less than the previous case. Between 5 and 650 m from the well the porosity increase is about 7%. At 5 m around the well not only has the brine been pushed away from the well, but also complete drying out has occurred. This vaporization leads to mineral precipitation, such as dolomite and anhydrite, decreasing the porosity by 0.1 to 1%. However, the precipitation is under estimated in this zone as TOUGHREACT uses the Debye-Hückel model to determine the activity coefficients of dissolved species, which is limited to solutions with ionic strength less than 0.5. In fact, the comparison of the results of the drying out zone with the ones from SCALE2000 using the Pitzer formalism gives significant differences, especially for carbonate and halite saturation indices. Carbonate and halite saturation indices are underestimated by TOUGHREACT with respect to SCALE2000. This is especially critical for halite because SCALE2000 predicts halite precipitation whereas TOUGHREACT does not.

2.1.5. Thermal processes

Different thermal processes take place during the CO_2 injection, e.g. the heat transfer between the host rock and confining layers, the heat of dissolution, latent heat of water vaporisation, the Joule-Thompson effect and injection temperature. André et al. (2010) investigated the thermal processes and their effect on geochemical reactivity. They carried out simulations with TOUGHREACT on a radial model of a carbonate reservoir, Dogger. They used two injection temperatures, 75°C and 40°C, whereas the reservoir temperature was 85°C. According to the simulation results the main cause of the

temperature gradients in the reservoir are due to injection temperature and the thermal effects are greater around the injection point. It is estimated that the Joule-Thompson effect is small (less than 1-2°C) at pressures higher than 150 bar. The combined effect of latent heat of vaporisation and the Joule-Thompson effect is not more than 2-3°C. The effect of heat of CO_2 dissolution increases the reservoir temperature by about 1°C. The major change of temperature is caused by the temperature of the injected CO_2. Due to the cooling of the reservoir around the injection well, more dissolution of carbonates is observed. Dolomite and siderite are the minerals most influenced by the temperature change. However the dissolution is followed by the precipitation due to the drying-out around the wellbore at high flow rates. Again dolomite is the most reactive mineral and precipitates first. Siderite shows the same behaviour, whereas calcite does not. Increasing the flow rate changes the location of chemical processes further from the injection well.

2.1.6. Impurities in CO_2 stream

Another question related to CO_2-brine-rock interactions, which is rarely studied, is whether impurities in the CO_2 stream can change the geochemical reactions. The question is important because the injected CO_2 is rarely pure and the separation of CO_2 from the waste stream is expensive. Knauss et al. (2005) investigated the injection of CO_2 with H_2S and SO_2 in the Frio formation, and compared it with the injection of pure CO_2. 1D radial simulations were run using the CRUNCH code. Compared to pure CO_2 injection, the co-injection of H_2S with CO_2 did not have significant impact on mineral reactions or pH. On the other hand, co-injection of SO_2 with CO_2 lowered the pH substantially, which caused significant mineral changes. These results are in agreement with the simulations of Xu et al. (2007) on the Gulf Coast formation and of Xiao et al. (2009) on siliciclastic and carbonate formations.

2.2 Experimental evidence

Only few experimental studies have been conducted to investigate the CO_2-brine-rock interactions. These experiments give useful information on the reactivity of CO_2 and the prediction of long term containment of CO_2. They are also useful to validate the numerical models. The reviewed literature is listed in Table 2.2.

Table 2.2 Experimental studies on CO_2-brine-rock reactions

Rock	T (°C)	P (bar)	Dissolution	Precipitation	Reference
Sandstone	80	200	K-feldspar Dolomite	Clays Halite	Pearce et al. (1996)
Glauconitic sandstone	105	90	-	-	Gunter et al. (1997)
Arkose and shale	200	200	K-feldspar Quartz Biotite	Magnesite Smectite	Katzuba et al. (2003, 2005)
Sandstone / Limestone	25 / 120	100 - 600	-	-	Rosenbauer et al. (2005)
Sandstone	70	100	Calcite Dolomite		Bateman et al. (2005)
Sandstone	80	150	Fe-carbonates Feldspar Mica	Calcite Siderite K-rich clays	Bertier et al. (2006)
Carbonate	18-50	34	-	-	Izgec et al. (2005)
Carbonate	90	100	Calcite	Anhydrite	Egermann et al. (2005)
Sandstone	60	150	K-feldspar Albite Dolomite	Montmorillonite	Wigand et al. (2008
Sandstone	48	108	Plagioclase Chlorite Calcite	-	Mito et al. (2008)
Sandstone	200	100-150	K-feldspar Calcite	Kaolinite	Ketzer et al. (2009)
Albite Anorthite	200-300	40-150	-	-	Hangx et al. (2009)
Basalt	15	?	Carbonates	-	Matter et al. (2007) Assayag et al (2009)
Basalt	40	20	-	Carbonates Silica Clays	Gysi and Stefansson (2009)
Sandstone	40	55	Plagioclase K-feldspar Anhydrite	Albite	Fischer et al. (2010)
Forsterite	35/95	1/100	Forsterite	Magnesite Silica	Giammar et al. (2005)
Olivine	150	150	Olivine	Magnesite Silica	Garcia et al. (2010)

Batch and core flooding experiments were conducted on sandstone samples from Cleveland, Cheshire and Wessex basin to represent the southern North Sea reservoirs at 80°C and 200 bar (Pearce et al., 1996). Most significant change common to all samples is the K-feldspar corrosion. In most cases corrosion of dolomite was also observed. Precipitation of secondary clays was tentatively identified. Extensive halite precipitation was observed above the CO_2-seawater interface suggesting the vaporisation of water in CO_2.

Gunter et al. (1997) conducted experiments on crushed samples of glauconite sandstone aquifer in Alberta Basin, Canada at 105°C and 90 bar. They did not observe any change in minerals for one month. However they observed large increase in alkalinity (from 200 mg/l to up to 1600 mg/l) of the brine sample which can indicate the minor mineral reactions. They ran simulations with Patharc.94 code to interpret the alkalinity change. The simulations indicated that K-feldspar, albite and biotite (proxy for glauconite) would dissolve and calcite, dolomite, siderite, quartz, kaolinite and muscovite would precipitate in 6 to 40 years. The authors concluded that experimental duration of one month is too short to observe changes in mineralogy.

Katzuba et al. (2003) investigated the reactive behaviour of CO_2 on arkose and shale samples. The experiments were conducted at 200°C and 200 bar for 59 days of exposure. Alteration of silicates (K-feldspar, quartz and biotite) and magnesite and smectite precipitation were observed. Cl^- increased by 25% and the authors believe that this is due to the vaporization of brine into CO_2. In another experiment Katzuba et al. (2005) observed biotite and shale dissolution and analcime precipitation.

The results of the experiments on plagioclase-rich arkosic sandstones at 25°C and 120°C and from 100 to 600 bar conducted by Rosenbauer et al. (2005) are in line with the results of Katzuba et al. These authors also conducted experiments on limestones at the same conditions as arkosic sandstones. They concluded that porosity changes are dependent on the content of dissolved sulphate in the initial brine. With high-sulphate brine (5100 mg/l of SO_4), dolomitization of calcite and anhydrite precipitation, with a final decrease of porosity of 4.5% was observed, whereas with low-sulphate brine (454 mg/l of SO_4), dissolution of calcite with a final increase of porosity of 2.6% was observed.

Bateman et al. (2005) conducted experiments on a synthetic mixture similar to Utsira formation. The experiments ran at 70°C and 100 bar for 7.5 months. Significant dissolution of calcite and dolomite was observed. There was no sign of change in silicates. The experiments were modelled using the British Geological Survey in-house code PRECIP. The model predictions overestimated the degree of reactions and some minerals such as dawsonite predicted in large quantities were not observed in the experiments.

CO_2 flooding was performed on samples from three sandstone aquifers in Belgium by Bertier et al (2006). Experiments were carried out at 80°C and 150 bar for eight months. Fe-rich carbonates were dissolved and replaced by pure end members (calcite/aragonite and siderite). Alteration of Al-silicates (feldspar, mica) and precipitation of K-rich clays were observed.

Izgec et al. (2006) investigated the effect of injection rate, formation temperature and brine salinity on the chemical reaction kinetics in carbonate formations. They found that horizontal flow resulted in larger calcite precipitation than vertical flow. Due to the absence of gravitational forces in horizontally oriented cores the CO_2 does not move easily to the end of the core. This increases the porosity near the inlet and then the dissolved calcite particles deposit along the flow path. The changes in salinity and injection rate have a small effect on changes in rock properties. The porosity and permeability alteration trends were similar for the temperature range tested (18°C – 50°C). The authors suggest that injection rate has less of an effect compared than the area and duration of CO_2-rock contact. This is contrary to the conclusions of Egermann et al. (2005), who also studied the effect of flow rate on chemical reactions in limestone cores. In their experiments high and low flow rates favoured the wormhole and compact dissolution patterns respectively. Moreover anhydrite precipitated at low rates, which impacted the permeability.

A CO_2 injection field test was conducted in order to investigate CO_2-fluid-rock interactions in a basaltic aquifer at the Lamont-Doherty Earth Observatory test site in Palisades, USA (Matter et al., 2007; Assayag et al., 2009). Rapid neutralization of carbonic acid was observed within hours with an increase in Ca and Mg concentrations.

The dominant process was the dissolution of the carbonates. However, the shallow depth and low temperature of the site makes it less relevant to CO_2 storage.

Experiments were performed on a Bunter sandstone formation sample at 60°C and 150 bar for 62.37 days by Wigand et al. (2008). K-feldspar, albite and dolomite dissolution and montmorillonite precipitation were observed. No change was observed in quartz crystals and illite cements. The concentration of Ca, Mg and K decreased with time, indicating precipitation or cation exchange. However, geochemical modelling did not explain the decrease of the concentrations.

Mito et al. (2008) conducted field and laboratory experiments at the Nagaoka CO_2 injection site, which is Japan's first CO_2 storage pilot site. Compositional changes in the formation waters during the CO_2 injection suggest plagioclase, chlorite and calcite dissolution in the early stage of CO_2 storage in the field test, which were in agreement with the laboratory experiments. Numerical models also showed that mineral trapping could occur within a few years.

The experiments of Ketzer et al. (2009) on sandstone cores of Rio Bonito formation in Brazil at 200°C and 100-150 bar for a 100 hour reaction time showed similar results with the other experiments on sandstones discussed above such as K-feldspar and calcite dissolution. In these experiments kaolinite precipitation was also observed.

Hangx et al. (2009) investigated the trapping potential of albite and anorthite. The experiments were conducted on pure crushed minerals at 200-300°C and 40 to 150 bar. Although the precipitation of calcite and kaolinite from anorthite, and dawsonite and quartz from albite were observed in the literature, no calcite, dawsonite or other carbonates were detected in this study.

Batch experiments and reaction path simulations were carried out on basalts (Gysi and Stefansson, 2009) for the pilot study in SW Iceland. The main secondary minerals formed were carbonates and silica (opal/chalcedony). Mineralization of clays and aluminum silicates were also observed. The interpretation of the results and geochemical modelling were found to be very dependent on the accuracy of the thermodynamic and kinetic data.

The experimental study with longest duration (15 months) was carried out on sandstone samples of Ketzin at 40°C and 55 bar (Fischer et al., 2010). The experiment indicated plagioclase, K-feldspar and anhydrite dissolution and albite precipitation.

The CO_2 sequestration potential of olivine has been studied by Giammar et al. (2005) and Garcia et al. (2010), as these rocks have high potential for CO_2 mineralization due their high content of MgO. The overall reaction for olivine (forsterite) can be expressed as:

$$Mg_2SiO_4 + 2CO_2 \rightarrow 2MgCO_3 + SiO_2$$

Giammar et al. (2005) investigated the dissolution of forsterite due to CO_2 injection. The batch experiments were carried out at 35°C or 95°C and at partial pressure of CO_2 of 1 bar or 100 bar. The experiments revealed that the dissolution of forsterite increases with both increasing temperature and increasing pressure. The precipitation of magnesite did not happen immediately and occurred when the saturation index reached a critical degree of supersaturation for nucleation which is between 0.25 and 1.14 at 95°C.

Garcia et al. (2010) investigated the CO_2 sequestration potential of olivine. The experiments were performed at 150°C and 150 bar. The precipitation of magnesite and amorphous silica was observed. The CO_2 mineralization capacity was up to 57%.

2.2.1 Caprock

Pearce et al. (1996) investigated the effects of CO_2 saturated water on the anhydrite and mudstone samples from the Cheshire Basin which can represent the southern North Sea caprocks. Core plugs were half submerged in either CO_2 saturated synthetic seawater or deionized water, with the remaining half filled with supercritical CO_2. Experiments were conducted at 80°C and 200 bar lasting up to eight months. Severe corrosion by CO_2 saturated fluids was observed on anhydrite samples. Although porosity was increased up to 50%, extensive secondary calcite precipitation was observed on the outer surface of the sample reacted with CO_2 saturated sea water. Hence it is unlikely that the sealing capacity is altered. On the other hand, mudstone samples disintegrated into small fragments, probably due to sodium exchange for calcium in smectite clays,

which causes swelling. Porosity was enhanced due to the dissolution of dolomite and K-feldspar. Precipitation of calcite was also observed in association with dolomite dissolution. However the changes on mudstones were very small.

Wollenweber et al. (2010) investigated the seal properties of two caprock formations from North West Germany by capillary breakthrough tests and diffusion experiments. The first sample is marl from 128 m depth with 40% calcite content and some anorthite, smectite and quartz. The second sample is limestone from 813 m depth with 90% calcite content and some quartz and anhydrite. The CO_2 breakthrough tests were performed at room temperature for up to 150 h and the CO_2 diffusion tests were carried at 45°C for up to 240 h. The confining pressures were up to 50MPa (at least 10 MPa higher than the pore fluid pressure). After the CO_2 diffusion tests, the marl sample showed a reduction of anorthite from 13.9 to 1.1 volume % and an increase of calcite from 10.1 to 56 volume %. The limestone sample did not show any significant mineralogical changes. After CO_2 breakthrough tests, the permeability had increased from 32-34 nD to 40-43 nD and water permeability increased from 7 nD to 12 nD for the limestone sample. In the marl sample a similar trend was observed. After the CO_2 diffusion tests the absolute permeability increased from 5 nD to 12 nD in limestone sample and 33 nD to 56 nD in the marl sample. The capillary breakthrough pressures decreased in both samples by 33% for the marl sample and 56% for the limestone sample. This reduction is associated with an increase in the effective gas permeability values by a factor of 3 for the marl sample and a factor of 8 for the limestone sample.

2.3 Natural Analogues

As reviewed in the previous section, the experimental studies are limited to short time scales, and we need other evidence for long term interactions. Naturally occurring CO_2 fields can provide evidence of CO_2-brine-rock interactions and give insights into how CO_2 behaves during long term storage. However, natural analogue studies also have their limitations, as the natural systems are complex and identification of the CO_2 associated processes and the geochemical reaction kinetics can be difficult. Besides, many of the natural occurrences of CO_2 are found in volcanic regions and they are not comparable to the sedimentary basins where CO_2 will be stored.

Natural occurrences of CO_2 are common and can be in the form of CO_2 rich waters, CO_2 gas accumulations or dry CO_2 gas vents (Pearce et al., 2004). The origin of CO_2 can be mantle degassing, volcanic activity, metamorphism of carbonates, maturation of hydrocarbons and decomposition of organic matter (Baines and Worden, 2004). In some fields CO_2 leaks to atmosphere while in others it does not reach surface. Natural analogues have been studied in the recent years for caprock integrity, CO_2-brine-rock interactions, migration along fractures, near surface processes and diagenetic processes. Here only the studies relevant to CO_2-brine-rock interactions are reviewed (Table 2.3).

The most comprehensive studies are the comparison study of Baines and Worden (2004) and the NASCENT (Natural analogues for the geological storage of CO_2) project (IEAGHG, 2010). Baines and Worden (2004) compared three pairs of reservoirs in which each pair contains the similar geological formations but one is CO_2-rich and the other is CO_2-poor. The first comparison is of two adjacent carbonate reservoirs, Blue Whale and Dolphin in Da Nang basin, Vietnam. Blue Whale and Dolphin contain more than 70% CO_2 and less than 1% CO_2 by volume, respectively. In Blue Whale, extensive late diagenetic dissolution and minimal cement growth were observed, whereas in Dolphin, on the contrary, minimal dissolution and well developed calcite and dolomite cements were observed. The comparison shows that high partial pressure of CO_2 induced mineral dissolution and inhibited mineral precipitation. Sequestration of CO_2 has not occurred in these carbonate reservoirs.

The second pair in the study is the quartzose sandstone reservoirs, Magnus and Miller fields in the UK North Sea. Miller field contains circa 28% of CO_2 by volume and Magnus field contains only 2% of CO_2. In Miller extensive mineral dissolution with the creation of secondary porosity was followed by minor ferroan dolomite and calcite precipitation. The authors assume that the dissolved phase was feldspar mineral. In Miller not all the CO_2 has been sequestered because there was a shortfall of feldspar to source divalent cations, hence CO_2 accumulated in the gas phase. In the Magnus sandstones, compared to Miller, extensive ferroan dolomite cementation was observed. Probably Magnus had a higher initial feldspar content, which had buffered the pH and induced carbonate cementation.

Table 2.3 Reviewed CO_2 natural analogues: CO_2 associated mineral reactions are given.

Analogue	Rock	Compared to	Dissolution	Precipitation	Reference
Bravo Dome (USA)	Sandstone Anhydrite	-	Dolomite Anhydrite Plagioclase	Kaolinite Zeolite Gibbsite	Pearce et al. (1996)
Blue Whale (Vietnam)	Carbonate	Dolphin (Vietnam)	-	-	Baines and Worden (2004)
Miller (UK)	Sandstone	Magnus (UK)	Feldspar	Calcite Illite Quartz	Baines and Worden (2004)
Bravo Dome (USA)	Sandstone Anhydrite	Vert le Grand (France)	Feldspar Dolomite Sulphates Evaporites	Carbonates	Baines and Worden (2004)
Ladbroke Grove (Australia)	Sandstone	Katnook (Australia)	Feldspar Chlorite Calcite	Quartz Kaolinite Fe-carbonates	Watson et al. (2004)
Springville-St. Johns (USA)	Sandstone Anhydrite Dolomite	-	Feldspar Carbonates	Kaolinite Dawsonite	Moore et al. (2005)
Australia	Sandstone	-	Feldspar Illite	Dawsonite	Baker et al. (2005)
Pine Lodge (Australia)	Mudstone	-	Feldspar	Siderite Kaolinite	Watson et al. (2005)
North Sea gas reservoir (UK)	Sandstone?	-	-	Dawsonite Dolomite	Wilkinson et al. (2009)
Florina (Greece)	Sandstone	-	Calcite Iron oxide	Siderite	IEAGHG (2010)
Montmiral (France)	Sandstone	St. Lattier (France)	K-feldspar	-	IEAGHG (2010) Pauwels et al. (2007)

The third pair in the study is the feldspar-lithic-rich sandstone reservoirs, Bravo Dome in New Mexico and Vert le Grand in the Paris basin. Bravo Dome contains 100% CO_2 and the Vert le Grand field contains 2.5-2.8% of CO_2. In the Vert le Grand field extensive dissolution of feldspars followed by dominant carbonate cements was observed. Although there is evidence of dissolution of dolomites, feldspars, sulphates and evaporites, the Bravo Dome reservoir contains potentially reactive minerals such as plagioclase and zeolites in contact with CO_2. CO_2 entry to the system is recent in Bravo Dome (between 100000 and 8000 years ago). According to the authors there has not been enough time to reach thermodynamic equilibrium. On the contrary, Pearce et al (1996), who also studied the Bravo Dome, suggested that with the introduction of CO_2, dolomite, anhydrite and plagioclase dissolved, and kaolinite, zeolite and gibbsite cements were formed. The authors give the evidence for the association with CO_2 as the proximity of these cements to the tertiary faults through which the CO_2 may have migrated.

Watson et al. (2004) studied the Ladbroke Grove and Katnook gas fields in the Otway basin, Australia. Ladbroke Grove is a sandstone reservoir with 26-57 mol% CO_2 content whereas Katnook is within the same formation but has less than 1% of CO_2. The comparison of these two fields indicated that most of the feldspar, chlorite and calcite were dissolved or altered due to CO_2, and quartz, kaolinite and ferroan carbonates were precipitated in Ladbroke Grove. Despite the mineral reactions, porosity is only slightly increased. On the other hand, permeability is increased due to the dissolution of pore-lining clays and carbonate cements opening pore throats.

Moore et al. (2005) investigated the Springville-St. Johns field in Arizona and New Mexico. Springville-St. Johns represents a leaky shallow reservoir with circa 90% CO_2 content. Extensive travertine deposits are present over the entire reservoir. The source of the $CaCO_3$ could be the dissolution of the underlying limestone and dolomite due to the presence of CO_2 and subsequent exsolution of CO_2 from the waters that discharged as springs. The reservoir core samples consisted predominantly of fine grained siltstones intercalated with minor sandstone, mudstone, limestone, anhydrite and dolomite. Dissolution of carbonate cements and feldspar grains and precipitation of kaolinite and dawsonite were observed. As dawsonite and kaolinite were younger than

the carbonate cements on which they have grown, formation of these minerals can be attributable to CO_2. Baker et al. (1995) observed the dawsonite deposition in Australian basins and suggested that it is due to the formation waters that have become acidified and enriched in HCO_3.

In a recent study core samples of a southern North Sea natural gas reservoir with 50% of CO_2 content were analyzed by Wilkinson et al. (2009). They observed a trace amount of dawsonite and dolomite cements. The authors related the limited reactivity to the limited availability of cations.

The NASCENT (IEAGHG, 2010) project studied the analogues around Europe. For the study of geochemical interactions in the reservoir two fields were chosen: the Florina field in Greece and the Montmiral field in France. Florina is a shallow sandstone reservoir (25°C, 5 bar) with CO_2 content more than 99.5%. Montmiral is a deep sandstone reservoir (103°C, 360 bar) with 97-99 % CO_2 content (Pauwels et al., 2007). In Florina the secondary porosity development is minor. The replacement of siderite by iron oxide and calcite corrosion were observed. In Montmiral there is a greater degree of secondary porosity (3.8%) due to dissolution of K-feldspar. The field was compared with the St. Lattier field with broadly equivalent lithology that does not contain CO_2. As there is no developed secondary porosity and the presence of calcite cements, which are absent in Montmiral, the differences between the two field can be attributable to CO_2.

2.3.1 Caprock

The sealing capacity of the seals of the Pine Lodge field in Otway Basin were analysed by Watson et al. (2005). They found that precipitation of CO_2 in the form of siderite enhanced the seal capacity. The seal is a Belfast mudstone which consists of silty mudstones, interbedded siltstones and fine grained sandstones. Alterations occurred in all units. In the siltstone/sandstone units dissolution of feldspar and precipitation of kaolinite and siderite were observed. In the mudstones siderite precipitated through the dissolution of iron rich volcanic fragments: siderite fills the fractures and the pore space. Mercury injection capillary pressure tests indicated an increase of seal capacity by 114-144% compared to the non-CO_2 affected seals.

2.4 Conclusions

The objective of this chapter is to outline the current knowledge of CO_2-brine-rock interactions by reviewing the literature. This review was divided into numerical studies, experimental studies and analysis of natural analogues. All the three categories of studies have their limitations. Most of the modelling studies are batch or 1D models. These studies tell us which minerals dissolve or precipitate but they do not explicitly indicate where they take place and what the impact on three dimensional flow patterns will be. Moreover batch models are closed systems that do not take into account transport, and most of the studies assume homogeneous systems. This is an oversimplification as it is well known that physical and chemical heterogeneities almost always exist. Besides, numerical models are dependent on the underlying geochemical databases and activity models. The work presented in this thesis will not only seek to extend the modelling beyond 1D but will also use the most frequently used numerical codes to compare results.

The major limitation of the field and laboratory experiments is the limited duration of the experiments compared to the time scales needed by some of the chemical reactions to happen. The major limitations of natural analogue studies are the difficulty in isolating the CO_2 associated processes due to the complexity of the natural systems and to identify the reaction kinetics. Regardless of the limitations, previous findings have significantly improved our understanding. The reviewed studies suggest that:

- Reactions observed are mainly dissolution of feldspars, mica and carbonates with secondary precipitation of carbonates, clays and silica.
- Carbonate aquifers have very limited potential to trap CO_2 by fluid-rock interactions.
- Sandstone reservoirs have greater potential to trap CO_2 in minerals if they contain Fe/Ca/Mg bearing aluminosilicates.
- Magnesium silicates have the highest mineral trapping capacity among the rocks studied.
- Non-equilibrium conditions can occur over long time frames as co-existence of CO_2 and reactive minerals was observed.

- Chemical reactions are highly site specific, not only because the reactivity of minerals is significant for some and minor for others, but also because the reactions are dependent on reservoir temperature and pressure.
- Diffusion of CO_2 into the caprock is a slow process. It can be further retarded due to the chemical reactions.
- Contrary to common belief, the dissolution of minerals can take place in several weeks and mineral precipitation can occur within a short time scale.
- Even minimal mineral alteration could have a significant impact on the flow properties of the formations.

This review suggests that any general geochemical modelling activity should concentrate on sandstone systems when considering the possibility of long term mineralisation of CO_2. The driver for this work is modelling of CO_2 sequestration in North Sea saline formations, which will, in any case predominantly mean CO_2 injection into sandstone rocks.

This review also indicates that close attention needs to be paid to the exact mineralogy in each system considered, and by extension, the exact formation water composition, as the processes involved are very system dependent.

2.5 References

André, L., Audigane, P., Azaroual, M. and Menjoz, A., 2007, Numerical modeling of fluid-rock chemical interactions at the supercritical CO_2-liquid interface during CO_2 injection into a carbonate reservoir, the Dogger aquifer (Paris Basin, France), Energy Conversion and Management, 48(6): 1782.

André, L., Azaroual, M. and Menjoz, A., 2010, Numerical simulations of the thermal impact of supercritical CO_2: Injection on chemical reactivity in a carbonate saline reservoir, Transport in Porous Media, 82(1): 247-274.

Assayag, N., Matter, J., Ader, M., Goldberg, D. and Agrinier, P., 2009, Water-rock interactions during a CO_2 injection field-test: Implications on host rock dissolution and alteration effects, Chemical Geology, 265(1-2): 227-235.

Audigane, P., Gaus, I., Czernichowski-Lauriol, I., Pruess, K. and Xu, T., 2007, Two-dimensional reactive transport modeling of CO_2 injection in a saline aquifer at the Sleipner site, North Sea, Am J Sci, 307(7): 974-1008.

Baines, S.J. and Worden, R.H, 2004, The long term fate of CO_2 in the subsurface: natural analogues for CO2 storage. In: Baines, S.J. and Worden, R.H (eds) Geological Storage of Carbon Dioxide, Geological Society, London, Special publications, 233: 59–85.

Baker, J.C., Bai, G.P., Hamilton, P.J., Golding, S.D. and Keene, J.B., 1995, Continental-scale magmatic carbon dioxide seepage recorded by dawsonite in the Bowen-Gunnedah-Sydney Basin system, eastern Australia, Journal of Sedimentary Research, 65(3a): 522-530.

Bateman, K., Turner, G., Pearce, J.M., Noy, D.J., Birchall, D., Rochelle, C.A, 2005, Large-scale column experiment: study of CO_2, pore water, rock reactions and model test case, Oil and Gas Science and Technology - Review IFP, 60(1): 161–175.

Bertier, P., Swennen, R., Laenen, B., Lagrou, D. and Dreesen, R., 2006, Experimental identification of CO_2-water-rock interactions caused by sequestration of CO_2 in Westphalian and Buntsandstein sandstones of the Campine Basin (NE-Belgium), Journal of Geochemical Exploration, 89(1-3): 10-14.

Calabrese, M., Masserano, F. and Blunt, M.J., 2005, Simulation of physical-chemical processes during carbon dioxide sequestration in geological structures, SPE Annual Technical Conference and Exhibition, Society of Petroleum Engineers, Dallas, Texas, SPE 95820-MS.

Cantucci, B., Montegrossi, G., Vaselli, O., Tassi, F., Quattrocchi, F., Perkins, E.H., 2009, Geochemical modeling of CO_2 storage in deep reservoirs: The Weyburn Project (Canada) case study, Chemical Geology, 265(1-2): 181-197.

Cipolli, F., Gambardella, B., Marini, L., Ottonello, G. and Vetuschi Zuccolini, M., 2004, Geochemistry of high-pH waters from serpentinites of the Gruppo di Voltri (Genova, Italy) and reaction path modeling of CO_2 sequestration in serpentinite aquifers, Applied Geochemistry, 19(5): 787-802.

Czernichowski-Lauriol, I., Sanjuan, B., Rochelle, C., Bateman, K., Pearce, J. and Blackwell, P., 1996, Inorganic geochemistry. In: S. Holloway (ed.), The Underground Disposal of Carbon Dioxide, Final Report of Joule II Project Number CT92-0031.

Egermann, P., Bazin, B. and Vizika, O., 2005, An experimental investigation of reaction-transport phenomena during CO_2 injection, SPE 93674

Fischer, S., Liebscher, A. and Wandrey, M., 2010, CO_2-brine-rock interaction: First results of long-term exposure experiments at in situ P-T conditions of the Ketzin CO_2 reservoir, Chemie der Erde-Geochemistry, doi: 10.1016/ j.chemer.2010.06.001.

Garcia, B., Beaumont V., Perfetti E., Rouchon V., Blanchet D., Oger P., Dromart G., Huc A.Y. and Haeseler F., 2010, Experiments and geochemical modelling of CO_2 sequestration by olivine: Potential, quantification, Applied Geochemistry, 25(9): 1383-1396.

Gaus, I., Azaroual, M. and Czernichowski-Lauriol, I., 2005, Reactive transport modelling of the impact of CO_2 injection on the clayey cap rock at Sleipner (North Sea), Chemical Geology, 217(3-4): 319-337.

Gherardi, F., Xu, T. and Pruess, K., 2007, Numerical modeling of self-limiting and self-enhancing caprock alteration induced by CO_2 storage in a depleted gas reservoir, Chemical Geology, 244(1-2): 103-129.

Giammar, D.E., Bruant Jr, R.G. and Peters, C.A., 2005, Forsterite dissolution and magnesite precipitation at conditions relevant for deep saline aquifer storage and sequestration of carbon dioxide, Chemical Geology, 217(3-4): 257-276.

Gunter, W.D., Wiwehar, B. and Perkins, E.H., 1997, Aquifer disposal of CO_2-rich greenhouse gases: Extension of the time scale of experiment for CO_2-sequestering reactions by geochemical modelling, Mineralogy and Petrology, 59(1): 121-140.

Gunter, W.D., Perkins, E.H. and Hutcheon, I., 2000, Aquifer disposal of acid gases: modelling of water-rock reactions for trapping of acid wastes, Applied Geochemistry, 15(8): 1085-1095.

Gysi, A.P. and Stefansson, A., 2009, CO_2-water-basalt interaction: Geochemical modelling and experiments, Geochimica et Cosmochimica Acta, 73 (13, Supplement 1): A483.

Hangx, S.J.T. and Spiers, C.J., 2009, Reaction of plagioclase feldspars with CO_2 under hydrothermal conditions, Chemical Geology, 265(1-2): 88-98.

IEAGHG, Natural Analogues for the geological storage of CO_2: NASCENT project final report, 2005/06, 2010.

Izgec, O., Demiral, B., Bertin and H., Akin S., 2006, Experimental and numerical modeling of direct injection of CO_2 into carbonate formations, SPE 100809.

Johnson, J.W., Nitao, J.J. and Knauss, K.G., 2004, Reactive transport modelling of CO_2 storage in saline aquifers to elucidate fundamental processes, trapping mechanisms and sequestration partitioning, Geological Society, London, Special Publications, 233(1): 107-128.

Kaszuba, J.P., Janecky, D.R. and Snow, M.G., 2003, Carbon dioxide reaction processes in a model brine aquifer at 200° C and 200 bars: implications for geologic sequestration of carbon dioxide, Applied Geochemistry, 18(7): 1065.

Kaszuba, J.P., Janecky, D.R. and Snow, M.G., 2005, Experimental evaluation of mixed fluid reactions between supercritical carbon dioxide and NaCl brine: Relevance to the integrity of a geologic carbon repository, Chemical Geology, 217(3-4): 277.

Ketzer, J.M., Iglesias, R., Einloft, S., Dullius, J., Ligabue, R. and de Lima, V., 2009, Water-rock-CO_2 interactions in saline aquifers aimed for carbon dioxide storage: Experimental and numerical modeling studies of the Rio Bonito Formation (Permian), southern Brazil, Applied Geochemistry, 24(5): 760-767.

Knauss, K.G., Johnson, J.W. and Steefel, C.I., 2005, Evaluation of the impact of CO_2, co-contaminant gas, aqueous fluid and reservoir rock interactions on the geologic sequestration of CO_2, Chemical Geology, 217(3-4): 339.

Matter, J.M., Takahashi, T. and Goldberg, D., 2007, Experimental evaluation of in situ CO_2-water-rock reactions during CO_2 injection in basaltic rocks: Implications

for geological CO_2 sequestration, Geochemistry, Geophysics, Geosystems, 8: 1-19.

Mito, S., Xue, Z. and Ohsumi, T., 2008, Case study of geochemical reactions at the Nagaoka CO_2 injection site, Japan, International Journal of Greenhouse Gas Control, 2(3): 309-318.

Moore, J., Adams, M., Allis, R., Lutz, S. and Rauzi, S., 2005, Mineralogical and geochemical consequences of the long-term presence of CO_2 in natural reservoirs: An example from the Springerville-St. Johns Field, Arizona, and New Mexico, U.S.A, Chemical Geology, 217(3-4): 365-385.

Nitao, J., 1998, Reference manual for the NUFT flow and transport code, version 2.0, Lawrence Livermore National Laboratory, UCRL-MA-130651.

Okamoto, I., Mito, S. and Ohsumi, T., 2009, A sensitivity study of CO_2 mineralization using GEM-GHG simulator, Energy Procedia, 1(1): 3323-3329.

Ozah, R.C., Lakshminarasimhan, S., Pope, G.A., Sepehrnoori, K. and Bryant, S.L., 2005, Numerical simulation of the storage of pure CO_2 and CO_2-H_2S gas mixtures in deep saline aquifers, SPE Annual Technical Conference and Exhibition, Society of Petroleum Engineers, Dallas, Texas, SPE 97255-MS.

Pauwels, H., Gaus, I., le Nindre, Y.M., Pearce, J. and Czernichowski-Lauriol, I., 2007, Chemistry of fluids from a natural analogue for a geological CO_2 storage site (Montmiral, France): Lessons for CO_2-water-rock interaction assessment and monitoring, Applied Geochemistry, 22(12): 2817-2833.

Pearce, J.M., Holloway S., Wacker H., Nelis M. K., Rochelle C. and Bateman K., 1996, Natural occurrences as analogues for the geological disposal of carbon dioxide, Energy Conversion and Management, 37(6-8): 1123-1128.

Pearce, J., Czernichowski-Lauriol, I., Lombardi, S., Brune, S., Nador, A., Baker, J., Pauwels, H., Hatziyannis, G., Beaubien, S. and Faber, E., 2004, A review of natural CO_2 accumulations in Europe as analogues for geological sequestration. In: Baines, S.J. and Worden, R.H (eds) Geological storage of carbon dioxide, Geological Society, London, Special publications, 233: 29-41.

Rosenbauer, R.J., Koksalan, T. and Palandri, J.L., 2005, Experimental investigation of CO_2-brine-rock interactions at elevated temperature and pressure: Implications for CO_2 sequestration in deep-saline aquifers, Fuel Processing Technology, 86(14-15): 1581.

Thibeau, S., Chiquet, P., Mouronval, G. and Lescanne, M., 2009, Geochemical assessment of the injection of CO_2 into Rousse depleted gas reservoir, Energy Procedia, 1(1): 3383-3390.

Thibeau, S., Nghiem, L. and Ohkuma, H., 2007, A Modeling study of the role of selected minerals in enhancing CO_2 mineralization during CO_2 aquifer storage, SPE Annual Technical Conference and Exhibition, Anaheim, California, USA, SPE 109739.

Watson M.N., Daniel R.F., Tingate P.R., Gibson-Poole C.M., 2005, CO_2-related seal capacity enhancement in mudstones: Evidence from the Pine Lodge natural CO_2 accumulation, Otway Basin, Australia. In: Wilson M, Morris T, Gale J, and Thambimuthu K (eds), Greenhouse Gas Control Technologies, Proceedings from the 7th Greenhouse Gas Control Technologies Conference, Vol. 2: 2313-2316.

Watson, M.N., Zwingmann, N. and Lemon, N.M., 2004, The Ladbroke Grove-Katnook carbon dioxide natural laboratory: A recent CO_2 accumulation in a lithic sandstone reservoir, Energy, 29(9-10): 1457-1466.

Wigand, M., Carey, J.W., Schütt, H., Spangenberg, E. and Erzinger, J., 2008, Geochemical effects of CO_2 sequestration in sandstones under simulated in situ conditions of deep saline aquifers, Applied Geochemistry, 23(9): 2735.

Wilkinson, M. Haszeldine, R.S., Fallick, A.E., Odling, N., Stoker, S.J. and Gatliff, R.W., 2009, CO_2-mineral reaction in a natural analogue for CO_2 storage - Implications for modeling, Journal of Sedimentary Research, 79(7): 486-494.

Wollenweber, J., Alles, S., Kronimus, A., Busch, A., Stanjek, H. and Krooss, B.M., 2009, Caprock and overburden processes in geological CO_2 storage: An experimental study on sealing efficiency and mineral alterations, Energy Procedia, 1(1): 3469-3476.

Xiao, Y. Maze, W., Teletzke, G. and Wilkinson, J., 2009, Coupled reactive transport models of Acid Gas Injection (AGI) in siliciclastic and carbonate reservoirs: Understanding fundamental controls on injection performance and storage security, International Petroleum Technology Conference, Doha, Qatar, SPE 13279.

Xu, T., Apps, J.A. and Pruess, K., 2004, Numerical simulation of CO_2 disposal by mineral trapping in deep aquifers, Applied Geochemistry, 19(6): 917.

Xu, T., Apps, J.A. and Pruess, K., 2005, Mineral sequestration of carbon dioxide in a sandstone-shale system, Chemical Geology, 217: 295-318.

Xu, T., Apps, J.A., Pruess, K. and Yamamoto, H., 2007, Numerical modeling of injection and mineral trapping of CO_2 with H_2S and SO_2 in a sandstone formation, Chemical Geology, 242(3-4): 319-346.

Xu, T., Kharaka, Y.K., Doughty, C., Freifeld, B.M. and Daley, T.M., 2010, Reactive transport modeling to study changes in water chemistry induced by CO_2 injection at the Frio-I Brine Pilot, Chemical Geology, 271(3-4): 153-164.

Zerai, B., Saylor, B.Z. and Matisoff, G., 2006, Computer simulation of CO_2 trapped through mineral precipitation in the Rose Run Sandstone, Ohio, Applied Geochemistry, 21(2): 223-240.

Zhang, W., Li, Y., Xu, T., Cheng, H., Zheng, Y. and Xiong, P., 2009, Long-term variations of CO_2 trapped in different mechanisms in deep saline formations: A case study of the Songliao Basin, China, International Journal of Greenhouse Gas Control, 3(2): 161-180.

Zwingmann, N., Mito, S., Sorai, M. and Ohsumi, T., 2005, Preinjection characterisation and evaluation of CO_2 sequestration potential in the Haizume formation, Niigata basin, Japan, Oil & Gas Science and Technology - Rev. IFP, 60(2): 249-258

CHAPTER 3

GEOCHEMICAL MODELLING: STATE OF THE ART

After reviewing the previous research and the evidence of CO_2 - brine - rock processes during CO_2 storage, another step towards understanding these processes is to build a theoretical framework which is described in this chapter.

Our goal is to understand and predict the geochemical changes in the reservoir due to the injection of CO_2 by modelling. A model is an abstract representation of a real system with two distinct parts: one from reality (data) and one from theoretical conceptualization. A mathematical model is a system of equations with variables that characterize the essential parameters of the system. Natural systems are complex and our models are the simplification of these systems, but they are still useful aids to understanding and the prediction of the system behaviour.

There are three main processes that form the basis of geochemical models: thermodynamics, reaction kinetics, and flow and transport processes. The models that do not consider the flow and transport processes are referred to as batch models. Batch models can be conceptualized as a stirred tank reactor. The models that couple geochemical reactions, flow and transport are referred as reactive transport models. All models are based on the principles of conservation of mass.

This chapter gives an overview of the thermodynamic and kinetics modelling approaches in the context of batch modelling and reactive transport simulation, defines the parameters and the type of data needed for application to CO_2 storage, and their limitations. The thermodynamic background of this chapter is taken from Bethke (1996), Lewis and Randall (1961), Garrels and Christ (1965), and Anderson (2005), and more detailed information can be found in these references.

3.1 Thermodynamic Equilibrium Modelling

The most common geochemical modelling is speciation modelling. It predicts the distribution of species, their activities, redox state, degree of saturation of the brine with respect to minerals, and the fugacities of the gases in the system. Speciation modelling is based on an assumption of thermodynamic equilibrium.

Equilibrium is the basis for thermodynamic modelling. Thermodynamics tells us the direction and the amount of reactions that should take place as the chemical system reaches equilibrium. In thermodynamic equilibrium models, equilibrium is defined in terms of chemical potential: the equilibrium is an absolute rest. In real systems equilibrium means a state in which the properties of a system undergo no change during an indefinite period of time.

As natural systems are evolving constantly, in order to apply the thermodynamics to natural systems we need to conceptualize our models with the assumption of local or partial equilibrium. Under the local equilibrium assumption, we apply the thermodynamics to the parts of the system which are not far from equilibrium. For example, if we inject CO_2 into a chalk reservoir, the chalk will start to dissolve and the rock - brine system is no longer in equilibrium. However if we take a sample of brine, we observe no change in that brine, then we can say that the brine is in local equilibrium. Under the partial equilibrium assumption, the overall reaction can be divided into a series of steps, where at each step thermodynamic equilibrium can be applied.

There are two approaches that are used to find the equilibrium composition of the system:

1. Law of mass action (LMA) approach: uses the equilibrium constants as a constraint and adjust the mass of the species until the equilibrium is reached.
2. Gibbs energy minimization (GEM) approach: directly minimizes the total Gibbs energy of the system subject to material balance constraints.

LMA approach is the most commonly used approach and the codes used in this thesis use this approach as well.

3.1.1. Chemical equilibrium in aqueous solutions

We know from the thermodynamics that transformations proceed in the direction of lowest energy and of increased entropy. A general criterion for chemical equilibrium is given by Lewis and Randall (1961) as: "... *with respect to every possible change, that the free energy remain unchanged in any infinitesimal process occurring at constant temperature and pressure.*" In other words, a chemical system is in equilibrium when the Gibbs free energy of reactants and products are equal.

The Gibbs free energy is defined as

$$G = H - TS \tag{3.1}$$

where G is the Gibbs free energy, H is the enthalpy, T is temperature in K and S is the entropy.

The Gibbs free energy for a species is related to its chemical potential through

$$\Delta G = \sum \alpha_i \mu_i \tag{3.2}$$

where ΔG is the Gibbs free energy, μ_i is the chemical potential, α_i is the stoichiometric number of species *i*.

The chemical potential for ideal solutions is expressed by the Nernst equation

$$\mu_i = \mu_i^{\circ} + RT \ln(m_i) \tag{3.3}$$

where μ_i° is the chemical potential at standard state, R is the universal gas constant and m_i is the concentration of the species i in solution.

Therefore a hypothetical reaction bB + cC ↔ dD + eE at equilibrium satisfies

$$d\mu_D + e\mu_E - b\mu_B - c\mu_C = 0 \tag{3.4}$$

The total Gibbs free energy change for the reaction from equations (3.2) and (3.3) is

$$\Delta G = \Delta G^\circ + RT \ln Q \tag{3.5}$$

where ΔG° is the standard state Gibbs free energy change of the reaction and $Q = \left[\frac{m_D^d m_E^e}{m_B^b m_C^c} \right]$.

At equilibrium $\Delta G = 0$, and Q is called as thermodynamic equilibrium constant (K):

$$Q = K \tag{3.6}$$

This equation is named the law of mass action. It is the second governing equation after the mass balance equation in thermodynamic equilibrium modelling, and the distribution of species is calculated according to these two equations.

At equilibrium equation (3.5) becomes

$$K = e^{-\frac{\Delta G^\circ}{RT}} \tag{3.7}$$

This equation depends on the standard molal Gibbs free energy. This is useful in two ways: first we can use the tabulated standard state values, and secondly it is dependent only on temperature and pressure.

From equation (3.1) we can write the standard Gibbs free energy of the reaction as

$$\Delta_r G^\circ = \Delta_r H^\circ - T\Delta_r S^\circ \tag{3.8}$$

where $\Delta_r G^\circ$ is the standard Gibbs free energy of the reaction, $\Delta_r H^\circ$ is the standard heat of the reaction and $\Delta_r S^\circ$ is the standard entropy change of the reaction. By convention, Δ_r is products minus reactants.

Typical adopted standard state for solids and liquids is pure phase. For gases it is ideal gas at 1 bar, and for aqueous species it is hypothetical 1 molal solution at infinite dilution.

As only differences in Gibbs free energy and enthalpy are measurable and not the absolute values, for any substance the formation Gibbs free energy ($\Delta_f G^\circ$) and formation enthalpy ($\Delta_f H^\circ$) are measured. $\Delta_f G^\circ$ (and $\Delta_f H^\circ$) are the difference between the Gibbs free energy (and enthalpy) of the substance and the sum of the Gibbs free energy (and enthalpy) values of its constituents at the most stable state. S° can be measured directly. The equilibrium constants also can be determined from direct measurements of solubility. The direct measurements are preferable because they are less prone to errors (Zhu and Anderson, 2002).

Geochemical modelling codes provide databases where logK or $\Delta_f G^\circ$, $\Delta_f H^\circ$ and S° are tabulated and the codes solve the equilibrium state by equilibrium constants or Gibbs free energies.

3.1.2. Activity

In the previous section we defined the general equation of chemical potential for ideal solutions. For the geochemical modelling of CO_2 storage we deal with real solutions. In real solutions electrostatic forces of the ions become stronger and because of this the Gibbs free energy of the real solutions is lower than in the ideal ones. For the same reason the chemical potential of the species are also lower. Hence we need to introduce a new parameter for the non-ideality, which is termed activity. Activity is the effective concentration of a species in a chemical reaction. Activity of an ion is lower than its concentration and it depends on the pressure, temperature and the solution composition.

Equation (3.3) becomes

$$\mu_i = \mu_i^\circ + RT \ln(a_i) \tag{3.9}$$

and the law of mass action becomes

$$K = \left[\frac{a_D^d a_E^e}{a_B^b a_C^c} \right] \tag{3.10}$$

where a_i is the activity of species i.

The activity of a species is related to its molality by

$$a_i = \gamma_i m_i \tag{3.11}$$

where γ_i is the activity coefficient of the species *i*.

Every pure substance in its standard state has unit activity and for an ideal solution the activity coefficient is equal to unity.

Although the activities of aqueous solute species are defined in molalities, the activity of water is defined in mole fraction.

Activity coefficients of individual ions cannot be measured because real solutions are electrically balanced. Therefore only neutral electrolytes are measurable and the activity coefficients of individual ions are expressed by the mean activity coefficient of neutral electrolytes. The mean activity of generic neutral electrolyte MX is given by

$$\log \gamma_{\pm} = \frac{\nu_M \log \gamma_M + \nu_X \log \gamma_X}{\nu_M + \nu_X} \tag{3.12}$$

where ν_M and ν_X are the number of moles of cation and anion produced by dissociation of one mole of electrolyte, respectively. The value of individual activity coefficients are separated on a conventional basis.

3.1.3. Activity models

Geochemical codes provide activity models to calculate the activity coefficients of aqueous species and water. There are two main approaches to model activity: Debye-Hückel methods and Pitzer methods.

The Debye-Hückel model takes account of only long range coulombic forces and calculates the activity coefficient of a species as a function of the species' size and the ionic strength of the solution by

$$\log \gamma_i = -\frac{A z_i^2 \sqrt{I}}{1 + \mathring{a} B \sqrt{I}} \tag{3.13}$$

where A and B are the solvent parameters which depend on temperature, density and dielectric constant of water, z_i is the ionic charge of the species i, $\mathring{a}$ is the ion size parameter, I is the ionic strength of the solution.

I is defined as

$$I = \frac{1}{2} \sqrt{m_i z_i^2} \tag{3.14}$$

The Debye-Hückel equation works well up to ionic strengths 0.1 molal as the method takes account only of long range coulombic forces. There are extended Debye-Hückel methods with additional terms to the equation (3.13) for the more concentrated solutions. The two most widely used ones are the Davies equation and the B-dot equation.

The Davies equation (Davies, 1962) is a simple extended Debye- Hückel equation:

$$\log \gamma_i = -A z_i^2 \left(\frac{\sqrt{I}}{1 + \sqrt{I}} - 0.3I \right) \tag{3.15}$$

$0.3I$ is an empirical term ($0.2I$ also is used). This equation is normally applied at temperatures close to 25°C and works for ionic strengths up to 0.5 molal. Activity coefficients of all neutral species are assumed to be unity. This is inaccurate because the activity coefficients of the non polar neutral species increase with increasing ionic strength (salting-out effect) (Garrels and Christ, 1965). Besides the activity coefficients of two polar neutral species ($MgSO_4$(aq) and $CaSO_4$(aq)) decrease with increasing ionic strength (Reardon and Langmuir, 1976).

The B-dot equation (Helgeson, 1969) is another extended Debye- Hückel equation:

$$\log \gamma_i = -\frac{Az_i^2\sqrt{I}}{1+\mathring{a}B\sqrt{I}} + \dot{B}\,I \tag{3.16}$$

where $\dot{B}$ is the B-dot parameter which depends on the electrical charge of the species and it varies with temperature. Activity coefficients of polar neutral species are assumed to be unity. The activity coefficients of non polar neutral species are assigned the activity coefficient CO_2(aq) in NaCl solutions of the same ionic strength and are calculated by power series such as (Bethke, 1996):

$$\log \gamma_i = aI + bI^2 + cI^3 \tag{3.17}$$

so the activity coefficients increase sharply at high ionic strengths which represents the salting out effect. a, b, c are the coefficients that vary with temperature. B-dot model is widely used in geochemical models as it is valid up to 300°C and ionic strengths up to 3 molal in which NaCl is the dominant solute, and up to 1 molal for others.

At high ionic strengths ions are bounded by water and short range forces become important. Besides, as the water molecules bound the individual ions, there are less free water molecules available as solvent. Therefore we need another approach that takes account of these effects.

The second main approach, a virial expansion method or generally referred to as the Pitzer method, takes account the short range forces and the solvent effect in addition to a modified Debye-Hückel term for long range coulombic forces.

The excess Gibbs free energy G^{EX} (free energy in excess with respect to the free energy of an ideal solution) is expressed as (Pitzer, 1973):

$$\frac{G^{EX}}{RT} = n_w f(I) + \frac{1}{n_w}\sum_{ij}\lambda_{ij}(I)n_i n_j + \frac{1}{n_w^2}\sum_{ijk}\mu_{ijk}n_i n_j n_k \tag{3.18}$$

where n_w and n_i are the number of kilograms of solvent and solute respectively, $f(I)$ is the modified Debye-Hückel term, λ_{ij} and μ_{ijk} are the second and third order ion interaction terms taking into account the short range forces between species *i* and *j*. λ_{ij} varies with ionic strength whereas μ_{ijk} is an empirical constant at a given temperature.

From the derivative of equation (3.18) the activity coefficient is derived as

$$\ln \gamma_i = \frac{z_i^2}{2} f' + 2\sum_j \lambda_{ij} m_j + \frac{z_i^2}{2} \sum_{jk} \lambda'_{jk} m_j m_k + 3\sum_{jk} \mu_{ijk} m_j m_k \qquad (3.19)$$

where $f' = \frac{df}{dI}$, $\lambda'_{ij} = \frac{d\lambda_{ij}}{dI}$ and $m_i = \frac{n_i}{n_w}$.

The Pitzer method gives accurate results at high ionic strengths but it requires a large number of parameters. The available data is limited and silica and aluminum components are missing. At present there is no general model available either to estimate interaction parameters for aqueous species or to extrapolate over wide ranges of temperature and pressure (Oelkers et al., 2009). On the other hand, Debye-Hückel methods are simple. They can be easily extrapolated over the range of temperatures and new species can be added easily. Unlike the Pitzer method they give information about the distribution of the species. However they are not reliable at higher ionic strengths and for solutions where the dominant solute is not NaCl.

3.1.4. Numerical Implementation

In a geochemical model the aqueous composition is described in terms of a set of basis components. Components are mathematical tools for describing a composition. Basis components are the minimum number of fundamental species that describe all the species in the solution. The basis components satisfy the following three rules:

1. They must be able to form all the species and phases considered in the model.
2. The number of the components is the minimum necessary to satisfy the first rule.
3. They must be mutually independent.

For example, water containing dissolved CO_2 can be described in terms of basis components H_2O, H^+ and $CO_2(aq)$. The secondary species can be expressed by independent chemical reactions among basis components:

$$OH^- = H_2O - H^+$$
$$H_2CO_3 = CO_2(aq)$$
$$HCO_3^- = CO_2(aq) + H_2O - H^+$$
$$CO_3^{2-} = CO_2(aq) + H_2O - 2H^+$$

There are three types of governing equations that need to be solved:

1. Mass balance equations: The total mass of each element is constant.
2. Mass action equations: Each independent reaction has an associated equilibrium constant, hence a mass action equation.
3. Charge balance equations: The aqueous solutions are electrically neutral.

The governing equations are a set of nonlinear algebraic equations and iterative methods are needed for the solution. The most common method is the Newton-Raphson method. The mathematic formulation is described in Bethke (1996).

3.2 Kinetics Modelling

We defined the conditions for equilibrium as the reactions proceed towards the equilibrium but the thermodynamic equilibrium models do not give any information about how long it will take to reach equilibrium, nor the transition states. Therefore, a thermodynamic equilibrium approach is suitable for fast reactions or when the time scale of interest is long enough that the system reaches equilibrium. In the case of CO_2 storage we would like to know the length of time required for the reservoir to reach equilibrium after the CO_2 injection. For slow reactions we need to introduce a time variable in order to model the reaction progress through time. This is achieved by the kinetics modelling approach. In the context of CO_2 storage, mineral dissolution and precipitation reactions are relatively slow with respect to the reactions involving only aqueous solutions and gases, and they are usually treated by the kinetics approach.

When a mineral comes into contact with CO_2 saturated brine with which it was not in equilibrium previously, the mineral starts to dissolve in order to reach equilibrium with the brine. The dissolution of the mineral changes the brine composition and can drive the precipitation of secondary minerals. For example, if K-feldspar comes into contact with CO_2 saturated brine, it dissolves. The release of Al, Si and K ions enriches the

brine, and it becomes supersaturated with respect to muscovite. If it is sufficiently supersaturated for nucleation, muscovite precipitates.

In thermodynamic equilibrium models supersaturation of a mineral is not allowed. On the other hand, whether or not a mineral actually precipitates depends on the kinetic rate of the reaction. Therefore, kinetics reaction modelling allows for the supersaturation of the mineral phases in the solution. For this reason a kinetic law is used for the dissolution and precipitation of minerals. The reaction rate depends on how much of the mineral is available, how fast the reaction is, and how far it is from equilibrium.

Mineral dissolution and precipitation involves five main processes: diffusion of the reactants and products from and to the mineral surface, surface reactions involving the breaking and creation of bonds, adsorption of the reactants and desorption of the products. The overall rate of dissolution and precipitation are controlled by the slowest step. Adsorption and desorption steps are rapid. Hence there are two classes of rate limiting steps (Lasaga, 1984). If the surface reactions are fast with respect to the diffusion processes the reaction is "transport controlled". If the diffusion processes are fast with respect to surface reactions the reaction is "surface controlled". In natural systems the majority of the silicate mineral reactions are surface controlled (Stumm and Wollast, 1990). On the other hand there are numerous non-silicate minerals, such as calcite, that are transport controlled at neutral to acidic conditions (Oelkers, 1996).

Almost all rate laws are based on transition state theory (Lasaga, 1981). The theory provides an approach to extrapolate rates near to equilibrium conditions found in natural systems. According to the theory, an activated complex forms during the reaction at the transition state forming products from reactants. Transition state is an unstable state at highest free energy. The rate at which the activated complex decays controls the rate of the reaction. The link between the thermodynamic approach and the kinetics approach is that at equilibrium the dissolution rate and the precipitation rate are equal.

There are two commonly used scales to quantify the distance from equilibrium: saturation index and chemical affinity. Saturation ratio (Ω) is defined by

$$\Omega = \frac{Q}{K} \tag{3.20}$$

where Q is the ionic activity product and K is the equilibrium constant. $\log\Omega$ is termed saturation index. At equilibrium the saturation index is equal to zero, and it is more than zero when the reactants are supersaturated. The chemical affinity (A) represents the energy difference between the reactants and the products. It is related to saturation ratio and is defined as

$$A = -\Delta_r G = -RT \ln \Omega \tag{3.21}$$

where $\Delta_r G$ is the Gibbs free energy of the reaction, R is the gas constant and T is the temperature in K. Chemical affinity is equal to zero at equilibrium and less than one when the reactants are supersaturated. The chemical affinity is a molar property whereas saturation index is dimensionless.

The rate of the dissolution or the precipitation of a mineral can be expressed by

$$\begin{aligned} r &= Akf(a_i) f(\Delta G) \\ &= \operatorname{sgn}\left(\log(\Omega)\right) Ak \prod a_i^p \left|(\Omega)^M - 1\right|^n \end{aligned} \tag{3.22}$$

where A is the reactive surface area of the mineral, k is the rate constant, $f(a_i)$ is the function of individual ions in solution and $f(\Delta G)$ is the function of the free energy of the solution. $f(a_i)$ represents the inhibiting or catalyzing effect of the ions in solution. $\operatorname{sgn}\left(\log(\Omega)\right)$ gives the sign of the expression: negative if the fluid is undersaturated, positive if the fluid supersaturated with respect to the mineral. p, M and n are empirical powers. a_i is the activity of the inhibiting or catalyzing species.

The temperature dependence of the rate constant can be expressed by the Arrhenius equation (Lasaga, 1984):

$$k = k_{T_0} \exp\left[-\frac{E_a}{R}\left(\frac{1}{T} - \frac{1}{T_0} \right) \right] \tag{3.23}$$

where k_{T_0} is the rate constant at T_0, E_a is the activation energy and T_0 is the reference temperature in K.

3.3 Reactive Transport Modelling

The injection of CO_2 induces fluxes through the reservoir and perturbates the equilibrium conditions; the extent of the chemical reactions is dependent on the flow and transport processes. Therefore we need to couple the static system described in the previous sections of this chapter to the flow and transport processes.

Reactive transport modelling is a coupled transport and reaction approach that simulates how the geochemical reactions evolve in time and space. The coupled transport and reaction models can be pictured as discretizing the flow into a sequence of interconnected stirred tank reactors.

3.3.1. Governing equations and coupling between various processes

The main components of reactive transport calculations are flow equations for fluid movement, transport equations for aqueous species and equations describing homogeneous and heterogeneous reactions. Two sets of equations are solved: the partial differential equations that describe flow, transport and reaction kinetics and nonlinear algebraic equations that describe chemical reactions. Theoretical formulations can be found in Lichtner (1996), Steefel and Lasaga (1994) and Yeh and Tripathi (1989).

The governing equations for a single phase are given in Figure 3.1 (Steefel et al., 2005).

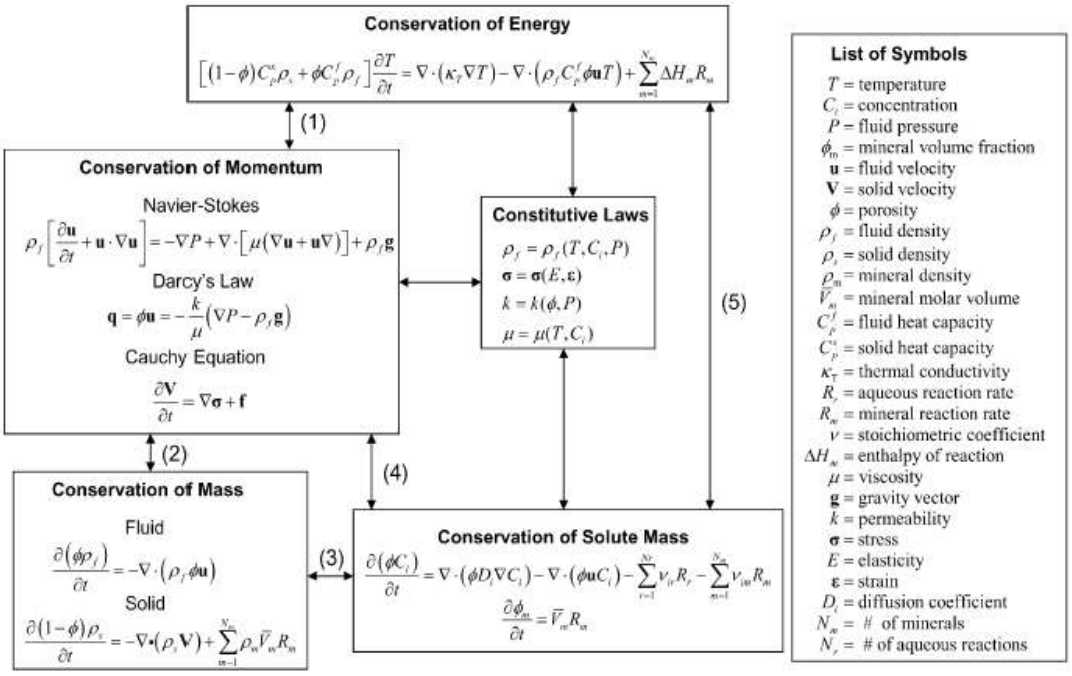

Figure 3.1 Governing equations for a single phase coupled reactive transport system (Steefel et al, 2005)

Some of the first order couplings are given below (shown with numbered arrows in Figure 3.1):

1. Coupling between energy and fluid flow (conservation of momentum), primarily through the advection of heat and the effect of temperature on the fluid density;
2. Coupling between the conservation of momentum and the conservation of fluid or solid mass, typically treated by solving the two together to obtain the flow field or the deformation of the solid phase;
3. The effect of dissolution or precipitation of minerals on concentrations of solutes and the mass of minerals;
4. Coupling between fluid flow and solute concentrations, primarily through the advection of solutes and/or colloids and the effect of concentration on fluid density and coupling between the deformation of the solid matrix and solute concentrations through the effect of stress on reactions (i.e., pressure solution) and through modifications on the porosity and permeability as a result of mineral dissolution or precipitation;
5. Coupling between temperature (conservation of energy) and solute concentrations through the effects of temperature on the thermodynamics and on

reaction rates and the effect of chemical reactions on the thermal regime where heats of reaction are significant.

3.3.2. Numerical implementation

The major difficulties in reactive transport models are the computational difficulties in terms of computer time and memory, and numerical stability. The governing equations are solved both in time and space. The numerical methods used to solve these equations are finite element or finite difference methods. In both cases generation of a grid on the spatial domain of interest is needed. In the finite difference method the spatial derivatives are approximated as linear difference equations between neighbouring nodes and the fluid exists at the nodes. In the finite element model the fluid occupies the space between the nodes and the concentrations are represented as extrapolating polynomials between the nodes. Spatial derivatives are approximated as the derivative of the polynomials. In both methods time derivatives are approximated as finite difference equations on discrete time steps.

The reactive models couple transport and reaction processes with one of the following (Steefel and Maher, 1996):

1. One-step (or global implicit) approach: by substituting directly the reaction equations into the transport equation, transport and reaction equations are solved simultaneously. It is the most CPU time and memory demanding approach. This method is implemented by Nghiem (2004) in GEM.
2. Sequential non iterative (or operator splitting) approach: consists of a single time step in which a transport step is followed by a reaction step using the transported concentrations. It is less CPU demanding. The greatest difficulties arise in kinetic systems at the physical boundaries of the system where the same amount of reaction is applied to a fluid parcel which just entered the system as is applied to a parcel which has been in the system for the entire time step. This approach is implemented by Xu et al. (2006) in TOUGHREACT as an option.
3. Sequential iterative approach: based on the sequential non iterative approach, except that a source/sink term is updated after each reaction step in the transport equation and an iterative loop within the time step is added. This approach is

implemented by Parkhurst and Appelo (1999) in PHREEQC and by Xu et al. (2006) in TOUGHREACT.

Steefel and Maher (1996) compared the coupling schemes and concluded that:

- Sequential non iterative approach may result in operator splitting errors[1].
- Global implicit approach is free from operator splitting errors but can have significant numerical dispersion.
- Global implicit approach required significantly more time than any other method.
- Sequential iterative approach is the most effective at reducing operator splitting error at lowest computational cost, although it had some difficulty in converging in some simulations.
- Global implicit approach may be more efficient in long time scales because of its ability to take larger time steps.

Xu et al. (1999) test the accuracy of the sequential non iterative and sequential iterative approaches and they concluded that the accuracy of sequential non iterative approach depends on space discretization, time step size and the type of chemical process. For courant[2] numbers smaller than one the difference between the two approaches is small and sequential non iterative approach can be used by enforcing a courant number less than one during the simulation.

Another study of the influence of the coupling approaches on the accuracy of the results can be found in Kervévan et al. (2007) where they indicate that the choice of time step has crucial importance on the accuracy of the results. Both too large and too small time steps may lead to inconsistent results.

[1] Numerical errors associated with the operator splitting approach in which the transport and chemistry equations are solved separately. The potential problem with operator splitting approach is that the reactions begin after the transport.

[2] Courant number is defined as the product of fluid velocity and time step size divided by grid size.

3.4 Model Requirements for the Geochemical Modelling of CO_2 Storage

Due to the complex interactions between the flow, transport and chemical processes ideally we need a model that can couple these processes. Besides, we need a model that is capable of predicting temporal and spatial distribution of the geochemical reactions. Moreover the reactivity potential differs between the batch and reactive transport models due to the differences between the static and dynamic systems. Hence reactive transport modelling is more appropriate for the geochemical modelling of CO_2 storage. On the other hand, reactive transport codes require as input the initial water composition, aqueous species, primary and secondary minerals. Batch models are useful in order to identify the key reactions, and aqueous species and minerals to be included in the reactive transport models.

An accurate modelling of thermophysical properties of pure CO_2 as well as the CO_2 - brine mixtures over a wide range of temperature, pressure and salinity is needed. The model should not only estimate the CO_2 solubility in brine but also the water solubility in CO_2 if the drying phenomenon is to be modelled. Density change of the brine with CO_2 dissolution should also be modelled as it enhances the CO_2 solubility by convective mixing.

Both aqueous reactions and mineral dissolution and precipitation reactions need to be considered ideally as equilibrium and kinetic reactions, because the reactions can be very fast or slow in the time scale of interest. A comprehensive and flexible thermodynamic and kinetic database should be provided by the code. An adequate activity model applicable to higher salinity brines is required for accurate modelling of geochemical reactions.

Thermodynamic equilibrium constants and reaction rates are required to be temperature and pressure dependent. There are uncertainties on equilibrium constant at high pressure and temperature because laboratory data are not available. However, current codes do not take into account the dependence of equilibrium constant on pressure. An adequate activity model applicable to high salinity brines is required for accurate modelling of geochemical reactions. The Pitzer model for high salinity brines does not contain Al and Si species. Another uncertainty associated with the equilibrium constants is the compositional variations of the complex minerals. Some equilibrium

constants in the databases are for pure minerals or minerals with specific composition (e.g. illite) but reservoir minerals have different composition (e.g. solid solutions).

Redox state is a critical parameter that needs to be considered in the models as the redox state determines the formation of redox sensitive iron bearing minerals. For example, the siderite, which is an important mineral for CO_2 trapping in mineral forms, depends on the redox state of the system.

The uncertainties in the input parameters for reaction rates in geochemical modelling can be several orders of magnitude. There are large discrepancies between the physical and chemical parameters from laboratory and field data. The main sources of the discrepancies are due to the effects of chemical affinity and solution composition on the dissolution rates and the differences between the surface areas of minerals in the field versus laboratory (Oelkers, 1996). Moreover there are significant differences between the reported laboratory measured rates.

The surface area can be calculated from the geometric surface areas of particles or by the BET[3] (Brunauer-Emmett-Teller) method (Brunauer et al., 1938). The geometric surface area, which is based on the shape and size of the grains, underestimates the natural surface area because it does not include the surface roughness[4] and porosity (Kump et al., 2000). The true surface area is measured by the BET method, but in this case there are uncertainties in reactive surface area due to the channelling reactive fluid flow (Oelkers, 1996) and the contribution of unreactive surface parts such as etch pit walls (Gautier et al., 2001). Moreover, there are significant differences between the surface roughness of mineral samples used in the laboratory experiments and of naturally weathered rocks. Anbeek (1992) reported that the freshly grounded silicate mineral surfaces have surface roughnesses ranging from 2.5 to 11, whereas the surface roughness of naturally weathered silicates ranges from 130 to 2600. Furthermore, with

[3] BET method measures the adsorption of an inert gas such as N_2 and Kr, on the surface. The surface area is proportional to the gas adsorbed.

[4] Surface roughness is defined as the ratio of the reactive surface area to the equivalent geometric surface area.

the dissolution and precipitation of minerals the surface area can change. While it is easy to calculate the porosity changes it is difficult to quantify the surface area.

Reaction rates have a high degree of uncertainty. For most of the minerals, precipitation rates are unknown because in the experiments metastable products often precipitate instead of the desired minerals. Besides, rates calculated from the field data are up to three orders of magnitude slower than the rates calculated from laboratory experiments. This is mainly due to the physical controls because in natural systems not the entire potential available mineral surface contacts with the pore fluids (Velbel, 1993).

Reactions that are surface controlled in the laboratory can be transport controlled in the field. A transport limitation can be the slow advection of reactants or products (Kump et al., 2000). Flow rate has an impact on the rate controlling mechanism. At low values of the flow rate to mass ratio, transport limits weathering of silicates, but at higher rates surface controls weathering (Schnoor, 1990). In transitional state theory, rate laws stem from the surface controlled mechanism, as the majority of the minerals in basic conditions in natural systems are surface controlled (Stumm and Wollast, 1990). However, in acidic conditions of CO_2 storage, the rate control mechanism may change.

The model should be able to deal with physical and chemical heterogeneity. Heterogeneities are always present in porous media, and the predictive capability of the reactive transport model depends on the characterization of the system. One of the biggest challenges in reactive transport modelling is the scale dependence of the reactive transport processes. There are physical heterogeneities that affect the flow and transport, but also there are chemical heterogeneities that affect the geochemical reactions. It is impossible to fully characterize the system because of lack of data.

The model should be able to calculate porosity and permeability changes due to mineral dissolution and precipitation. In multiphase flow the model should be able to deal with the wettability changes of the medium due to chemical reactions. The model should also be able to simulate drying out near the injection well.

The dissolution and precipitation of minerals can cause porosity and permeability changes. Dissolution of minerals increases the porosity and permeability of the formation which can lead to preferential flowpaths. On the other hand precipitation of minerals decreases the porosity and permeability. Mineral precipitation can lead to

solids depositing on the pore walls in the pore space, individual particles blocking the pore throat and bridging of several grains across the pore throat (MacQuarrie and Mayer, 2005). It is difficult to quantify the permeability changes because the permeability depends not only on porosity but on the geometry of the pore network, hence total porosity, pore size, tortuosity, and connectivity. Several models are developed to describe permeability-porosity relationship such as the Kozeny - Carman model (Oelkers, 1996). These models express permeability as a function of porosity and a parameter such as grain size, specific surface or pore radius. These models do not fit well with a variety of permeability data (Oelkers, 1996; Saripalli et al., 2001). Kozeny - Carman models often fail at low porosities where permeability decreases much more with decreasing porosity. Improved models were developed, but they require additional parameters such as shape factors and roughness (Panda and Lake, 1995).

Although CO_2 is considered as the non-wetting phase, CO_2 wettability can be mixed at CO_2 storage conditions. Chriquet et al. (2005) showed that the wettability of minerals such as quartz and mica is altered with CO_2 injection. Those minerals changed from strongly water wet to intermediate wet.

3.5 Codes used in this study

The codes used in this thesis are briefly summarised below. More detailed information on the codes can be found in the cited references.

PHREEQC v.2.15 (Parkhust and Appelo, 1999) is mainly a general purpose geochemical code, including the capability to simulate monophase 1D reactive transport. A feature of PHREEQC is its ability to be adapted to specific geochemical problems by modifying its database (reactions and species can be added or suppressed easily) and/or adding specific modules (programmed in BASIC) to take into account, for instance, a particular kinetic law. Coupling between chemistry and transport is based on the operator splitting technique (advective, dispersive and reaction operators are split) with a specific sequential iterative algorithm. PHREEQC uses the law of mass action approach. PHREEQC may be used in batch mode or as a one dimension discretized linear transport model.

GEM v.2009.13 (Nghiem et al., 2004) is a fully coupled geochemical compositional equation of state simulator for modelling CO_2 and acid gas enhanced oil recovery (EOR) and storage processes. GEM uses a one step approach and can model convective and dispersive flow; phase equilibrium between oil, gas and brine; chemical equilibrium reactions among aqueous components; and mineral dissolution and precipitation kinetics. The simulator uses an adaptive implicit discretization technique to model the component transport in porous media in one, two or three dimensions. The oil and gas phases are modelled with an equation of state, and the gas solubility in the aqueous phase is modelled with Henry's law. Vaporization of H_2O into the gas phase, thermal effects and leakage through cap rock, and sealing faults also are modelled. GEM also uses the law of mass action approach.

TOUGHREACT v.1.21 (Xu et al., 2006) is a non-isothermal reactive transport code. It was developed by introducing reactive chemistry into the framework of the existing multi phase fluid and heat code TOUGH2. It uses a sequential coupling scheme. TOUGHREACT can be used for batch geochemical modelling and to model reactive transport in one, two and three dimensions. The model can include any number of chemical species in liquid, gas and solid phases. Aqueous chemical complexation and gas dissolution/exsolution are considered under the local equilibrium assumption. Mineral dissolution/precipitation can proceed either subject to local equilibrium or kinetic conditions with coupling to changes in porosity with permeability and capillary pressure in undersaturated systems. TOUGHREACT uses the ECO2N module, which is a fluid property module for the TOUGH2 simulator (Version 2.0) that was designed for applications to geologic sequestration of CO_2 in saline aquifers. It includes a comprehensive description of the thermodynamics and thermophysical properties of H_2O-NaCl-CO_2 mixtures, which reproduces fluid properties largely within experimental error for the temperature, pressure and salinity conditions of interest (10 °C $\leq$ T $\leq$ 110 °C; P $\leq$ 600 bar; salinity up to halite saturation) (Pruess and Spycher, 2005).

MoReS v2011_1_alpha (Wei, 2009; 2010) is the non released version of the Shell's in-house simulator coupled with PHREEQC. The coupling scheme between MoReS and PHREEQC is sequential coupling. All the features of PHREEQC are implemented in MoReS. MoReS is a fully interactive reservoir simulator, with flexible scripting interface, capable of black oil, equation of state and K-value compositional simulations.

MoReS uses fully implicit, or implicit pressure, explicit saturation and composition, or adaptive implicit method. CO_2 fugacity calculated by MoReS is used in PHREEQC to calculate solubility of CO_2. Vaporization of H_2O into the gas phase is modelled with equation of state formulations. The effect of gas dissolution on water density is modelled by the Garcia model (Garcia, 2001).

3.6 Criteria for geochemical modelling code selection

From the discussion above, the criteria for code selection for the geochemical modelling of CO_2 storage are the following:

- Capability to handle equilibrium and kinetic modelling approaches
- An adequate activity model
- An accessible internal thermodynamic and kinetic database
- Ability to model accurately CO_2 solubility
- Ability to model reactive transport
- Ability to model diffusion
- Capability to handle multiphase flow
- Capability to handle heterogeneity of medium
- High computational efficiency and numerical robustness

In addition to the technical criteria the following criteria are important for the selection:

- Versatile pre and post processors
- Code availability
- Code documentation
- Code support
- Code validation

Today there is no code that meets all the criteria. A matrix to define how the four codes which are used in this thesis (PHREEQC, GEM, TOUGHREACT and MoReS) perform against the above criteria is given in Table 3.1 with the legend in Table 3.2. The selection of the code can be made by judging the most important criteria for a specific scenario and the purpose of the study.

As PHREEQC is a predominantly a geochemical modelling code, its main advantage is the batch equilibrium modelling. It is also the only code among PHREEQC, GEM and TOUGHREACT which implemented the Pitzer activity model. Although the Pitzer model is available to use the database was only validated at 25°C and its performance is uncertain above 25°C. It has versatile thermodynamic databases which can be modified easily. It has great flexibility in modelling kinetics as the modeller needs to program the rate equations in the BASIC language. There is also a kinetics database ready to use for few minerals such as calcite, albite and K-feldspar. The disadvantage is the computational time in case of kinetics models. The main disadvantage is inability to model CO_2 solubility because of the ideal gas assumption. The other disadvantages are that it can only simulate simple one dimensional reactive transport and the inability to simulate multiphase transport.

Since MoReS uses PHREEQC as the geochemical solver it incorporates all the advantages of PHREEQC. The disadvantages of PHREEQC are tackled in MoReS. The computational time is improved significantly and the code is faster than the other three codes. Modelling CO_2 solubility is also improved by calculating the correct fugacities with MoReS and using them in PHREEQC calculations. However, it still overestimates the CO_2 solubility. The code is fully flexible due to the scripting interface. MoReS is a fully interactive simulator which allows visualisation of the results during time-stepping, and any input data, except the grid dimensions, can be changed after reservoir initialisation. It also has an advanced pre and post processor. The main disadvantage of the code is its availability; it is an in-house simulator for the exclusive use of Shell.

The main advantages of GEM are its ability to simulate complex three dimensional models, multiphase, multicomponent flow and the advanced pre and post processors. The major disadvantage is the necessity to input initial brine composition including the H^+ and the trace components such as Al^{3+} which are not usually included in the brine analysis. An external geochemical code is needed to obtain the brine speciation. The mineral reactions are only modelled by kinetics approach and the code has no kinetic database. Other disadvantages are the inflexible internal database, the lack of Pitzer activity model and the need for tedious numerical tuning. Basis switching is also not possible.

The advantages of TOUGHREACT compared to GEM are the ability to model mineral reactions either by equilibrium or kinetics approach, run batch models, the cost and more widespread use for geochemical modelling than GEM. It has a flexible database and a utility for basis switching. The necessity to input initial brine and lack of kinetics database is also valid for TOUGHREACT. It can only model three components: water, salt and CO_2. Hence it can only be used for aquifer modelling. It has a less accurate CO_2 solubility model. Its major limitation is the lack of a pre and post processing. The PetraSim pre-processor can be purchased separately, but it is not advanced as the GEM pre-processor Builder. For a detailed three dimensional model the code needs to be compiled by a FORTRAN compiler.

Table 3.1 How PHREEQC, GEM, TOUGHREACT and MoReS meets the criteria for code selection

Criteria	PHREEQC	GEM	TOUGHREACT	MoReS
Equilibrium approach	●●●	●	●●	●●●
Kinetics approach	●●●	●	●●	●●●
Activity model	●●	●	●	●●
Thermodynamic database	●●●	●	●●	●●●
Kinetics database	●			●
CO_2 solubility model		●●	●	●
Batch modelling	●●		●	●●
Reactive transport	●	●●●	●●	●●●
Flow mechanism	●●	●	●●	●●
Multiphase flow		●	●	●
Multicomponent flow		●●	●	●●
Handling heterogeneity		●●	●	●●
Computational efficiency	●	●●	●	●●●
Pre and post processor		●●	●	●●
Code availability	●●●	●●	●●	●
Code documentation	●	●	●	●
Code support	●●	●●●	●	●●●
Code validation	●●	●	●●	●

Table 3.2 Criteria legend

	Equilibrium approach
●	Compute equilibrium calculations only for aqueous species
●●	Compute equilibrium calculations for aqueous species and minerals
●●●	Both of the above and compute flash speciation calculations
	Kinetics approach
●	Compute kinetic calculations
●●	Compute kinetic calculations with different rate for different mechanism
●●●	Flexible kinetics modelling
	Activity model
●	Pitzer model is not implemented
●●	Pitzer model is implemented
	Thermodynamic database
●	Inflexible, inaccessible internal database
●●	Flexible database
●●●	Various flexible databases
	Kinetics database
●	Kinetics database for few minerals
	CO_2 solubility model
●	CO_2 solubility model
●●	More accurate CO_2 solubility model

Table 3.2 Contiued

	Batch modelling
●	Batch modelling with initial data requirement
●●	Batch modelling
	Reactive transport
●	1D limited reactive transport
●●	3D reactive transport
●●●	Complex 3D reactive transport
	Flow mechanism
●	Advection only for aqueous phase
●●	Advection and diffusion for aqueous phase
	Multiphase flow
●	Simulate multiphase flow
	Multicomponent flow
●	Water, NaCl and CO_2
●●	Water, NaCl, hydrocarbons, CO_2 and user input components
	Handling heterogeneity
●	Needs to be compiled
●●	Geological models can be imported, easier grid generation
	Computational efficiency
●	Slower
●●	Intermediate
●●●	Faster

Table 3.2 Continued

	Pre and post processor
●	Limited
●●	Advanced
	Code availability
●	In-house code
●●	Research code (not free) or commercial
●●●	Research code, freeware
	Code documentation
●	Manual with sample datasets
	Code support
●	Limited author support
●●	Email author support
●●●	Commercial support
	Code validation (for geochemical calculations)
●	New code
●●	Extensively tested code
●●●	Established code

3.7 Conclusions

The critical parameters for geochemical modelling of CO_2 storage are divided into two categories: reaction specific parameters and site specific parameters. Reaction specific parameters are equilibrium constants, kinetic rate constants, activation energies and solubility models. Site specific parameters are temperature, pressure, composition of brine, composition of rock, specific surface area and redox state.

In the case of reactive transport modelling, in addition to the parameters above, porosity, permeability, flow rate, equation of state, pressure and temperature gradients and diffusion coefficients indirectly affect the extent of the geochemical reactions.

The codes used in this study are not ideal; nevertheless, they are the most commonly used codes. To date a code that meets all the required criteria has not been identified.

As discussed, major limitations of geochemical modelling include the high uncertainty about input parameters and lack of knowledge in coupled processes. Even if the aforementioned issues are resolved and we have an ideal code, the predictions of the models are influenced very much by the way the modeller conceptualizes the model. Furthermore, due to the complexity of the models and the time scales involved, often it is not possible to validate the models thoroughly.

3.8 References

Anbeek, C., 1992, The dependence of dissolution rates on grain size for some fresh and weathered feldspars, Geochimica et Cosmochimica Acta, 56(11): 3957-3970.

Anderson, G., 2005, Thermodynamics of Natural Systems, Cambridge University Press.

Bethke, C., 1996, Geochemical Reaction Modeling: Concepts and Applications, Oxford University Press, USA.

Brunauer, S., Emmett, P.H. and Teller, E., 1938, Adsorption of gases in multimolecular layers, Journal of the American Chemical Society, 60(2): 309-319.

Chiquet, P., Broseta, D.F. and Thibeau, S., 2005, Capillary alteration of shaly caprocks by carbon dioxide, SPE Europec/EAGE Annual Conference, Society of Petroleum Engineers, Madrid, Spain, SPE 94183-MS.

Davies, C., 1962, Ion Association, Butterworths, London, UK.

Garcia, J.E., 2001, Density of aqueous solutions of CO_2, Lawrence Berkeley National Laboratory Report, LBNL-49023.

Garrels, R. and Christ, C., 1965, Solutions, Minerals, and Equilibria, Freeman, Cooper and Co.

Gautier, J.-M., Oelkers, E.H. and Schott, J., 2001, Are quartz dissolution rates proportional to B.E.T. surface areas?, Geochimica et Cosmochimica Acta, 65(7): 1059-1070.

Helgeson, H.C., 1969, Thermodynamics of hydrothermal systems at elevated temperatures and pressures, Am J Sci, 267: 729-804.

Kervevan, C., Lanini, S., Audigane P., 2007, Chemistry-transport coupling: numerical experiments on the influence of the coupling algorithm on the results accuracy, RP-54907-FR, BRGM.

Kump, L., Brantley, S. and Arthur, M., 2000, Chemical weathering, atmospheric CO_2, and climate, Annual Review of Earth and Planetary Sciences, 28(1): 611-667.

Lasaga, A., 1981, Transition state theory, Reviews in Mineralogy and Geochemistry, 8(1): 135.

Lasaga, A., 1984, Chemical kinetics of water-rock interactions, Journal of Geophysical Research, 89(B6): 4009-4025.

Lewis, G. and Randall, M., 1961, Thermodynamics, revised by KS Pitzer and L. Brewer, Mc-GrawHill, New York.

Lichtner, P.C., 1996, Continuum formulation of multicomponent-multiphase reactive transport, Reviews in Mineralogy and Geochemistry, 34(1): 1-81.

MacQuarrie, K.T.B. and Mayer, K.U., 2005, Reactive transport modeling in fractured rock: A state-of-the-science review, Earth-Science Reviews, 72(3-4): 189.

Nghiem, L., Sammon, P., Grabenstetter, J., Ohkuma, H., 2004, Modeling CO_2 storage in aquifers with a fully-coupled geochemical EOS, SPE 89474.

Oelkers, E.H., 1996, Physical and chemical properties of rocks and fluids for chemical mass transport calculations, Reviews in Mineralogy and Geochemistry, 34(1): 131-191.

Oelkers, E.H., Benezeth, P. and Pokrovski, G.S., 2009, Thermodynamic databases for water-rock interaction, Reviews in Mineralogy and Geochemistry, 70(1): 1-46.

Panda, M. and Lake, L., 1995, A physical model of cementation and its effects on single-phase permeability, AAPG Bulletin-American Association of Petroleum Geologists, 79(3): 431-443.

Parkhurst, D.L. and Appelo, C.A.J., 1999, User's Guide to PHREEQC (Version 2)-A Computer Program for Speciation, Batch-Reaction, One-dimensional Transport and Inverse Geochemical Calculations.

Pitzer, K.S., 1973, Thermodynamics of electrolytes: I. Theoretical basis and general equations, J. Phys. Chem., 77(2): 268-277.

Reardon, E.J. and Langmuir, D., 1976, Activity coefficients of $MgCO_3$ and $CaSO_4$ ion pairs as a function of ionic strength, Geochimica et Cosmochimica Acta, 40(5): 549-554

Saripalli, K., Meyer, P., Bacon, D. and Freedman, V., 2001, Changes in hydrologic properties of aquifer media due to chemical reactions: a review, Critical Reviews in Environmental Science and Technology, 31(4): 311-349.

Schnoor, J., 1990, Kinetics of chemical weathering: a comparison of laboratory and field weathering rates, Aquatic Chemical Kinetics: Reaction Rates of Processes in Natural Waters, Environmental Science and Technology Series, John Wiley & Sons, New York.

Steefel, C.I. and Lasaga, A.C., 1994, A coupled model for transport of multiple chemical species and kinetic precipitation/dissolution reactions with application to reactive flow in single phase hydrothermal systems, Am J Sci, 294(5): 529-592.

Steefel, C.I. and Maher, K., 2009, Fluid-rock interaction: A reactive transport approach, Reviews in Mineralogy and Geochemistry, 70(1): 485-532.

Steefel, C.I., DePaolo, Donald J., Lichtner, Peter C., 2005, Reactive transport modeling: An essential tool and a new research approach for the earth sciences, Earth and Planetary Science Letters, 240(3-4): 539.

Stumm, W. and Wollast, R., 1990, Kinetics of the surface-controlled dissolution of oxide minerals, Rev. Geophysics, 28: 53–69.

Velbel, M.A., 1993, Constancy of silicate-mineral weathering-rate ratios between natural and experimental weathering: implications for hydrologic control of differences in absolute rates, Chemical Geology, 105(1-3): 89-99.

Wei, L. and Saaf, F., 2009, Estimate CO_2 storage capacity of the Johansen formation: numerical investigations beyond the benchmarking exercise, Computational Geosciences, 13(4): 451-467.

Wei, L., 2010, Rigorous water chemistry modelling in reservoir simulations for waterflood and EOR studies, Abu Dhabi International Petroleum Exhibition and Conference, SPE 138037.

Xu, T., Samper, J., Ayora, C., Manzano, M. and Custodio, E., 1999, Modeling of non-isothermal multi-component reactive transport in field scale porous media flow systems, Journal of Hydrology, 214(1-4): 144.

Xu, T., Sonnenthal, E., Spycher, N. and Pruess, K., 2006, TOUGHREACT--A simulation program for non-isothermal multiphase reactive geochemical transport in variably saturated geologic media: Applications to geothermal injectivity and CO_2 geological sequestration, Computers & Geosciences, 32(2): 145.

Yeh, G. and Tripathi, V., 1989, A critical evaluation of recent developments in hydrogeochemical transport models of reactive multichemical components, Water Resources Research, 25(1): 93-108.

Zhu, C. and Anderson, G., 2002, Environmental Applications of Geochemical Modeling Cambridge University Press Cambridge, New York.

CHAPTER 4

CO_2 SOLUBILITY IN BRINE

An accurate calculation of CO_2 solubility in brine is essential not only for the storage capacity estimation of the aquifer, but also for studies of the fluid-rock interactions as the dissolved CO_2 acidifies the brine. Therefore we need to integrate CO_2 solubility models in numerical codes.

The solubility of the CO_2 depends on pressure, temperature and salinity of solution. CO_2 solubility decreases with increasing temperature over the range of temperatures applicable to CO_2 storage. CO_2 solubility decreases with increasing salinity and decreasing pressure. Therefore, the solubility models should be valid over the range of temperature, pressure and salinity conditions of the storage reservoir. Several experimental data on CO_2 solubility have been published. However, the data are sparse over the temperature and pressure ranges of interest and most of the P-T space over 200 bars has no data. Hence the CO_2 solubility models are not only needed to interpolate the experimental data, but also to predict the CO_2 solubility over the entire temperature, pressure and salinity ranges. The review and evaluation of the published data can be found in Duan and Sun (2003) and Akinfiev and Diamond (2010).

In this chapter the theoretical basis for identifying CO_2 solubility in brine is established and a description of the several CO_2 solubility models is given. The fugacity calculations with different equations of state are evaluated, and the CO_2 solubility calculated by different models is compared, and their applicability to CO_2 storage is discussed.

4.1 CO_2 -H_2O System

Un-ionized dissolved CO_2 may be present in two forms: in the hydrated form, as the true carbonic acid $H_2CO_3^\circ$ and in the non-hydrated form CO_2°. The sum of these two forms gives the total dissolved CO_2, which is called aqueous CO_2, $CO_2(aq)$.

The hydration reaction can be expressed as

$$CO_2^\circ + H_2O = H_2CO_3^\circ \tag{4.1}$$

This reaction lies far to the left, the majority of the un-ionized CO_2 is in the form of CO_2°, and the total dissolved CO_2 can be approximated to CO_2°.

The carbonic acid dissociates and forms bicarbonate and carbonate ions:

$$H_2CO_3^\circ = HCO_3^- + H^+ \tag{4.2}$$

$$HCO_3^- = CO_3^{2-} + H^+ \tag{4.3}$$

From this series of reactions it can be seen that dissolved CO_2 acidifies the brine, and the acidification, which is important for fluid - rock interactions depends on the CO_2 solubility.

As the dissolution rate of CO_2 in water is fast, it can be expressed by the chemical equilibrium reaction

$$CO_2(g) = CO_2(aq) \tag{4.4}$$

where $CO_2(g)$ and $CO_2(aq)$ are the CO_2 in the gas and in the aqueous phases respectively.

The thermodynamic equilibrium for the reaction (4.4) is defined as the equality of the chemical potentials in the coexisting phases:

$$\mu_{CO_2(g)} = \mu_{CO_2(aq)} \tag{4.5}$$

The chemical potential of CO_2 in the gas phase, following the analogy of activity, can be expressed in terms of fugacity

$$\mu_{CO_2(g)} = \mu^{\circ}_{CO_2(g)} + RT \ln f_{CO_2(g)} \tag{4.6}$$

where f_{CO_2} is the fugacity of CO_2 in the gas phase and $\mu^{\circ}_{CO_2(g)}$ is the standard state chemical potential of CO_2 (ideal gas at 1 bar).

The condition for thermodynamic equilibrium is the equality of the fugacities of the components in the gas and aqueous phases.

The fugacity of CO_2 in the gas phase is defined as

$$f_{CO_2(g)} = \Phi P_{CO_2} \tag{4.7}$$

where $f_{CO_2(g)}$ is the fugacity of CO_2 in the gas phase, P_{CO_2} is the partial pressure of CO_2 and Φ is the fugacity coefficient. The fugacity coefficient depends on temperature and pressure.

The fugacity of CO_2 in the aqueous phase is equal to its activity:

$$f_{CO_2(aq)} = a_{CO_2(aq)} = m_{CO_2}\gamma_{CO_2} \tag{4.8}$$

and the chemical potential of CO_2(aq) is

$$\mu_{CO_2(aq)} = \mu^{\circ}_{CO_2(aq)} + RT \ln a_{CO_2(aq)} = \mu^{\circ}_{CO_2(aq)} + RT \ln(m_{CO_2}\gamma_{CO_2}) \tag{4.9}$$

where $f_{CO_2(aq)}$, $a_{CO_2(aq)}$, m_{CO_2}, γ_{CO_2} and $\mu_{CO_2(aq)}$ are, respectively the fugacity, activity, molality, activity coefficient and chemical potential of CO_2 in aqueous phase. $\mu^{\circ}_{CO_2(aq)}$

is the standard state chemical potential of CO_2 in the aqueous phase (ideal solution of 1 molality).

The thermodynamic equilibrium constant for equation (4.4) can be written as

$$\ln K = -\frac{\mu^{\circ}_{CO_2(aq)} - \mu_{CO_2(g)}}{RT} = \ln \frac{m_{CO_2}\gamma_{CO_2}}{P\Phi y_{CO_2}} \tag{4.10}$$

where y_{CO_2} is the mole fraction of CO_2 in the aqueous phase.

The solubility of gases is often expressed in terms of Henry's constant (H)[5]. The equation (4.8) can be written in terms of H as

$$f_{CO_2(aq)} = y_{CO_2} H \tag{4.11}$$

From equations (4.7) and (4.11) the mole fraction of CO_2 in the aqueous phase is derived:

$$y_{CO_2} = \frac{P_{CO_2}\Phi}{H} \tag{4.12}$$

Hence the solubility of CO_2 can be obtained by calculating the fugacity coefficient, provided that Henry's constant is known.

The fugacity coefficient can be calculated by

$$\ln \Phi_i = \int_0^P \left(\frac{\bar{V}}{RT} - \frac{1}{P} \right) dP = \int_0^P \frac{(Z-1)}{P} dP \tag{4.13}$$

where Z is the compressibility factor. This equation is solved by an equation of state (EOS). An EOS relates temperature, pressure, volume and mass of the system. At temperature ranges of CO_2 storage (<200°C), infinite H_2O dilution in the vapour phase

---

[5] The relation between K and H is defined by (Prausnitz et al., 1986) $H = \frac{N_w}{K}$, $H = \Phi^{\infty} P$ where $N_w = \frac{1000}{M_w} = 55.51\,\text{mole}$, Φ^{∞} is the fugacity coefficient at infinite dilution and M_w is the molar mass of water.

can be assumed and the fugacity of CO_2 can be approximated by the fugacity of pure CO_2. Hence an EOS for pure CO_2 can be used for the calculation of fugacity.

The cubic EOS, such as that of Redlich and Kwong (1948) and Peng and Robinson (1976), the Helmholtz free energy based EOS of Span and Wagner (1996), and the semi empirical virial EOS of Duan et al. (1992a; 1992b) can be used to calculate the fugacity coefficients of CO_2. Cubic equations of state are widely used because of their simplicity to implement in numerical codes and acceptable accuracy. On the other hand, Span and Wagner EOS and Duan and Sun EOS are accurate but difficult to apply because of their complex form. Fugacity coefficients calculated by Duan and Sun EOS are shown in Figure 4.1. It can be seen that the fugacity coefficient ranges between 0.28 and 0.84, which leads to CO_2 fugacity of 63 to 283 bar over the pressure range of 100-500 bar.

Dissolved salts have an influence on the phase equilibrium by decreasing the solubility of CO_2. This effect is called salting-out as the vapour pressure increases because of the decreased solubility of gas. In addition CO_2 solubility is a function of pressure. CO_2 solubility with respect to salinity and pressure at 50°C is given in Figure 4.2. As CO_2 solubility is a strong function of both salinity and pressure, these two effects should be integrated in CO_2 solubility modelling.

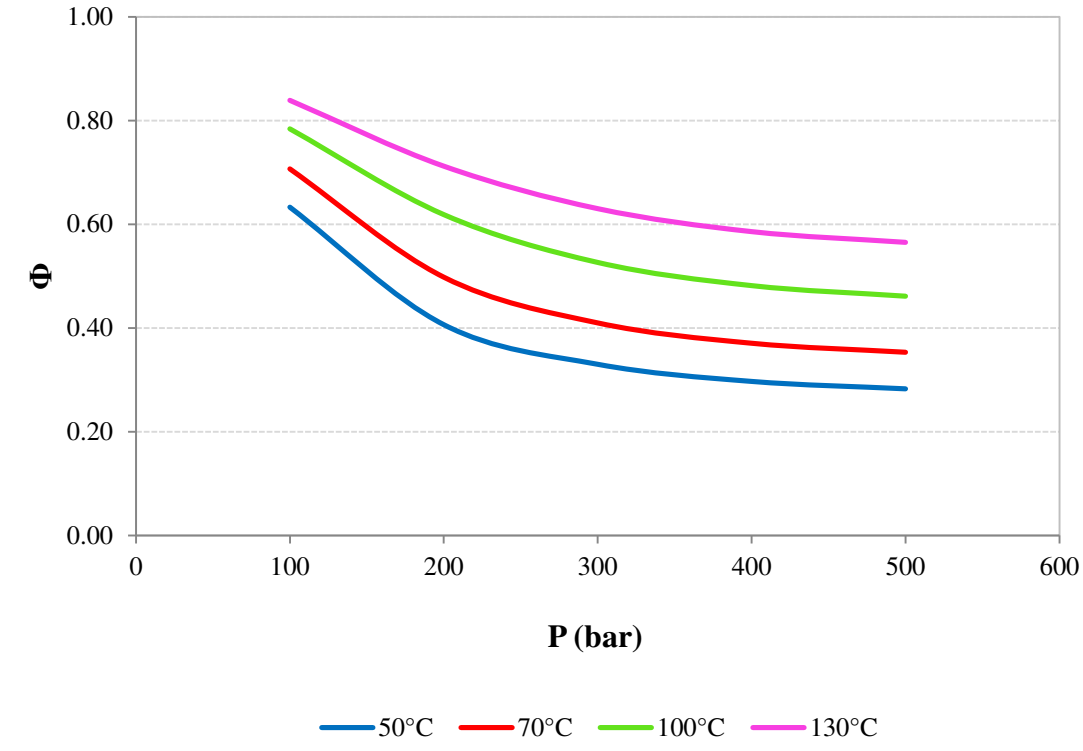

Figure 4.1 Fugacity coefficients of CO_2 vs. pressure calculated by Duan and Sun EOS

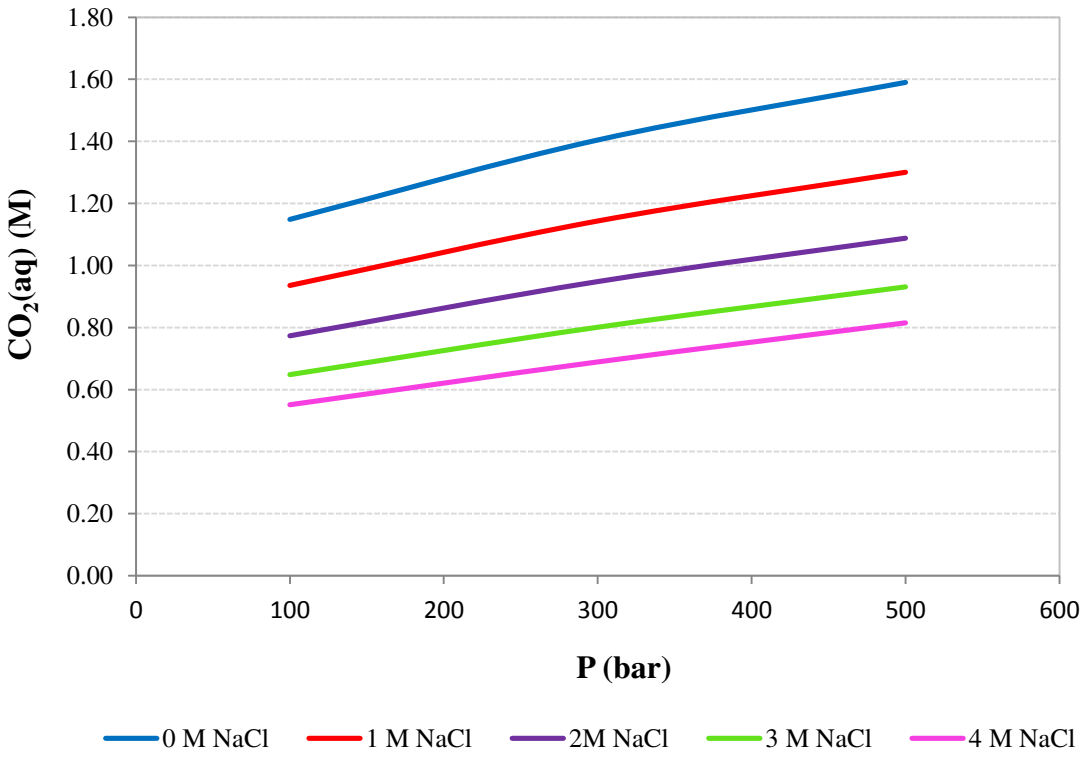

Figure 4.2 Change of CO_2 solubility with salinity and pressure at 50°C (Calculated by Duan and Sun model)

Although several EOS were developed for CO_2 - H_2O systems, e.g. Spycher and Reed (1988), Duan et al. (1992a; 1992b), Diamond and Akinfiev (2003), today a single EOS that can predict the phase behaviour of CO_2 and saline solution mixtures does not exist. There are, however, CO_2 solubility models that couple different equations to predict the CO_2 solubility in brines. These models are mixed models that use EOS for the gas phase, and activity models or Henry's constants for the aqueous phase. The solubility models are based generally on the equivalent NaCl approximation. If the brine has relatively low salinity and the main salt is NaCl, the approximation does not induce high errors. In the other cases, the error can be significant. Kervévan et al. (2005) quantified this error as being between 5% and 20% for the majority of the brines using SCALE 2000.

The next section will review how different models estimate the CO_2 solubility over the range of temperatures, pressures and salinities that are relevant to CO_2 storage.

4.2 CO_2 Solubility Models in Brine

Several researchers proposed solubility models of CO_2 in aqueous solutions such as Li and Nghiem (1986), Enick and Klara (1990), Pruess and Garcia (2002), Duan and Sun (2003), Xu et al. (2004), Portier and Rochelle (2005), Spycher and Pruess (2005; 2010), and Akinfiev and Diamond (2010). The temperature, pressure and salinity range and the EOS used for the calculation of the CO_2 fugacity are given in Table 4.1. As the Li and Nghiem model is not accurate (Duan and Sun, 2003) and Enick and Klara's model is approximate, these two models are not described. The Pruess and Garcia model was the previous solubility model implemented by TOUGH2, and was substituted by the Spycher and Pruess model. Hence the Pruess and Garcia model also is not described either.

Table 4.1 Application range and EOS used by the solubility models

Solubility Model	Temperature (°C)	Pressure (bar)	Salinity (up to) (M)	EOS
Akinfiev and Diamond	22 - 100	1 - 1000	any	Span and Wagner
Duan and Sun	0 - 260	0 - 2000	4.5	Duan et al.
Enick and Klara	25 - 250	30 - 850	5	Peng - Robinson
GEM	up to 150	up to 600	5.13	Peng - Robinson or Soave - Redlich-Kwong
Li and Nghiem	up to 200	up to 1000	4	Peng - Robinson
Portier and Rochelle	up to 300	1 - 300	3	Peng - Robinson
Pruess and Garcia	25 - 350	0 - 1000	5	Spycher and Reed
Spycher and Pruess (2003)	12 - 100	1 - 600	6	Modified Redlich - Kwong
Spycher and Pruess (2010)	12 - 300	1 - 600	6	Modified Redlich - Kwong
TOUGHREACT	50 - 350	1 - 500	6	Spycher and Reed

4.2.1. Duan and Sun model

Duan and Sun (2003) developed a model for CO_2 solubility in brines in a temperature range of 273-533K, pressures up to 2000 bar and salinity up to 4.3 molal. They compared the model predictions with the published experimental data and CO_2 solubility is within the accuracy of experiments (<7% in CO_2 solubility). The model also can be used in other aqueous electrolyte solutions such as aqueous $CaCl_2$, MgCl and seawater without needing experimental data for these solutions. The model is based

on the equality of the chemical potentials in aqueous and vapour phases. The chemical potential of CO_2 in the vapour phase is calculated by the EOS developed by Duan et al. (1992a; 1992b) and the chemical potential of CO_2 in the aqueous phase is calculated by the Pitzer model (Pitzer, 1973).

The EOS for CO_2 is given by

$$\begin{aligned} Z = \frac{P_r V_r}{T_r} &= 1 + \frac{a_1 + a_2 / T_r^2 + a_3 / T_r^3}{V_r} \\ &+ \frac{a_4 + a_5 / T_r^2 + a_6 / T_r^3}{V_r^2} + \frac{a_7 + a_8 / T_r^2 + a_9 / T_r^3}{V_r^4} \\ &+ \frac{a_{10} + a_{11} / T_r^2 + a_{12} / T_r^3}{V_r^5} \\ &+ \frac{a_{13}}{T_r^3 V_r^2}\left(a_{14} + \frac{a_{15}}{V_r^2} \right) \exp\left(-\frac{a_{15}}{V_r^2} \right) \end{aligned} \tag{4.14}$$

where P_r, T_r, V_r are the reduced pressure, reduced temperature and reduced volume defined by $P_r = \frac{P}{P_c}$, $T_r = \frac{T}{T_c}$, $V_r = \frac{VP_c}{RT_c}$, and where P_c and T_c are the critical pressure and temperature respectively. The parameters a_1 - a_{15} are given in the Appendix A.

The fugacity coefficient of CO_2 is calculated from:

$$\begin{aligned} \ln \Phi(T,P) = Z - 1 - \ln Z &+ \frac{a_1 + a_2 / T_r^2 + a_3 / T_r^3}{V_r} \\ &+ \frac{a_4 + a_5 / T_r^2 + a_6 / T_r^3}{2V_r^2} + \frac{a_7 + a_8 / T_r^2 + a_9 / T_r^3}{4V_r^4} \\ &+ \frac{a_{10} + a_{11} / T_r^2 + a_{12} / T_r^3}{5V_r^5} + \frac{a_{13}}{2T_r^3 a_{15}} \\ &\times \left[a_{14} + 1 - \left(a_{14} + 1 + \frac{a_{15}}{V_r^2} \right) \times \exp\left(-\frac{a_{15}}{V_r^2} \right) \right] \end{aligned} \tag{4.15}$$

The molality of CO_2 is calculated from:

$$\begin{aligned}\ln m_{CO_2} = &\ln\left(\frac{P-P_{H_2O}}{P}\Phi_{CO_2}P\right)-\frac{\mu^{l0}_{CO_2}}{RT}\\ &-2\lambda_{CO_2-Na}\left(m_{Na}+m_K+2m_{Ca}+2m_{Mg}\right)\\ &-\zeta_{CO_2-Na-Cl}m_{Cl}\left(m_{Na}+m_K+m_{Ca}+m_{Mg}\right)+0.07m_{SO_4}\end{aligned} \tag{4.16}$$

where λ_{CO_2-Na}, $\zeta_{CO_2-Na-Cl}$ and $\frac{\mu^{l0}_{CO_2}}{RT}$ are the second and third order interaction parameters and the dimensionless standard chemical potential respectively. They are calculated from the following equation:

$$\begin{aligned}Par(T,P) = &c_1+c_2T+\frac{c_3}{T}+c_4T^2+\frac{c_5}{630-T}+c_6P+c_7P\ln T\\ &+\frac{c_8P}{T}+\frac{c_9P}{630-T}+\frac{c_{10}P^2}{\left(630-T\right)^2}+c_{11}T\ln P\end{aligned} \tag{4.17}$$

The constants c_1 - c_{11} are given in the Appendix A.

The pure water pressure is given by

$$P_{H_2O} = \frac{P_cT}{T_c}\left(1+b_1\left(-t\right)^{1.9}\right)+b_2t+b_3t^2+b_4t^3+b_5t^4 \tag{4.18}$$

where $t=\frac{T-T_c}{T_c}$. The constants b_1 - b_5 are given in the Appendix A.

Since this model uses a fifth order virial EOS to calculate the fugacity coefficients iteratively, it is computationally demanding for reservoir scale simulations, and so Duan et al. (2006) proposed a non iterative equation to calculate the fugacity coefficient:

$$\begin{aligned}\Phi_{CO_2} = &d_1+\left(d_2+d_3T+\frac{d_4}{T}+\frac{d_5}{T-150}\right)P+\left(d_6+d_7T+\frac{d_8}{T}\right)P^2\\ &+\left(d_9+d_{10}T+\frac{d_{11}}{T}\right)\ln P+\frac{d_{12}+d_{13}T}{P}+\frac{d_{14}}{T}+d_{15}T^2\end{aligned} \tag{4.19}$$

where T is in K. The constants d_1 - d_{15} were fitted to the Φ_{CO_2} calculated from equation (4.15).

4.2.2. Akinfiev and Diamond Model

Akinfiev and Diamond (2010) evaluated the experimental CO_2 solubility data and developed a semi-empirical thermodynamic model for aqueous CO_2-H_2O-NaCl solutions from -22 to 100°C and from 0.1 to 100MPa, and for any NaCl concentration. The model is an extension of the previous model (Diamond and Akinfiev, 2003) for CO_2-H_2O systems. The model predicts the solubilities with a precision of better than 1.6%.

The model is based on the Pitzer approach. The Pitzer et al. EOS (Pitzer et al., 1984) is incorporated in the model for the H_2O-NaCl subsystem without any modification and the Diamond and Akinfiev model (2003) for the CO_2-H_2O subsystem. The Diamond and Akinfiev model uses Span and Wagner EOS (1996) for pure CO_2 properties.

The following relation for the activity coefficient of CO_2 in pure water is obtained:

$$\begin{aligned}\ln \gamma_{CO_2}^{w} = &(-0.099085 + 0.48977\times10^{-3}T - 0.962628\times10^{-6}T^2)m_{CO_2} \\ &+(0.218384 - 1.024319\times10^{-3}T + 1.222992\times10^{-6}T^2)\left(m_{CO_2}\right)^2\end{aligned} \tag{4.20}$$

where $\gamma_{CO_2}^{w}$ and m_{CO_2} are the activity coefficient of CO_2 in pure water and the molality of CO_2, respectively, and T is in K.

The activity coefficient of CO_2 in a saline solution is given by

$$\begin{aligned}\ln \gamma_{CO_2} = &2m_{CO_2}\lambda_{11} + 3\left(m_{CO_2}\right)^2\tau_{111} + 2m_{NaCl}B_{12} + 3\left(m_{NaCl}\right)^2 C_{122} \\ &+6m_{CO_2}m_{NaCl}C_{112}\end{aligned} \tag{4.21}$$

where γ_{CO_2} is the activity coefficient of CO_2 in saline water, m_{NaCl} is the molality of NaCl in solution, λ, τ, B and C indicate short range interaction parameters where subscript 1 stands for CO_2 and 2 for salt.

λ_{11} and τ_{111} are dependent on temperature and calculated as follows:

$$\lambda_{11} = -0.0495425 + 0.244885\times10^{-3}T - 0.481314\times10^{-6}T^2 \quad (4.22)$$

$$\tau_{111} = 0.0727795 - 0.34141\times10^{-3}T + 0.407664\times10^{-6}T^2 \quad (4.23)$$

where T is in K.

A fitting function $F\left(T, m_{NaCl}, m_{CO_2}, I\right)$ was used to find the other Pitzer interaction parameters from experimental data and the following equations are derived:

$$B_{12} = a_1 + a_2\left(\frac{100}{T-228}\right) + a_6 g(2I^{0.5}) \quad (4.24)$$

$$C_{122} = a_4 + a_3\left(\frac{1000}{T}\right) \quad (4.25)$$

$$C_{112} = a_5 \quad (4.26)$$

where a_1 = 0.057123, a_2 = 0.026994, a_3 = 0.034096, a_4 = -0.002380, a_5 = -0.000576, a_6 = 0.045635, $g(x) = \left(\frac{2}{x^2}\right)\left[1-\left(1+x\right)\exp\left(-x\right)\right]$, $x = 2I^{0.5}$ and I is the ionic strength.

4.2.3. Portier and Rochelle model

Portier and Rochelle (2005) presented a model for the CO_2 - H_2O - NaCl system up to 300°C, between 1 to 300 bar and ionic strengths up to 3 molal. They model the experimental data generated under Sleipner conditions and compare the results with previous published experimental data. The phase equilibrium is calculated by equality of the fugacities in the aqueous and vapour phases. The gas fugacity is calculated by Peng and Robinson EOS (1976). The fugacity of water is calculated using its vapour pressure with the following expression (Dhima et al., 1988)

$$f_{H_2O}^{aq} = a_{H_2O} P_{H_2O}^{sat} \exp\left(\frac{\bar{V}_{H_2O}^{aq}}{RT}\left[P - P_{H_2O}^{sat}\right]\right) \quad (4.27)$$

The saturation pressure of water $P_{H_2O}^{sat}$ and the saturated molar volume of water in the aqueous phase $\bar{V}_{H_2O}^{aq}$ are calculated from the Saul and Wagner correlation (Saul and Wagner, 1987).

The activity of the water is calculated by the Helgeson (1969) expression

$$\ln a_{H_2O} = -0.03603 I \Theta_{NaCl} \tag{4.28}$$

where Θ_{NaCl} is the osmotic coefficient, as in Helgeson (1969).

The fugacity of the dissolved CO_2 is calculated by Henry's law with the Krichevsky and Kasarnovsky correction for high pressures (Krichevsky and Kasarnovsky, 1935):

$$f_{CO_2}^{aq} = m_{CO_2} \gamma_{CO_2} H_{CO_2}(T, P_{H_2O}^{sat}) \exp\left(\frac{\bar{V}_{H_2O}^{\infty}}{RT} \left[P - P_{H_2O}^{sat} \right] \right) \tag{4.29}$$

The salinity dependence of the activity coefficient of dissolved CO_2 is represented by the Helgeson correlation (1969)

$$\ln \gamma_{CO_2} = \sigma_{CO_2}(T) I \tag{4.30}$$

where $\sigma_{CO_2}(T)$ is the salting coefficient which was determined by using experimental data.

Combining the equations gives the CO_2 solubility in brine as

$$m_{CO_2} = \frac{\Phi_{CO_2} x_{CO_2} P}{\gamma_{CO_2} H_{CO_2}(T, P_{H_2O}^{sat}) \exp\left(\frac{\bar{V}_{H_2O}^{\infty}}{RT} \left[P - P_{H_2O}^{sat} \right] \right)} \tag{4.31}$$

4.2.4. Spycher and Pruess Model

Spycher and Pruess (2005) proposed a model for CO_2 and chloride brine mixtures between 12-100°C and up to 600 bar. The model calculates the mutual solubilities of CO_2 and H_2O using a model previously developed by Spycher et al. (2003), and is extended with an activity coefficient for aqueous CO_2 and a correction to the activity of

water to account for the effect of dissolved salts. The model uses a geochemical approach and equilibrium constants rather than Henry's constants.

The CO_2 mole fraction in the aqueous phase is expressed by

$$x_{CO_2} = \frac{\Phi_{CO_2}(1 - y_{H_2O})P_{tot}}{55.508\gamma_{CO_2}K^0_{CO_2}} \exp\left(-\frac{(P - P^0)\bar{V}_{CO_2}}{RT}\right) \tag{4.32}$$

and the water mole fraction in the CO_2 rich phase is expressed by

$$y_{H_2O} = \frac{K^0_{H_2O}a_{H_2O}}{\Phi_{H_2O}P_{tot}} \exp\left(\frac{(P - P^0)\bar{V}_{H_2O}}{RT}\right) \tag{4.33}$$

where K^0 is the thermodynamic equilibrium constant for each component for reactions $H_2O_{(l)} = H_2O_{(g)}$ and $CO_{2(aq)} = CO_{2(g)}$ at temperature T and reference pressure $P^0 = 1$ bar. Activity coefficients are in mole fraction. The water activity coefficient is assumed to be unity.

For the calculation of the activity coefficients, the authors compare various activity formulations, and they concluded that both Pitzer models adopted by Rumpf et al (1994) and Duan and Sun (2003) give similar accuracy. However, they favour the Duan and Sun formulation because it was fitted over a wider P-T range than Rumpf et al., and it is easier to implement.

The model calculates the fugacities with the modified version of Redlich - Kwong EOS which is tuned to the experimental data for pure CO_2.

The Redlich - Kwong EOS is expressed by

$$P = \left(\frac{RT}{V - b}\right) - \left(\frac{a}{T^{0.5}V(V + b)}\right) \tag{4.34}$$

where *a* and *b* are the parameters representing intermolecular attraction and repulsion respectively. *V* is the volume of the compressed gas at P and T. Spycher et al. (2003) modified the equation by setting

$$a = k_0 + k_1 T \tag{4.35}$$

and fitting k_0, k_1 and b to reference PVT data.

The fugacity coefficient of pure CO_2 can be calculated as

$$\begin{aligned} \ln \Phi = \ln\left(\frac{V}{V-b}\right) + \left(\frac{b}{V-b}\right) - \left(\frac{2a}{RT^{1.5}b}\right)\ln\left(\frac{V+b}{V}\right) \\ + \left(\frac{a}{RT^{1.5}b}\right)\left[\ln\left(\frac{V+b}{V}\right) - \left(\frac{b}{V-b}\right)\right] - \ln\left(\frac{PV}{RT}\right) \end{aligned} \tag{4.36}$$

ECLIPSE300 simulator with the CO2STORE option for CO_2 storage in aquifers uses the Spycher and Pruess model. TOUGH2 has a fluid property module, ECO2N, for mixtures of water, NaCl, and CO_2. The fluid flow part of TOUGHREACT uses this model, with the modification that instead of Redlich - Kwong EOS it uses the tabular EOS based on Altunin's correlation (Altunin, 1975).

Spycher and Pruess extended this model to higher temperatures (Spycher and Pruess, 2010). At temperatures above 100°C the assumption regarding water activity is no longer valid. In the extended version an activity model using Margules expressions is implemented, and binary interaction parameters are added to the EOS for temperatures above 109°C. The Duan and Sun activity coefficient expression is also re-parameterized for temperatures above 109°C. At temperatures between 99 and 109°C the results of both high temperature and low temperature calculations are blended to give a smooth transition.

4.2.5. GEM

GEM uses the modified Henry's constant to model CO_2 solubility. Henry's constants are corrected for pressure and salting-out effects.

Henry's constant at P and T is given by

$$\ln H = \ln H^{sat} + \frac{1}{RT}\int_{P_{H_2O}^{sat}}^{P} \bar{V}_{CO_2} dP \tag{4.37}$$

where H^{sat} is the Henry's constant at the water saturation pressure, and it is estimated by the Harvey's correlation (Harvey, 1996):

$$\ln H^{sat} = \ln P_{H_2O}^{sat} - \frac{9.4234}{T_{r,H_2O}} + 4.0087\frac{\left(1-T_{r,H_2O}\right)^{0.355}}{T_{r,H_2O}} + 10.3199\frac{\exp\left(1-T_{r,H_2O}\right)}{T_{r,H_2O}^{0.41}} \tag{4.38}$$

where $P_{H_2O}^{sat}$ is the saturation pressure of water in MPa at T(K), $T_{r,H_2O} = \frac{T}{T_{c,H_2O}}$ is the reduced temperature of water and T_{c,H_2O} is the critical temperature of water (K).

The partial molar volume of CO_2 in the aqueous phase, $\bar{V}_{CO_2}$ is estimated from the correlation of Garcia (2001):

$$\bar{V}_{CO_2} = 37.51 - 9.585\times10^{-2}T + 8.74\times10^{-4}T^2 - 5.044\times10^{-7}T^3 \tag{4.39}$$

where $\bar{V}_{CO_2}$ is in cm^3/mol and T is in °C.

The fugacity of CO_2 in the gas phase can be calculated by Peng-Robinson (default) or Soave-Redlich-Kwong EOS.

The effect of salinity is defined by

$$\ln\left(\frac{H_{salt}}{H}\right) = k_{salt}m_{salt} \tag{4.40}$$

where H_{salt} is the Henry's constant of CO_2 in brine, k_{salt} is the salting-out coefficient and m_{salt} is the molality of the dissolved salt.

k_{salt} is estimated from the correlation of Bakker (2003):

$$k_{salt} = 0.11572 - 6.0293\times10^{-4}T + 3.5817\times10^{-6}T^2 - 3.7772\times10^{-9}T^3 \tag{4.41}$$

where T is in °C.

4.2.6. TOUGHREACT

TOUGHREACT's solubility model is based on the law of mass action (Xu et al., 2004):

$$K\Phi P_{CO_2} = \gamma m_{CO_2} \tag{4.42}$$

where K is the equilibrium constant of the equilibrium reaction $CO_2(g) = CO_2(aq)$. Φ is the fugacity coefficient of CO_2 in the gas phase, P_{CO_2} is the partial pressure of CO_2, γ and m_{CO_2} are the activity coefficient of the aqueous CO_2 and molality of CO_2 respectively.

The pressure dependence of the thermodynamic equilibrium constants is not considered. The equilibrium constant at temperature T is obtained from

$$\log K = b_1 \ln T + b_2 + b_3 T + \frac{b_4}{T} + \frac{b_5}{T^2} \tag{4.43}$$

where T is in K.

The constants are obtained from the logK values at 0, 25, 60, 100, 150, 200, 250 and 300°C from the EQ3/6 geochemical database (Wolery, 1992): b_1 = 65.48, b_2 = -425.5, b_3 = -0.05301, b_4 = 24010, and b_5 = -1.22*10^6.

The model assumes ideal mixing between CO_2 and water and the fugacity coefficients are calculated from the Spycher and Reed correlation (1988):

$$\ln \Phi = \left(\frac{a}{T^2} + \frac{b}{T} + c \right) P + \left(\frac{d}{T^2} + \frac{e}{T} + f \right) \frac{P^2}{2} \tag{4.44}$$

where P is the total pressure in bar and T is in K; a, b, c, d, e, f are empirical constants. For 50-350°C and up to 500bars, they have the following values: a = 1430.97, b = 3.598, c = -2.27376*10^{-3}, d = 3.47644, e = -1.04247*10^{-2} and f = 8.46271*10^{-6}.

The activity coefficient is corrected for the salting-out effect by the Drummond's activity coefficient expression (Drummond, 1981):

$$\ln\gamma = \left(C + FT + \frac{G}{T}\right)I - \left(E + HI\right)\left(\frac{I}{I-1}\right) \tag{4.45}$$

where T is in K and I is the ionic strength.

The constants have the following values: C = -1.0312, F = 0.0012806, G = 255.9, E = 0.4445, H = -0.001606.

4.2.7. PHREEQC

The PHREEQC's approach for the calculation of solubility is similar to TOUGHREACT. There are two differences. PHREEQC assumes that CO_2 behaves like an ideal gas, hence $\gamma = 1$. Besides, the temperature dependence of the equilibrium constants are expressed by

$$\log K = a + bT + \frac{c}{T} + d\log T + \frac{e}{T^2} \tag{4.46}$$

where T is in K and a = -10.5, b = 0.0217, c = 2520, d = 0.791, e = 39.4

4.3 Evaluation of EOS for CO_2 Fugacity Coefficient Calculation

In this section five EOS are compared for CO_2 fugacity coefficient calculation at 50-130°C and 100-500 bar. Duan-Møller-Weare EOS (Duan et al., 1992b) and Span and Wagner EOS (Span and Wagner, 1996) are recognized as references because of their accuracy. Peng-Robinson EOS (Peng and Robinson, 1976) and Soave-Redlich-Kwong EOS (Soave, 1972) are two widely used cubic EOS. These two EOS are implemented in GEM. Spycher and Reed EOS (Spycher and Reed, 1988) is another commonly used EOS for fugacity calculations and is used by TOUGHREACT.

The comparison is shown in Figures 4.3 to 4.6. Duan-Møller-Weare EOS and Span and Wagner EOS give almost identical values. Peng and Robinson EOS is very close to these two with a maximum of 2.3% fugacity difference over the entire temperature and pressure range. Soave-Redlich-Kwong EOS deviates from Duan-Møller-Weare EOS significantly with the deviation increasing with increasing pressure over the entire temperature range; the fugacity can be overestimated as much as 32%. Therefore this

EOS is not suitable for fugacity calculations. Spycher and Reed EOS differs from Duan-Møller-Weare EOS as much as 13% for the temperatures under 100°C. Above 100°C, the discrepancy diminishes with increasing temperature, and the EOS can be used for fugacity calculations.

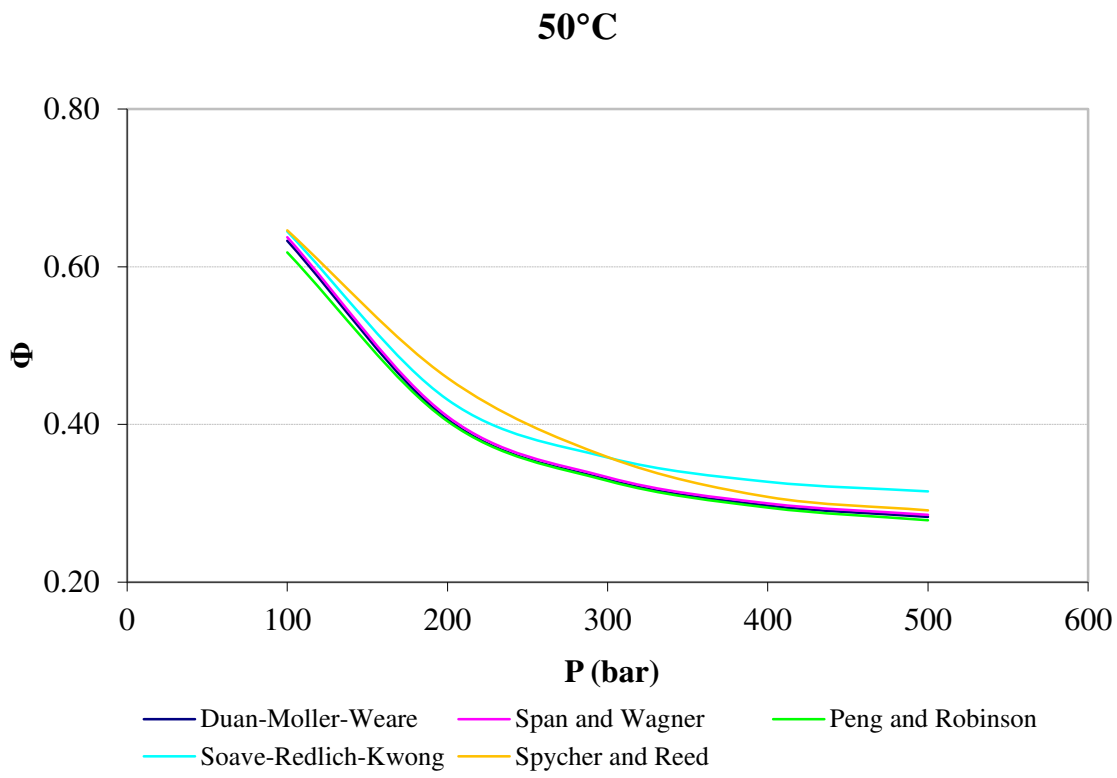

Figure 4.3 Fugacity coefficient comparison at 50°C

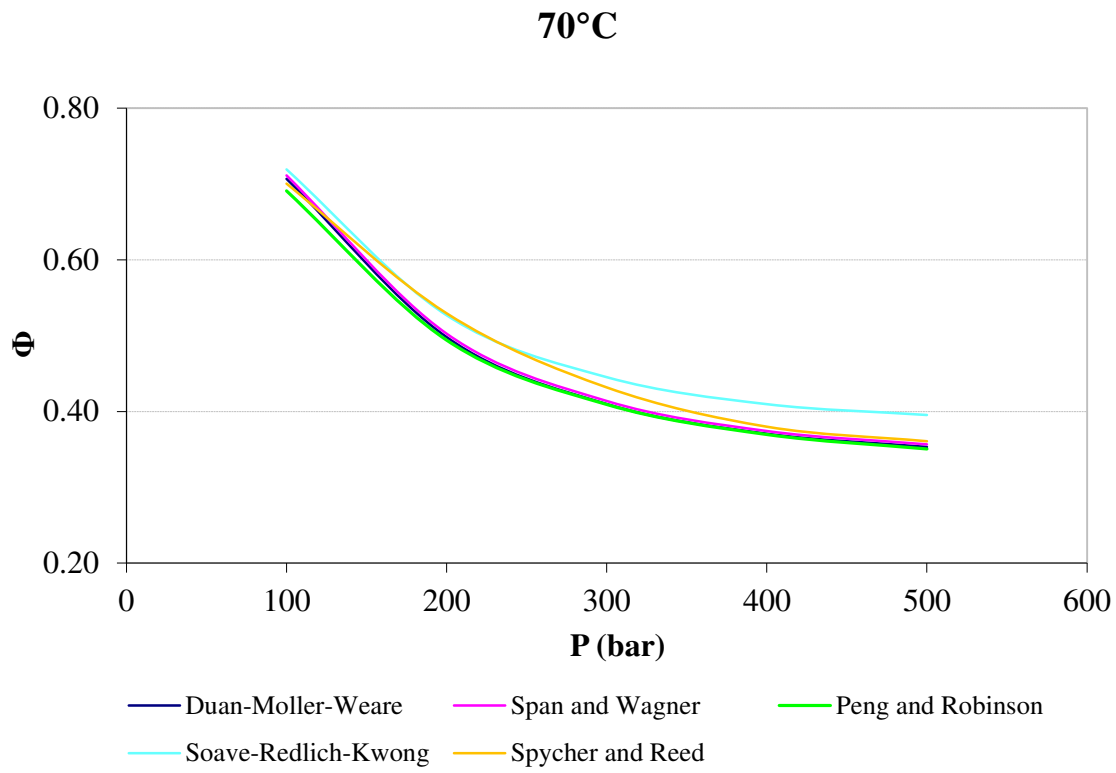

Figure 4.4 Fugacity coefficient comparison at 70°C

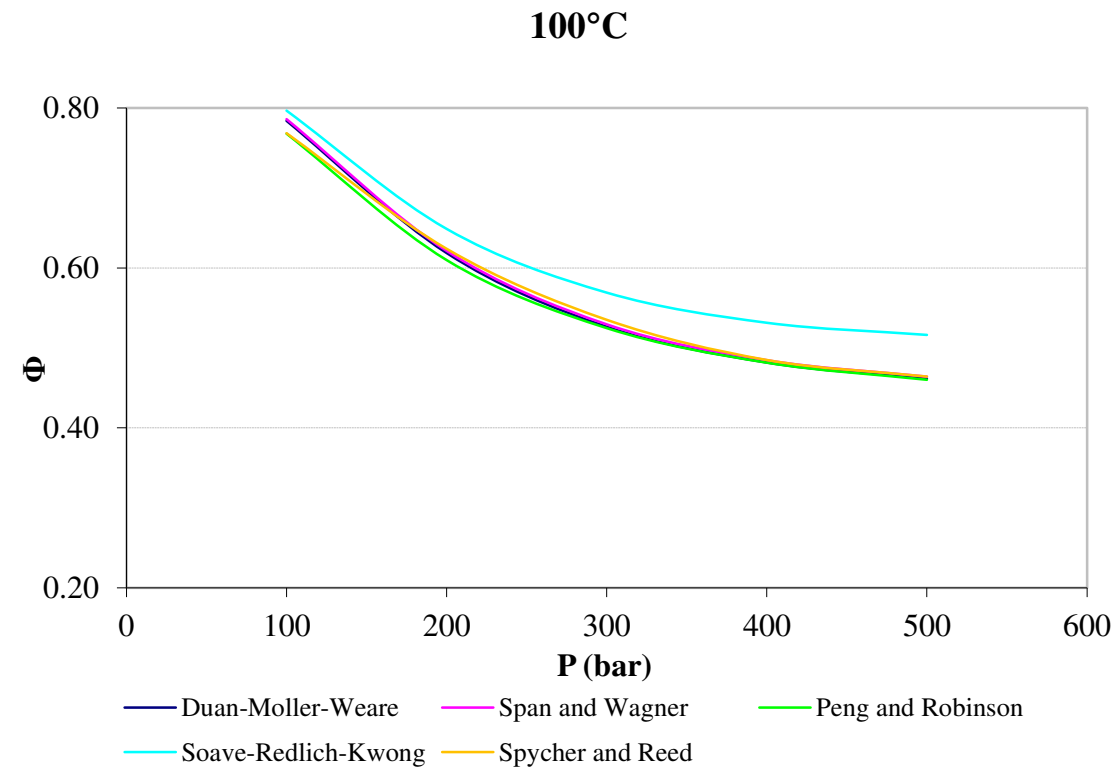

Figure 4.5 Fugacity coefficient comparison at 100°C

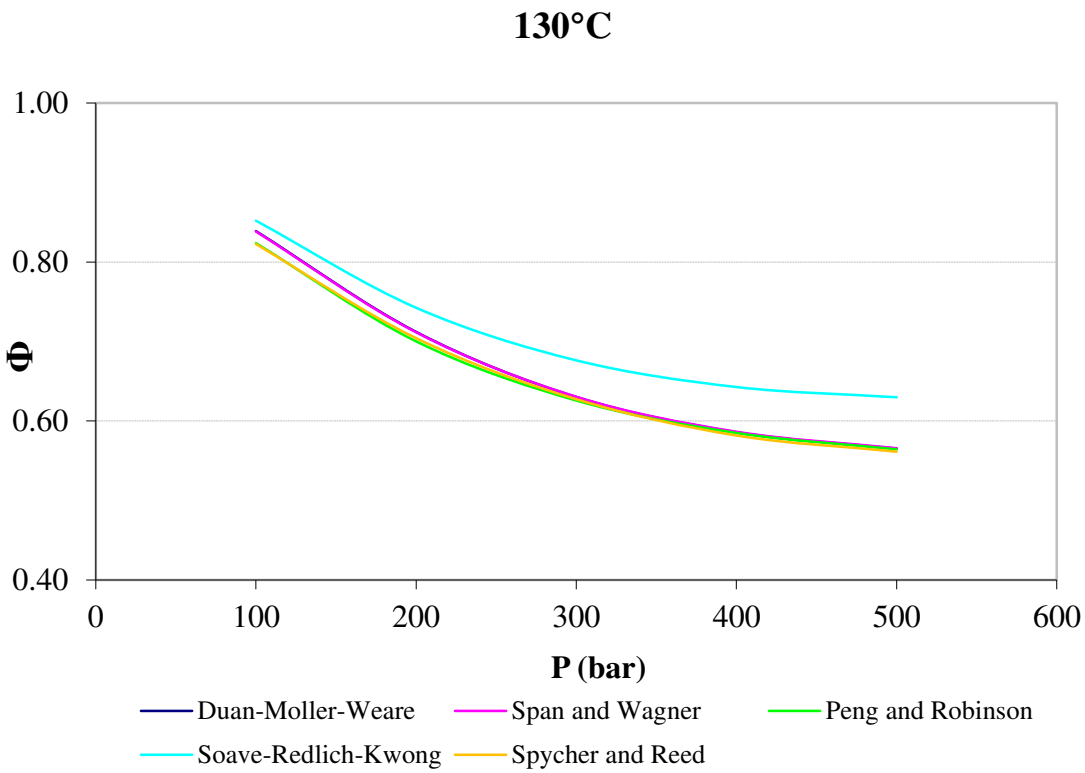

Figure 4.6 Fugacity coefficient comparison at 130°C

4.4 Comparison of CO_2 Solubility Models

CO_2 solubility predictions of the models reviewed in Section 4.2, except the Portier and Rochelle model, are compared over 50-100°C, 100-500 bar and 0-5M salinity. The Portier and Rochelle model is not compared because the aim of the comparison is to evaluate the CO_2 solubility predictions of the simulation codes. TOUGH2 and ECLIPSE use the Spycher and Pruess models as implemented by TOUGH2 ECO2N and ECLIPSE300 CO2STORE. The CO_2 solubilities at 50°C and 0-5M salinity are given in Figures 4.7 - 4.14. Since PHREEQC assumes ideal gas, the fugacity coefficients were calculated by Duan et al. (1992a; 1992b) fugacity model and inputted in the PHREEQC models. PHREEQC results with this fugacity correction are plotted. As may be seen from the figures, there are significant differences in the calculated solubilities and the differences increase with increasing salinity.

The two standalone models, Duan and Sun, and Diamond and Akinfiev are specifically designed for CO_2 solubility calculations, and they reproduce the experimental data

within the accuracy of experiments. Hence they are considered as the most accurate models among the models compared here. Over the entire range of comparison, the discrepancy between the two models is within 6%. For the comparison of the other models, the Duan and Sun model is chosen as a reference over the 0-4M salinity range. The Diamond and Akinfiev model is used for the 5M salinity range because the Duan and Sun model is only valid up to 4.5M.

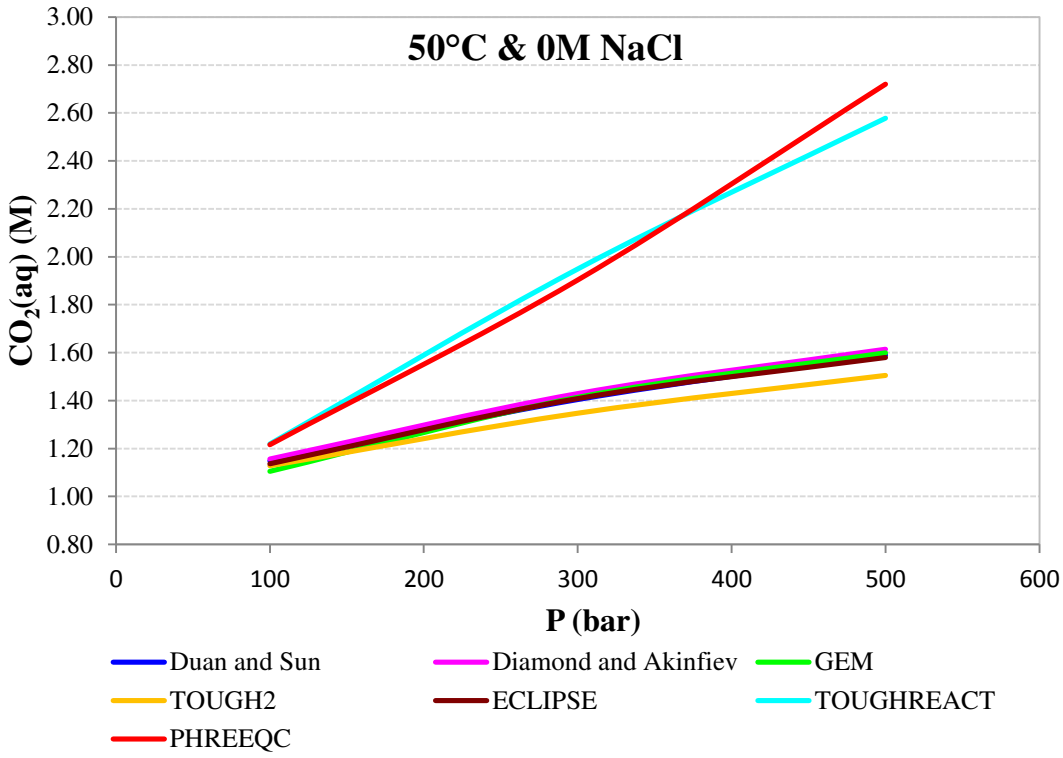

Figure 4.7 CO_2 solubility at 50°C and 0M salinity predicted by different models

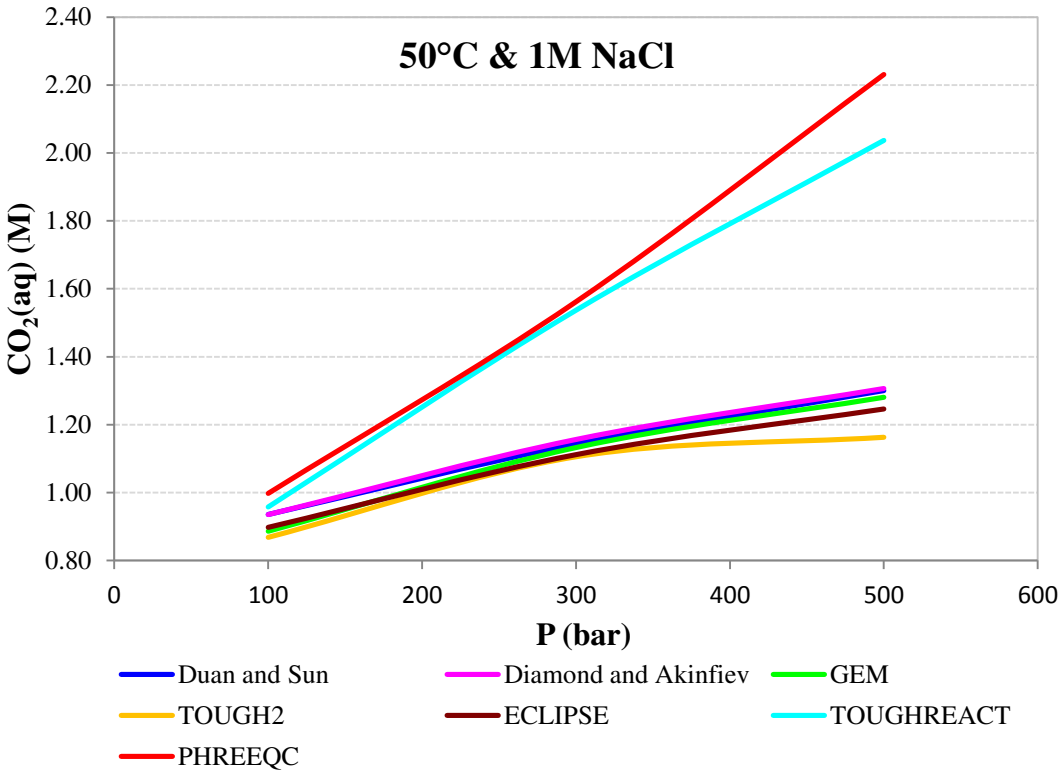

Figure 4.8 CO_2 solubility at 50°C and 1M salinity predicted by different models

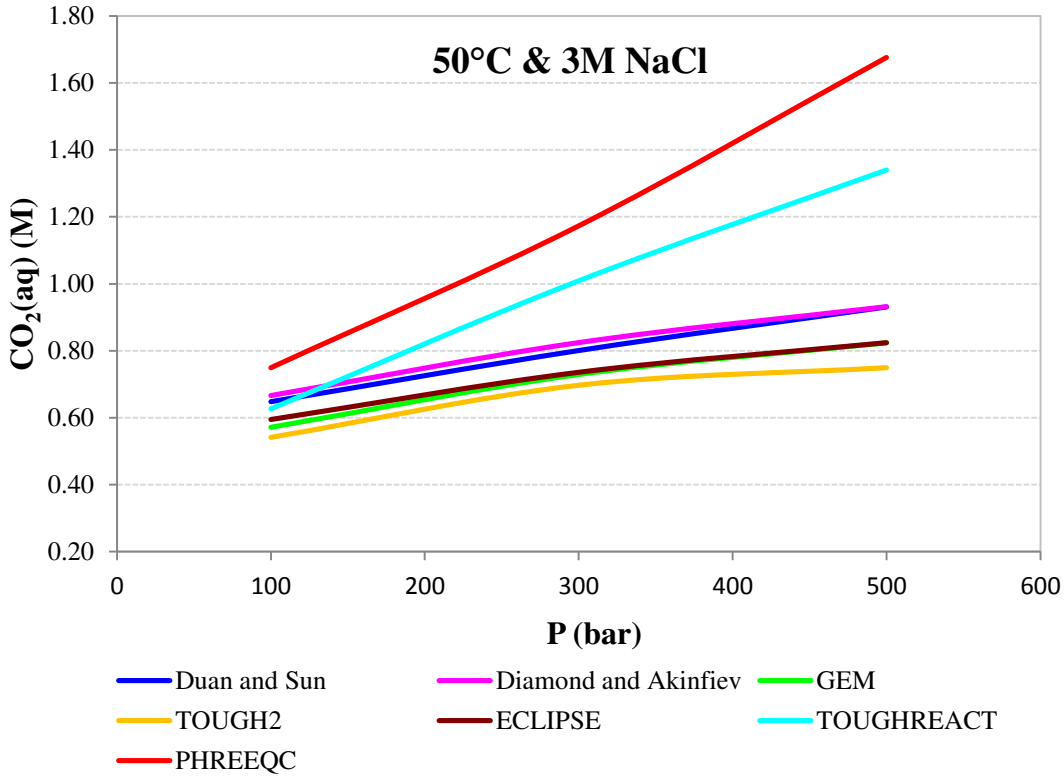

Figure 4.9 CO_2 solubility at 50°C and 3M salinity predicted by different models

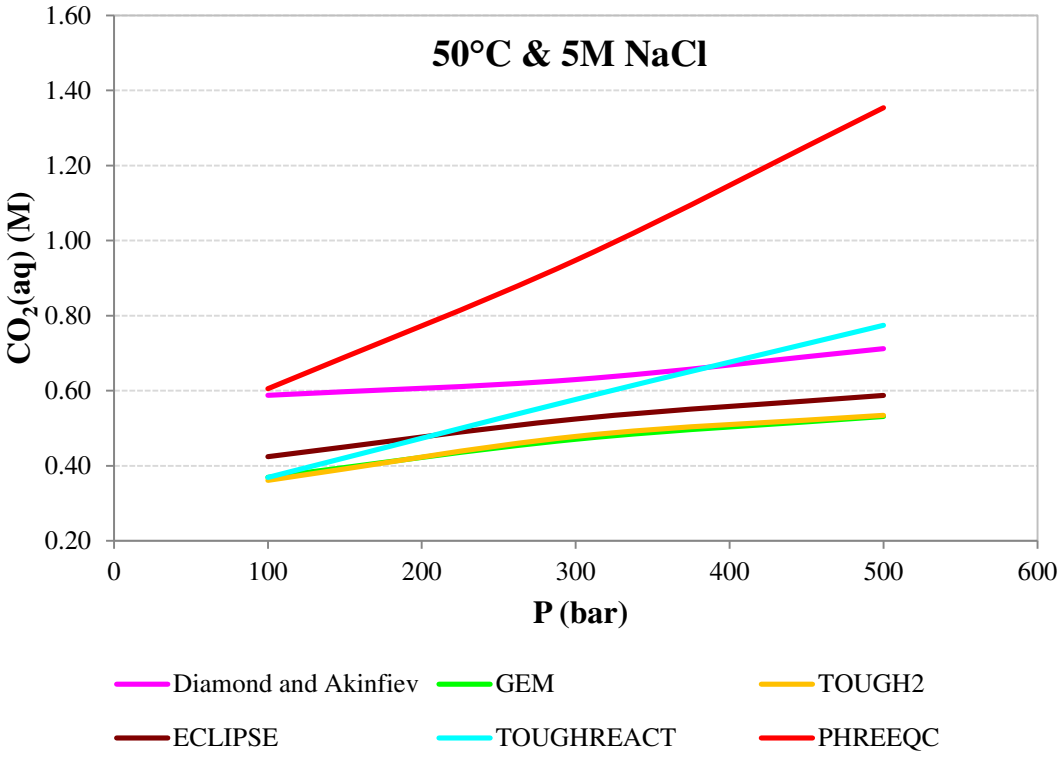

Figure 4.10 CO_2 solubility at 50°C and 5M salinity predicted by different models

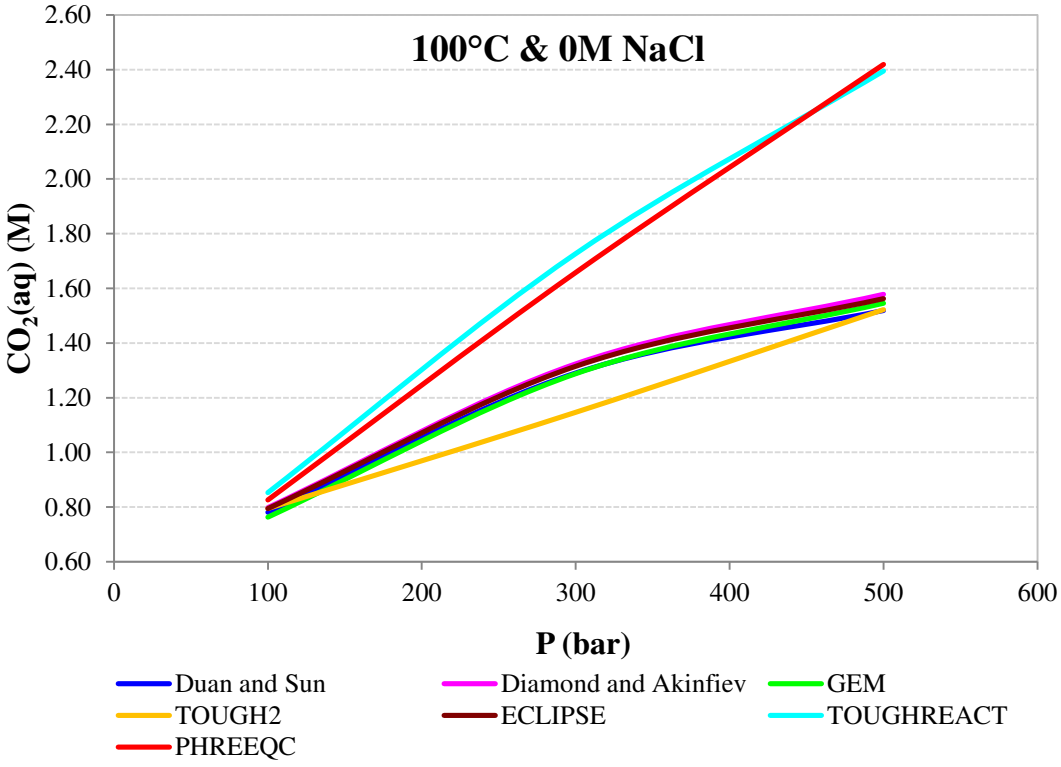

Figure 4.11 CO_2 solubility at 100°C and 0M salinity predicted by different models

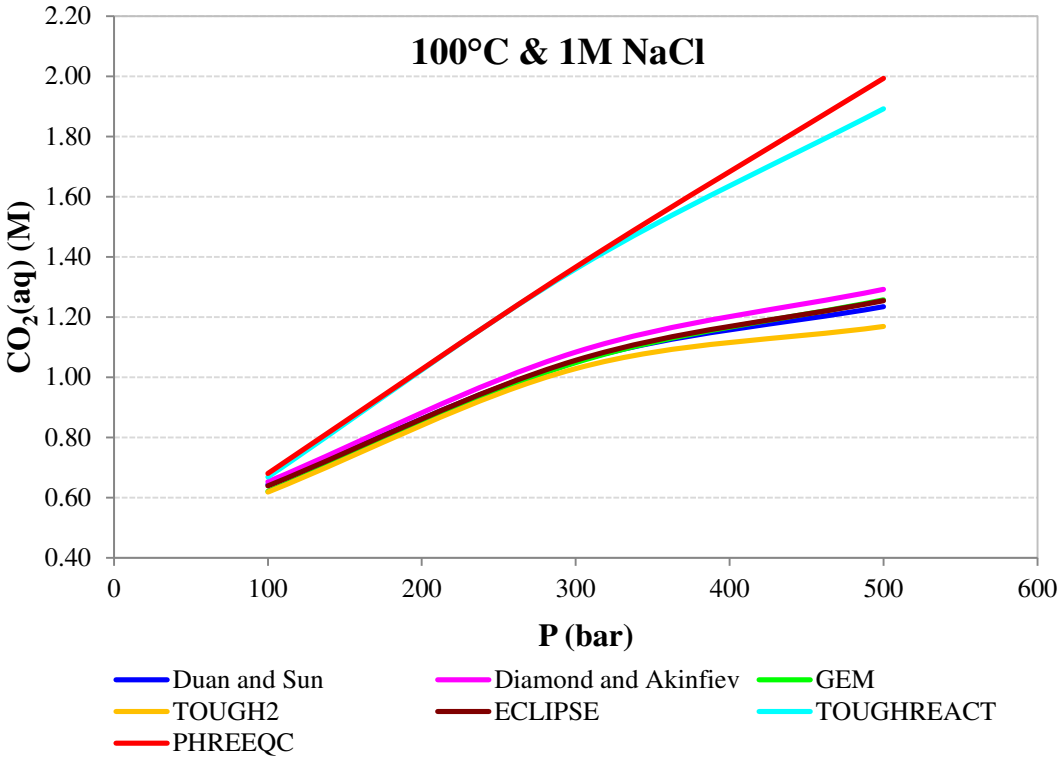

Figure 4.12 CO_2 solubility at 100°C and 1M salinity predicted by different models

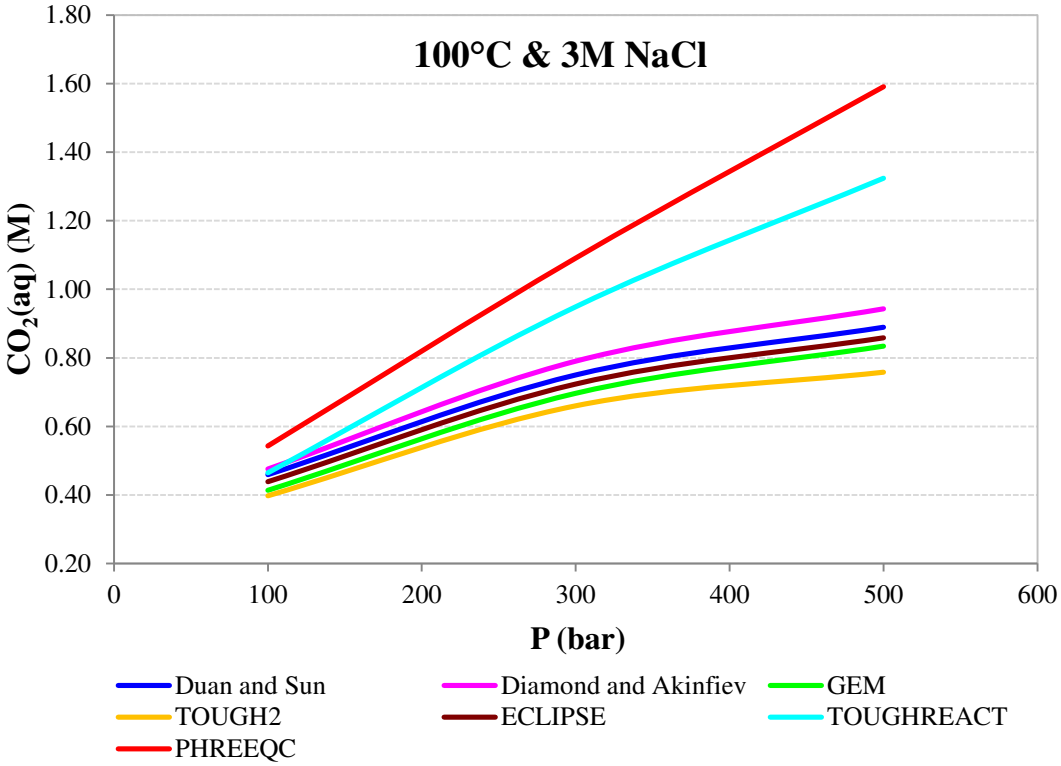

Figure 4.13 CO_2 solubility at 100°C and 3M salinity predicted by different models

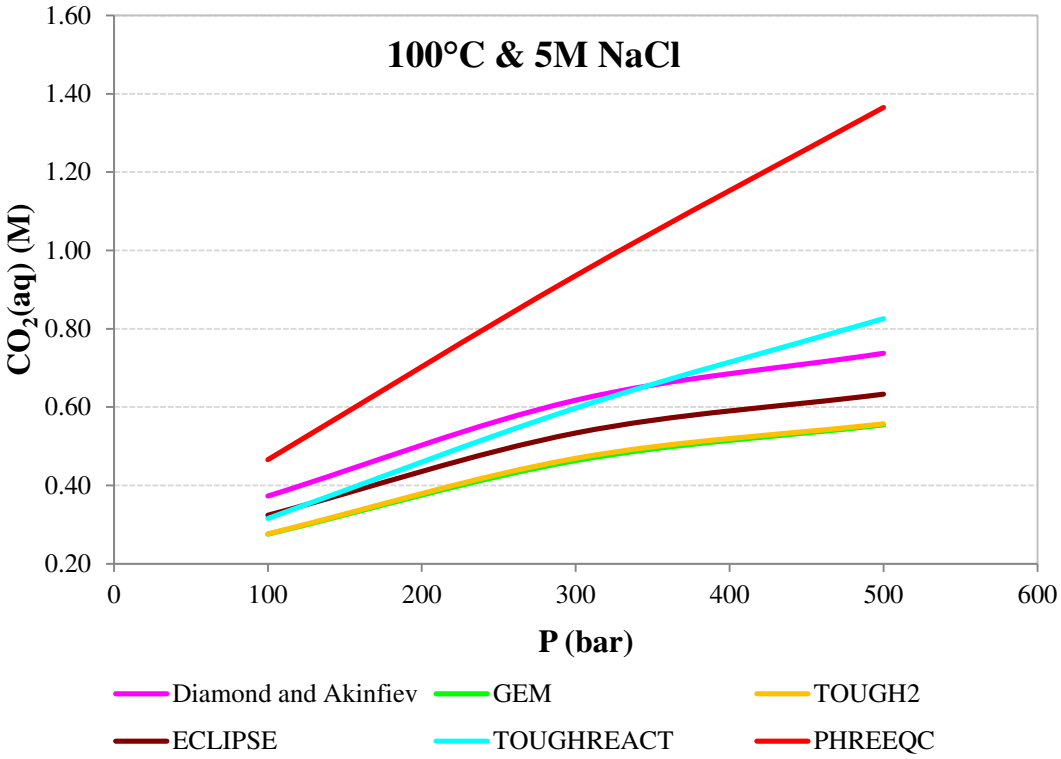

Figure 4.14 CO_2 solubility at 100°C and 5M salinity predicted by different models

The GEM, TOUGH2 and ECLIPSE models all underestimate the solubility, with TOUGH2 having the highest discrepancy over the entire range. The discrepancies increase with increasing salinity. The maximum discrepancy is 37.2% for GEM, 38.6% for TOUGH2 and 27.8% for ECLIPSE. Although ECLIPSE and TOUGH2 use the same solubility model, TOUGH2 underestimates the solubility with respect to ECLIPSE as much as 12%. This is because TOUGH2 calculates the fugacities from the tabulated molar volumes from the Altunin correlations.

The way in which the solubility is modelled by the two primarily geochemical modelling codes, PHREEQC and TOUGHREACT, is basically the same if the fugacities are corrected in PHREEQC. PHREEQC overestimates the solubility by as much as 590% if an ideal gas is assumed. If the fugacities are calculated by Duan-Møller-Weare EOS and then entered to the PHREEQC model, the predictions improve significantly, although the overestimation can still be as much as 90%. TOUGHREACT also gives significant divergence, up to 61.6%. The high degree of

divergence of these two models with respect to others is mainly due to the use of equilibrium constants without pressure correction and the activity models used.

The overestimation of CO_2 solubility leads to an underestimation of the pH. The lower pH enhances mineral dissolution. The comparison of the Ca concentration of CO_2 saturated brine with a salinity of 1M at 50°C in equilibrium with calcite with and without fugacity correction is given Figure 4.15. Since the error in CO_2 solubility does not propagate linearly, the resulting errors due to the pressure dependence of the Henry's constants are relatively small with respect to the resulting error due to the ideal gas assumption.

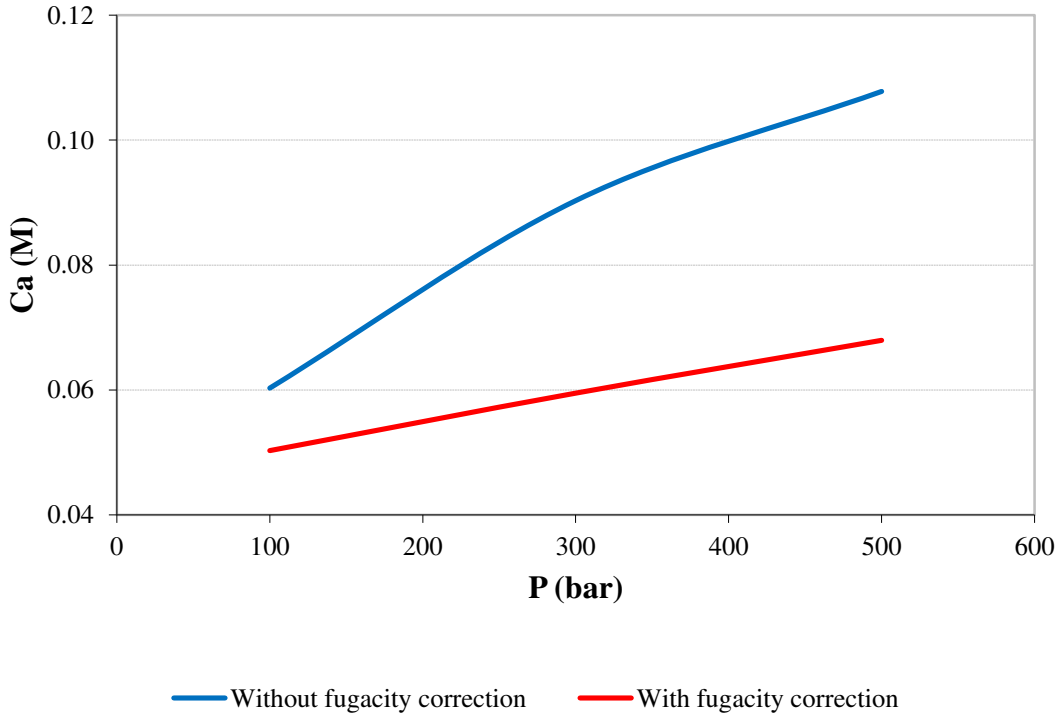

Figure 4.15 The Ca concentration of the CO_2 saturated brine in equilibrium with calcite at 50°C with and without fugacity correction

4.5 Conclusions

In this chapter the fugacity and solubility of CO_2 in brine by different models at conditions relevant to CO_2 storage were evaluated. The following conclusions can be drawn:

- A single EOS that can predict the solubility of CO_2 in brines does not exist.

- CO_2 solubility varies significantly between the various models tested. The divergence increases with increasing salinity.
- None of the models were tested at pressures over 200 bars, since there are no experimental data of CO_2 solubility in saline solutions over 200 bars.
- The three reservoir simulators, GEM, ECLIPSE300 and TOUGH2, underestimate the CO_2 solubility.
- The two geochemical codes, PHREEQC and TOUGHREACT overestimate the solubility of CO_2.
- The fugacity correction has the greatest impact on the accuracy of the CO_2 solubility calculation compared to salting-out and the pressure dependence of the Henry's constants.
- The Soave-Redlich-Kwong EOS is not suitable for CO_2 fugacity calculations.
- The Spycher and Reed EOS is not accurate at temperatures below 100°C.
- The Peng and Robinson EOS is the recommended EOS to implement in numerical codes because of its simplicity and relative accuracy.
- The overestimation of CO_2 solubility leads to an underestimation of pH, which results in an overestimation of mineral dissolution.

The comparison of the models indicates that close attention needs to be paid when primarily geochemical codes are used to simulate CO_2 storage. An accurate CO_2 solubility model needs to be implemented or the thermodynamic data needs to be tuned. However, since there are no data of CO_2 solubility at CO_2 storage conditions at present there is some level of uncertainty in all the models.

4.6 References

Akinfiev, N.N. and Diamond, L.W., 2010, Thermodynamic model of aqueous CO_2-H_2O-NaCl solutions from -22 to 100 °C and from 0.1 to 100 MPa, Fluid Phase Equilibria, 295(1): 104-124.

Altunin, V.V., 1975, Thermophysical Properties of Carbon Dioxide, Publishing House of Standards, Moscow.

Bakker, R.J., 2003, Package FLUIDS 1: Computer programs for analysis of fluid inclusion data and for modelling bulk fluid properties, Chemical Geology, 194(1-3): 3-23.

Dhima, A., de Hemptinne, J.-C. and Moracchini, G., 1998, Solubility of light hydrocarbons and their mixtures in pure water under high pressure, Fluid Phase Equilibria, 145(1): 129-150.

Diamond, L.W. and Akinfiev, N.N., 2003, Solubility of CO_2 in water from -1.5 to 100 °C and from 0.1 to 100 MPa: Evaluation of literature data and thermodynamic modelling. Fluid Phase Equilibria, 208(1-2): 265-290.

Drummond, S.E., 1981, Boiling and mixing of hydrothermal fluids: chemical effects on mineral precipitation, PhD Thesis, The Pennsylvania State University.

Duan, Z., Møller, N. and Weare, J.H., 1992a, An equation of state for the CH_4-CO_2-H_2O system: I. Pure systems from 0 to 1000°C and 0 to 8000 bar, Geochimica et Cosmochimica Acta, 56(7): 2605-2617.

Duan, Z., Møller, N. and Weare, J.H., 1992b, An equation of state for the CH_4-CO_2-H_2O system: II. Mixtures from 50 to 1000°C and 0 to 1000 bar, Geochimica et Cosmochimica Acta, 56(7): 2619-2631.

Duan, Z. and Sun, R., 2003, An improved model calculating CO_2 solubility in pure water and aqueous NaCl solutions from 273 to 533 K and from 0 to 2000 bar, Chemical Geology, 193(3-4): 257.

Duan, Z., Sun, R., Zhu, C. and Chou, I.M., 2006, An improved model for the calculation of CO_2 solubility in aqueous solutions containing Na^+, K^+, Ca^{2+}, Mg^{2+}, Cl^-, and SO_4^{2-}, Marine Chemistry, 98(2-4): 131-139.

Enick, R.M. and Klara, S.M., 1990, CO_2 Solubility in water and brine under reservoir conditions, Chemical Engineering Communications, 90: 23-33.

Garcia, J.E., 2001, Density of aqueous solutions of CO_2, Lawrence Berkeley National Laboratory Report, LBNL-49023.

Harvey, A.H., 1996, Semiempirical correlation for Henry's constants over large temperature ranges, AIChE Journal, 42(5): 1491-1494.

Helgeson, H.C., 1969, Thermodynamics of hydrothermal systems at elevated temperatures and pressures, Am J Sci, 267: 729-804.

Kervevan, C., Azaroual, M., Durst, P., 2005, Improvement of the calculation accuracy of acid gas solubility in deep reservoir brines: Application to the geological storage of CO_2, Oil & Gas Science and Technology Review 60(2): 357-379.

Krichevsky, I.R. and Kasarnovsky, J.S., 1935, Thermodynamical calculations of solubilities of nitrogen and hydrogen in water at high pressures, J. Am. Chem. Soc. 57: 2168-2171.

Li, Y.K. and Nghiem, L.X., 1986, Phase equilibria of oil, gas and water/brine mixtures from a cubic equation of state and Henry's law, The Canadian Journal of Chemical Engineering, 64(3): 486-496.

Peng, D.Y. and Robinson, D.B., 1976, A new two-constant Equation of State, Industrial & Engineering Chemistry Fundamentals, 15(1): 59-64.

Pitzer, K.S., 1973, Thermodynamics of electrolytes, I. Theoretical basis and general equations, J. Phys. Chem., 77(2): 268-277.

Pitzer, K.S., Peiper, J.C. and Busey, R.H., 1984, Thermodynamic properties of aqueous sodium chloride solutions, Journal of Physical and Chemical Reference Data, 13(1): 1-102.

Portier, S. and Rochelle, C., 2005, Modelling CO_2 solubility in pure water and NaCl-type waters from 0 to 300 °C and from 1 to 300 bar: Application to the Utsira Formation at Sleipner, Chemical Geology, 217(3-4): 187-199.

Pruess, K. and García, J., 2002, Multiphase flow dynamics during CO_2 disposal into saline aquifers, Environmental Geology, 42(2): 282-295.

Redlich, O. and Kwong, J.N.S., 1948, On the thermodynamics of solutions. V - An Equation of State. Fugacities of gaseous solutions, Symposium on Thermodynamics and Molecular Structure of Solutions under auspices of Division of Physical and Inorganic Chemistry - 114th Meeting of American Chemical Society, Portland, Oregon.

Rumpf, B., Nicolaisen, H., Öcal, C. and Maurer, G., 1994, Solubility of carbon dioxide in aqueous solutions of sodium chloride: Experimental results and correlation, Journal of Solution Chemistry, 23(3): 431-448.

Saul, A. and Wagner, W., 1987, International equations for the saturation properties of ordinary water substance, Journal of Physical and Chemical Reference Data, 16(4): 893-901.

Soave, G., 1972, Equilibrium constants from a modified Redlich-Kwong Equation of State, Chemical Engineering Science, 27(6-A): 1197-1203.

Span, R. and Wagner, W., 1996, A new Equation of State for carbon dioxide covering the fluid region from the triple-point temperature to 1100 K at pressures up to 800 MPa, Journal of Physical and Chemical Reference Data, 25(6): 1509-1596.

Spycher, N. and Pruess, K., 2005, CO_2-H_2O mixtures in the geological sequestration of CO_2.: II. Partitioning in chloride brines at 12-100°C and up to 600 bar, Geochimica et Cosmochimica Acta, 69(13): 3309-3320.

Spycher, N. and Pruess, K., 2010, A phase-partitioning model for CO_2–brine mixtures at elevated temperatures and pressures: Application to CO_2-enhanced geothermal systems, Transport in Porous Media, 82(1): 173-196.

Spycher, N., Pruess, K. and Ennis-King, J., 2003, CO_2-H_2O mixtures in the geological sequestration of CO_2: I. Assessment and calculation of mutual solubilities from 12 to 100°C and up to 600 bar, Geochimica et Cosmochimica Acta, 67(16): 3015-3031.

Spycher, N.F. and Reed, M.H., 1988, Fugacity coefficients of H_2, CO_2, CH_4, H_2O and of H_2O- CO_2-CH_4 mixtures: A virial equation treatment for moderate pressures and temperatures applicable to calculations of hydrothermal boiling, Geochimica et Cosmochimica Acta, 52(3): 739-749.

Wolery, T.J., 1992, EQ3/6: Software package for geochemical modeling of aqueous systems: Package overview and installation guide (version 7.0), Lawrence Livermore National Laboratory Report, UCRL-MA-110662 PT I.

Xu, T., Apps, J.A. and Pruess, K., 2004, Numerical simulation of CO_2 disposal by mineral trapping in deep aquifers, Applied Geochemistry, 19(6): 917.

CHAPTER 5

GEOCHEMICAL MODELLING: APPLICATION TO CORE SAMPLES

Computer codes such as PHREEQC, GEM and TOUGHREACT are widely used to simulate reactive processes during CO_2 storage (Gaus et al., 2005; Audigane et al., 2007; Wigand et al., 2008; Xu et al., 2005; Thibeau et al, 2007; Cantucci et al., 2009). In this chapter these simulators are compared with respect to brine - CO_2 - rock reactions in potential target sandstone formations in the North Sea. Since MoReS uses PHREEQC for the geochemical calculations, the results of PHREEQC can also be extrapolated to MoReS.

5.1 Model set up

5.1.1. Description of the reservoirs

Reservoirs suitable for CO_2 storage have good porosity and permeability, which allows injected CO_2 to displace the fluid in the host rock and occupies the pore space. In addition, the reservoirs also have caprock that prevents the escape of CO_2, and high enough pressure and temperature that the stored CO_2 will be in the supercritical state,

which maximizes the storage capacity. Rannoch, Oseberg and Forties formations of the northern part of the North Sea are candidate formations for CO_2 storage. In previous work (Prof. Eric Mackay, personal communication), three core samples were taken from these formations and analyses were performed to identify the mineralogy of these cores, and the composition of the formation water, although CO_2 injection was not performed.

In this study, modelling was performed at reservoir temperature and at an estimated maximum allowable pressure during injection (Table 5.1). The fugacity of CO_2 is calculated under these conditions with the Duan et al. (1992a; 1992b), and is given together with reservoir parameters in Table 5.1.

Table 5.1 Physical properties of the reservoirs

Property	**Rannoch**	**Oseberg**	**Forties**
Temperature (°C)	92	100	96
Pressure (bar)	460	280	172
Fugacity of CO_2 (bar) (calculated)	201.71	151.20	110.80
Porosity (%)	25	20	22
k (mD)	200	600	700

5.1.2. Modelling approach

As the objective is to compare the geochemical calculations of the codes, in order to simplify the problem, the transport effects are not considered. The easiest way to compare geochemical simulations is by batch modelling. While batch modelling is straightforward in PHREEQC and TOUGHREACT, it is not possible in GEM. In GEM a one-dimensional homogeneous model was used instead. A system was modelled with a constant CO_2 pressure, which supplies abundant CO_2 to the aqueous system throughout the simulations. This system represents more closely the top of the reservoir with a CO_2 cap.

5.2 The baseline geochemical conditions

It is necessary to define the initial geochemical conditions of the reservoir prior to CO_2 injection. This requires an assessment of the mineralogy and fluid composition of the reservoir. The data from the core and fluid samples of the candidate sandstone reservoirs from the North Sea are used.

5.2.1. Initial mineralogy

The mineralogy of the core samples was taken from the petrographic analysis data. In some cases these analyses were not specific enough and it was necessary to select some minerals as proxies. Muscovite was a proxy for mica, and clinochlore-14A was a proxy for chlorite. Since there is not enough specification of these minerals they are taken from the representative North Sea formation (Johnson et al, 2004). Feldspars were predominantly K-feldspar and modelled as K-feldspar. Chalcedony was used instead of quartz because natural waters at low temperature are usually oversaturated with respect to quartz, which also is the case in the North Sea reservoirs (Bazin et al, 1997; Gaus et al., 2005). The minerals containing less than 1% of the overall bulk volume fraction were not modelled. The chemical formula of the minerals and the mineralogical compositions used in the modelling are given in Tables 5.2 and 5.3 respectively.

Table 5.2 Chemical formula of the minerals used in this study

Mineral	Chemical formula
Calcite	$CaCO_3$
Chalcedony	SiO_2
Clinochlore	$Mg_5Al_2Si_3O_{10}(OH)_8$
Dolomite -dis	$CaMg(CO_3)_2$
K-feldspar	$KAlSi_3O_8$
Illite	$K_{0.6}Mg_{0.25}Al_{2.3}Si_{3.5}O_{10}(OH)_2$
Kaolinite	$Al_2Si_2O_5(OH)_4$
Magnesite	$MgCO_3$
Muscovite	$KAl_2(AlSi_3O_{10})(OH)_2$
Siderite	$FeCO_3$

Table 5.3 Mineralogical composition of the samples used in this study

Mineral	Rannoch		Oseberg		Forties	
	Vol.fr. (%)	mol/m^{3}rock	Vol.fr. (%)	mol/m^{3}rock	Vol.fr. (%)	mol/m^{3}rock
Calcite	0.0	0.0	1.0	271	2.0	542
Chalcedony	62.5	27548	62.0	27327	55.0	24242
Clinochlore	1.5	72	-	-	-	-
Dolomite -dis	0.0	0.0	0.0	0.0	1.0	155
K-feldspar	5.0	459	5.0	459	6.0	551
Illite	-	-	1.0	72	-	-
Kaolinite	-	-	4.0	402	2.0	201
Magnesite	0.0	0.0	0.0	0.0	-	-
Muscovite	4.0	284	0.0	0.0	0.0	0.0
Siderite	-	-	-	-	5.0	1746

5.2.2. Initial brine composition

Formation water compositions were taken from the Flow Assurance and Scale Team (FAST) research group Coreflood Database. These compositions had been supplied by operating companies who commissioned research at Heriot Watt University and the precise details of sample capture and presentation procedures were not available.

It is to be expected that the water compositions and the primary minerals are close to equilibrium, because these data are taken from reservoirs where the formation water will be in equilibrium with the rock substrate. It is certain that degasification will have taken place before the brine samples were analysed, but typically any precipitate will be re-dissolved before analysis, and the pH may be adjusted to ensure equilibrium with minerals present in the formation.

The thermodynamic equilibrium of the formation water with the mineralogy of the reservoir is assumed as the initial reference state for the fluid composition. Hence the formation water samples were equilibrated with the minerals of the core samples defined above by using PHREEQC. This simulated brine composition was used as the initial brine in the modelling of the CO_2 reactions in the cores.

Table 5.4 The composition of the initial brine sample data, the modelled initial brine and the initial brine after equilibration with mineralogy The first column under each formation (Sample) represents the composition of the water sample. The second column (Model) represents the modelled water sample. The third column (Eq. Model) represents the modelled water composition after equilibrated with the reservoir minerals.

	Oseberg			**Rannoch**			**Forties**		
	Sample	**Model**	**Eq. Model**	**Sample**	**Model**	**Eq. Model**	**Sample**	**Model**	**Eq. Model**
T (°C)	100	100	100	92	92	92	96	96	96
pH	6.04	6.04	6.04	6.90	6.90	6.34	7.00	7.00	5.77
Ionic strength	-	0.66	0.66	-	0.54	0.54	-	1.37	1.36
Composition (mol/kg H2O)									
Al	-	-	1.32E-07	-	-	7.27E-08	-	-	6.86E-08
Ca	2.20E-02	2.20E-02	2.15E-02	9.00E-03	9.00E-03	9.00E-03	7.00E-02	7.00E-02	6.22E-02
Cl	6.75E-01	6.80E-01	6.80E-01	5.50E-01	5.60E-01	5.60E-01	1.48E+00	1.46E+00	1.46E+00
CO_2	-	2.928e-03	2.669e-03	-	6.833e-04	1.868e-03	-	5.444e-04	3.714e-03
Fe	-	-	-	-	-	-	1.65E-04	1.65E-04	5.25E-04
HCO_3^-	3.0E-03	2.446e-03	2.221e-03	5.0E-05	4.288e-03	3.217e-03	8.13e-03	4.810e-03	1.933e-03
K	1.30E-02	1.30E-02	3.95E-03	1.40E-02	1.40E-02	4.20E-03	1.00E-02	1.00E-02	7.98E-03
Mg	5.00E-03	5.00E-03	9.90E-03	2.00E-03	2.00E-03	6.30E-03	2.10E-02	2.10E-02	2.69E-02
Na	6.16E-01	6.16E-01	6.16E-01	5.29E-01	5.29E-01	5.29E-01	1.28E+00	1.28E+00	1.28E+00
Si	-	-	1.45E-03	-	-	1.25E-03	-	-	1.35E-03

Before the equilibration with minerals, the water samples were analyzed to check the quality of the samples and the consistency with the thermodynamic data. The analytical

data (labelled Sample in Table 5.4) and the equilibrium model (labelled Model in Table 5.4) are in good agreement. Because the concentration of Cl^- was determined by the charge balance there are slight differences in the Cl concentration. As can be seen from Table 5.4, equilibration of the brine with the mineralogy of the cores (labelled Eq. Model) caused changes in the pH and composition. This is because minerals dissolved or precipitated in order to reach equilibrium.

5.2.3. Secondary minerals

Secondary minerals are the ones that are not present initially, but can be formed during the simulations. The secondary minerals were selected by evaluating their degree of saturation in the CO_2 saturated brine model using PHREEQC. The minerals that are supersaturated and can likely precipitate under reservoir conditions were selected as secondary minerals. One exception to this are the iron minerals other than siderite, since we do not model them because the redox state of the systems modelled are not known. The secondary minerals are denoted with zero initial volume fractions in Table 5.3.

5.3 Comparison of Results

5.3.1. Thermodynamic equilibrium modelling

One of the fundamental requirements of geochemical modelling is the calculation of the species in the aqueous phase. The main assumption is local thermodynamic equilibrium as the aqueous phase is dominated by fast reactions. To study a reaction we need to write the mass action equation that relates the activities of the species to the reaction's equilibrium constant. At equilibrium the ion activity product is equal to the equilibrium constant. The internal databases of GEM and TOUGHREACT and the Lawrence Livermore National Laboratory (LLNL) database of PHREEQC for thermodynamic data were used. The equilibrium constants are reported at 25°C in the databases, and these were extrapolated to the reservoir temperatures. The codes use the following equations to derive equilibrium constants at T in°C for GEM and in K for others:

PHREEQC: $$\log K_T = a + bT + c/T + d\log T + e/T^2 \quad (5.1)$$

TOUGHREACT: $$\log K_T = a\ln T + b + cT + d/T + e/T^2 \quad (5.2)$$

GEM: $$\log K_T = a + bT + cT^2 + dT^3 + eT^4 \quad (5.3)$$

where K_T is the equilibrium constant at temperature T, and *a, b, c, d, e* are the constants. Note that all three codes neglect the effect of pressure on the equilibrium constants, although the impact of pressure can be significant at high pressures.

Because speciation and mineral precipitation and dissolution calculations are based on mass action equations, activity models are crucial for the accuracy of these calculations. Activity models also are important for mineral precipitation or dissolution reactions. Because precipitation occurs when a solution becomes oversaturated with respect to a solid phase, activity models are essential when the degree of saturation with respect to a solid is calculated.

Activity corrections are based on the Debye–Hückel or the B-dot model for GEM. PHREEQC uses the B-dot model as default for the LLNL database but the Davies equation can also be used with modification of the database. In this study the B-dot model (Helgeson, 1969) is used in both GEM and PHREEQC.

PHREEQC calculates the activity coefficient of uncharged species specified with "-CO2-llnl-gamma" (essentially the nonpolar neutral species) with the following equation derived by Drummond (Wolery, 1992)

$$\ln\gamma = \left(a + b + \frac{c}{T}\right)I - \left(d + \frac{e}{T}\right)\left(\frac{I}{I+1}\right) \quad (5.4)$$

where T is the absolute temperature, a, b, c, d, e, are the constants and I is the ionic strength. The activities of the other uncharged species are assumed to be one.

In GEM, the activities of uncharged species are set to one.

TOUGHREACT uses the extended Debye-Hückel equation from Helgeson, Kirkham, and Flowers (Helgeson et al, 1981) to compute the activity coefficients of charged species and water:

$$\log\gamma_i = \frac{Az_i^2 - I^{0.5}}{1 + \mathring{a}BI^{0.5}} + \log\left(1 + 0.018153m^*\right) - \left(\omega_i b_{NaCl} + b_{Na^+,Cl^-} - 0.19\left(|z_i| - 1\right)\right)I \quad (5.5)$$

where γ_i, $\mathring{a}_i$, z_i are the activity coefficient, the ion size parameter, and the ionic charge of the species i, A and B are temperature dependent coefficients, m^* is the total molality, I is the ionic strength of the solution, ω_i is the Born coefficient, b_{NaCl} and b_{Na^+,Cl^-} are Debye-Hückel parameters.

The activity of dissolved gases (CO_2(aq), CH_4(aq), H_2(aq), H_2S(aq), O_2(aq), SO_2(aq)) are calculated by the equation derived by Drummond. For all the other uncharged species, activity coefficients are assumed to be one by default or can be computed by the Setchenow equation: $\ln \gamma = \dot{B} I$.

All these models are valid for salinities below 1M where the influence of the medium is calculated as a whole by ionic strength. For higher salinities it is necessary to take into account the influence of each specific species by using the Pitzer formalism. Only PHREEQC has a Pitzer database for more concentrated solutions, but this database does not include all the minerals used in this study. Since the ionic strengths of Oseberg and Rannoch samples are below one activity models used by the codes are suitable for these models, whereas the ionic strength of Forties formation is above one hence there is more uncertainty in modelling this formation with the activity models used.

The equilibrium constants used by the codes are compared in Table 5.5. There is good agreement between the logK values for chalcedony, clinochlore-14A, and carbonates at 100°C. On the other hand there are significant differences between the logK values of other minerals.

Table 5.5 Comparison of the equilibrium constants for the minerals used in this study

	logK at 25°C			logK at 100°C		
Minerals	**PHREEQC**	**GEM**	**TOUGHREACT**	**PHREEQC**	**GEM**	**TOUGHREACT**
Calcite	$Calcite + H^+ = Ca^{2+} + HCO_3^-$					
	1.82	1.71	2.15	0.79	0.69	0.77
Chalcedony	$Chalcedony = SiO_2(aq)$					
	-3.76	-3.74	-4.19	-2.84	-2.87	-2.86
Clinochlore-14A	$Clinochlore\text{-}14A + 16\ H^+ = 12\ H_2O + 5\ Mg^{2+} + 2\ Al^{3+} + 3\ SiO_2(aq)$					
	67.05	68.58	72.75	45.27	47.28	44.24
Dolomite-dis	$Dolomite\text{-}dis + 2\ H^+ = Ca^{2+} + Mg^{2+} + 2\ HCO_3^-$					
	2.47	4.06	4.93	1.24	1.24	1.20
Illite	$Illite + 8\ H^+ = 5\ H_2O + 0.6\ K^+ + 0.25\ Mg^{2+} + 2.3\ Al^{3+} + 3.5\ SiO_2(aq)$					
	8.88	9.80	7.27	2.15	3.76	-0.97
Kaolinite	$Kaolinite + 6\ H^+ = 5\ H_2O + 2\ Al^{3+} + 2\ SiO_2(aq)$					
	6.72	7.43	7.96	1.02	2.40	-0.09
K-feldspar	$K\text{-}feldspar + 4\ H^+ = 2\ H_2O + K^+ + Al^{3+} + 3\ SiO_2(aq)$					
	-0.38	0.07	0.72	-1.78	-1.10	-1.94
Magnesite	$Magnesite + H^+ = Mg^{2+} + HCO_3^-$					
	2.27	2.44	2.83	0.61	0.71	0.58
Muscovite	$Muscovite + 10\ H^+ = 6\ H_2O + K^+ + 3\ Al^{3+} + 3\ SiO_2(aq)$					
	13.45	14.57	16.42	4.3	6.41	4.19
Siderite	$Siderite + H^+ = HCO_3^- + Fe^{2+}$					
	-0.22	-0.22	0.08	-1.48	-1.51	-1.41

5.3.2. Solubility of CO_2

GEM and TOUGHREACT use corrected Henry's constants in order to take account of pressure and salinity effects. PHREEQC does not use fugacity coefficient and assumes that the fugacity of a gas is equal to its partial pressure. This overestimates the solubility at high pressures. The CO_2 fugacities calculated with the Duan and Sun model (2003) were used for PHREEQC calculations. As shown in Table 5.6, the correction of fugacity reduces the overestimation but there are still significant discrepancies. This is because PHREEQC does not consider the effect of pressure on

the equilibrium constants. On the other hand, TOUGHREACT overestimated the CO_2 solubility in the Rannoch model, which is the one with the highest fugacity of the three cases. These results are not unexpected as they are in agreement with CO_2 solubility modelling comparison in Chapter 4.

Table 5.6 Computed CO_2 solubility in different models (PHREEQC_gas is the PHREEQC model without fugacity correction, PHREEQC is the PHREEQC model with fugacity correction)

		CO_2(aq) (M)				
Sample	**f_{CO2} (bar)**	**Reference model**	**PHREEQC_gas**	**PHREEQC**	**GEM**	**TOUGHREACT**
Rannoch	201.71	1.31	4.59	2.01	1.35	1.98
Oseberg	151.20	1.11	2.56	1.39	1.13	1.19
Forties	110.80	0.82	1.44	0.93	0.83	0.76

5.3.3. pH

The decrease of the pH in the formation fluid with CO_2 injection is observed both in laboratory and field tests (Katzuba et al., 2005, Kharaka et al, 2006). Dissolved CO_2 forms a weak acid in the solution which can be expressed by the following chemical reactions:

$$CO_2(aq) + H_2O = H^+ + HCO_3 \quad (5.6)$$

$$HCO_3^- = H^+ + CO_3^{2-} \quad (5.7)$$

The equilibrium constants of these reactions are given in Table 5.7.

Table 5.7 The equilibrium constants of the dissociation reactions (5.6) and (5.7)

	logK at 25°C			**logK at 100°C**		
	PHREEQC	**GEM**	**TOUGHREACT**	**PHREEQC**	**GEM**	**TOUGHREACT**
CO_2(aq)	-6.37	-6.38	-6.52	-6.37	-6.43	-6.39
HCO_3^-	-10.35	-10.35	-10.55	-10.07	-10.24	-10.09

A sharp decrease of the pH was observed in all the three samples. Later, due to the mineral reactions, the pH started to increase. Because of the fast dissolution kinetics of

calcite, the pH of the brine increased, in just 1000 seconds, to 4.45 in the Oseberg rock type and to 4.51 in the Forties rock type and reached the final values by buffering of silicate minerals. On the other hand, as calcite is absent in the Rannoch sample, pH increased slowly throughout the simulation. The simulators are in reasonably good agreement, as seen from Table 5.8.

Table 5.8 pH values of the initial CO_2 saturated brine and final brine

	PHREEQC		**GEM**		**TOUGHREACT**	
Sample	Initial brine	Final brine	Initial brine	Final brine	Initial brine	Final brine
Rannoch	3.39	5.14	3.63	5.03	3.53	4.87
Oseberg	3.41	4.90	3.60	5.00	3.58	5.01
Forties	3.46	4.77	3.65	4.88	3.59	4.87

5.3.4. Mineral dissolution and precipitation

When a mineral comes into contact with CO_2 saturated brine which was not in equilibrium previously, the mineral starts to dissolve in order to reach equilibrium with the brine. The dissolution of the mineral changes the brine composition and can drive the precipitation of secondary minerals. For example, if K-feldspar comes into contact with CO_2 saturated brine, it dissolves. The release of Al, Si and K ions enriches the brine, and it becomes supersaturated with respect to muscovite. If it is sufficiently supersaturated for nucleation, muscovite precipitates.

In thermodynamic equilibrium models supersaturation of a mineral is not allowed. On the other hand, whether or not a mineral actually precipitates depends on the kinetic rate of the reaction. Therefore the kinetics reaction modelling allows the supersaturation of the mineral phases in the solution. For this reason a kinetic law was used for the dissolution and precipitation of minerals. The reaction rate depends on the how much of the mineral is available, how fast the reaction is and how far it is from the equilibrium.

A simplified kinetics rate law (Steefel and Lasaga, 1994) was considered:

$$r_\beta = k_\beta A_\beta \left(1 - \frac{Q_\beta}{K_\beta}\right) \tag{5.8}$$

where r_β is the dissolution/precipitation rate for mineral β per unit bulk volume of porous medium or per volume of aqueous phase [mol m^{-3} s^{-1}], A_β is the reactive surface area of mineral β [m^2], k_β is the rate constant [mol m^{-2} s^{-1}], K_β is the chemical equilibrium constant, and Q_β is the ionic activity product.

In the simulations A is expressed as per unit of rock volume in GEM and TOUGHREACT, whereas it is expressed as per mole in PHREEQC, so it is updated by the simulator with volume change and mole change respectively. Reactive surface areas are case specific and they need to be measured case by case. Because measurements of BET surfaces were not available, a universal value of 10^4 m^2 per m^3 of rock was assumed, except that for the phyllosilicates. Because of the fine grain size of phyllosilicates, the surface area for these minerals was set to 10^6 m^2 per m^3. To allow the precipitation of the secondary minerals, their volume fraction was set to 10^{-6}-10^{-7} so that their reactive surfaces were non-zero.

The Arrhenius equation can be used to describe the temperature dependence of the rate constant. The rate constants are reported usually at 25°C, and this is expressed as (Steefel and Lasaga, 1994):

$$k = k_{25} \exp\left(\frac{-E_a}{R}\left(\frac{1}{T} - \frac{1}{298.15}\right)\right) \tag{5.9}$$

where k_{25} is the rate constant at 25°C [mol m^{-2} s^{-1}], E_a is the activation energy [J/mol], R is the universal gas constant [8.3143 J K^{-1} mol^{-1}], and T is the temperature [K].

The rate constants and the activation energies used in this study (Table 5.9) were from Johnson et al. (2004 and references cited therein) with the exception of the activation energy of calcite (Svensson and Dreybodt, 1992). The kinetic data of disordered dolomite and siderite were assumed to be equal to those of magnesite, and the kinetic data of illite to those of muscovite.

Table 5.9 Reaction rate constants and activation energies for minerals used in the simulations

Mineral	k (25°C)	EA (kJ)
Calcite	1.50E-06	41.9
Chalcedony	3.45E-13	62.8
Clinochlore	3.00E-13	88.0
Dolomite-dis	1.00E-09	62.8
K-feldspar	1.78E-10	51.7
Illite	1.00E-13	22.0
Kaolinite	4.00E-13	29.0
Magnesite	1.00E-09	62.8
Muscovite	1.00E-13	22.0
Siderite	1.00E-09	62.8

In GEM and TOUGHREACT it is necessary to specify the aqueous species that will be modelled. The following species were modelled: H^+, Ca^{2+}, $SiO_2(aq)$, K^+, Al^{3+}, Na^+, Cl^-, HCO^{3-}, CO_3^{2-}, OH-, Fe^{2+}, Mg^{2+}, $AlOH^{2+}$. On the other hand, in the PHREEQC models all the aqueous species available in the database are used for modelling.

As the kinetic data are not well known, the length of time that the reactions take should be considered as qualitative rather than quantitative.

5.3.5. The mineral reactions observed in the simulations in Rannoch type

In Rannoch rock type, the decrease of pH by CO_2 dissolution initiated clinochlore and K-feldspar dissolution. The dissolution of these minerals released Mg, K, Al, and Si ions into the brine which lead to supersaturation and precipitation of magnesite, muscovite and chalcedony.

The overall reaction observed can be expressed as

Clinochlore + K-feldspar + 5 $CO_2(aq)$ = Muscovite + 3 Chalcedony +

$$5\ Magnesite + 3\ H_2O$$

The equation shows that for each mole of clinochlore dissolved, five moles of CO_2 is trapped as magnesite. The clinochlore was consumed in less than 10 years and K-feldspar continued to dissolve until the K-feldspar – muscovite equilibrium was reached. This reaction can be written as

$$K\text{-}feldspar + 2\ CO_2 + 2\ H_2O = Muscovite + 2\ K^+ + 6\ Chalcedony + 2\ HCO_3^-$$

As can be seen from Figure 5.1, the three simulators are in very good agreement for the five minerals after 10 years of simulation. It is difficult to identify the discrepancy between GEM and the other two simulators because GEM does not output the activities of the species or the saturation index of the minerals.

a) Chalcedony

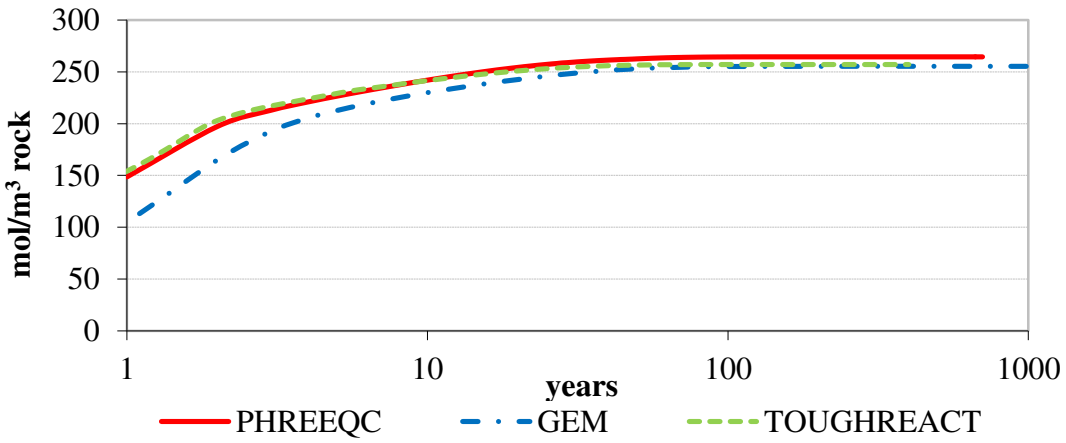

b) Clinochlore

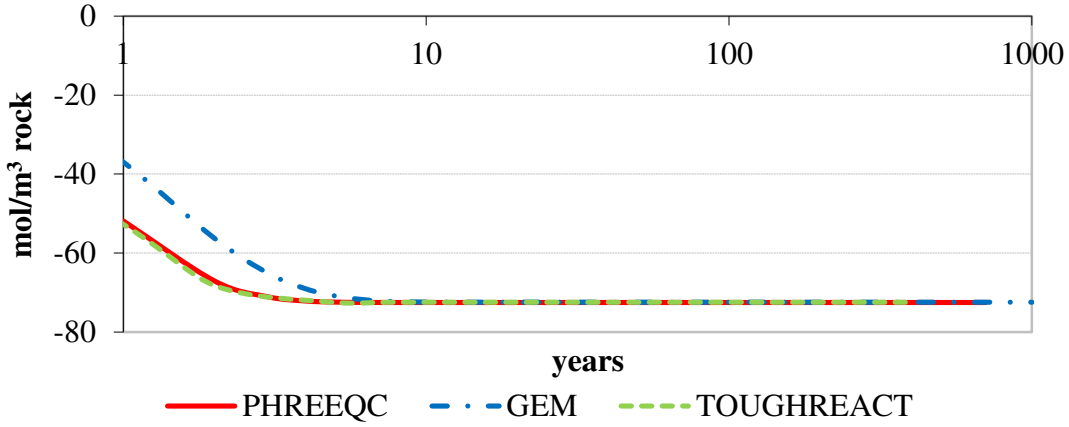

c) K-feldspar

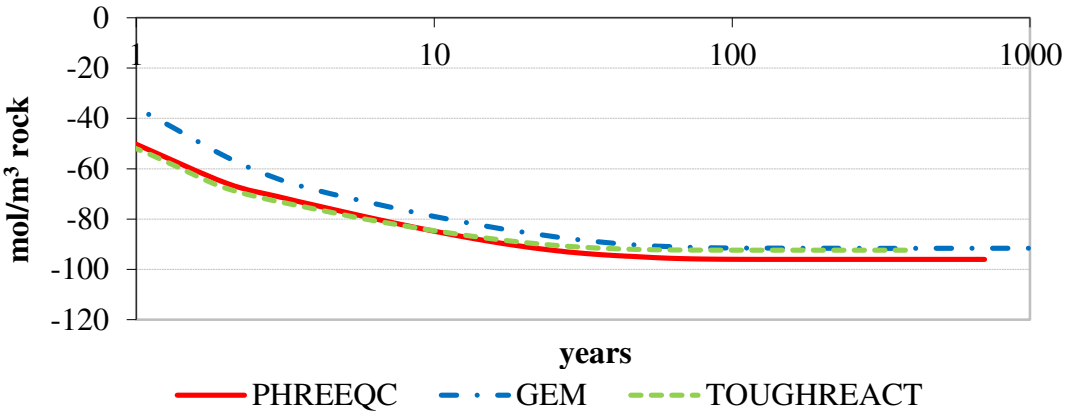

d) Magnesite

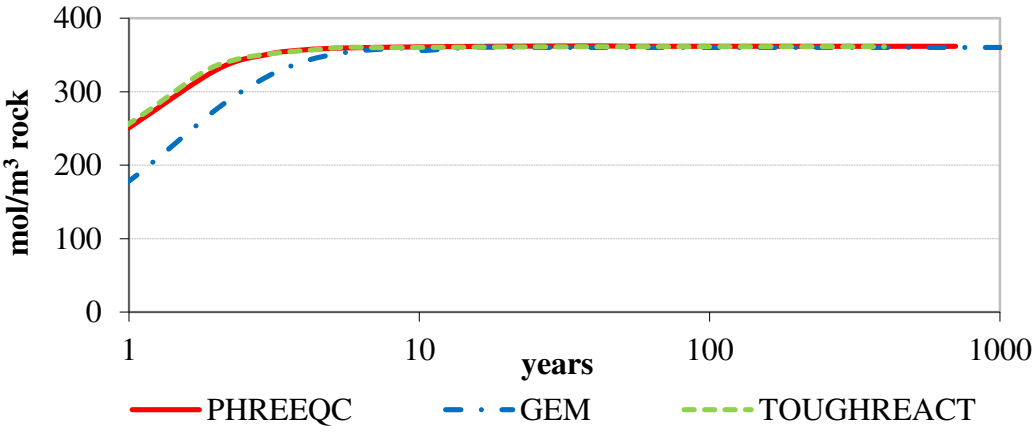

e) Muscovite

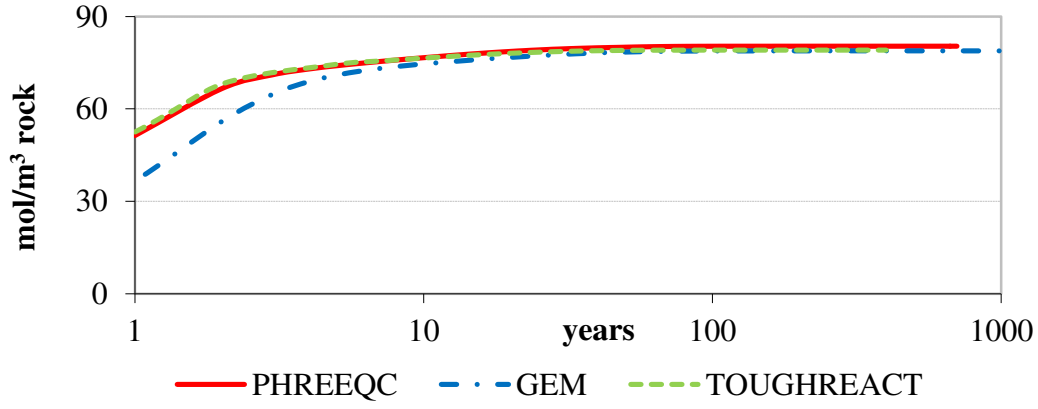

Figure 5.1 (a-e) Mineral changes in moles per m^3 of medium with time (positive values precipitation, negative values dissolution) for Rannoch rock type

5.3.6. The mineral reactions observed in the simulations in Oseberg type

For Oseberg rock type, PHREEQC and GEM predicted, in the early time of the simulations, the dissolution of illite which enriched the brine with K, Al, and Si ions. This enrichment initiated the precipitation of kaolinite, K-feldspar and chalcedony. The kaolinite and K-feldspar formed were not stable and they started to dissolve later on. Illite also released Mg^{2+} which induced a trace amount of dolomitization. Only after approximately 1000 years, when illite was consumed, rapid mineral change was observed due to K-feldspar and kaolinite dissolution, and muscovite and chalcedony precipitation by the following overall reaction:

K-feldspar + Kaolinite = Muscovite + 2 Chalcedony + H_2O

In contrast, TOUGHREACT simulated a low level of reactivity with a minor amount of illite precipitation and feldspar dissolution. Saturation index of muscovite was estimated negative throughout the simulation. Hence with no sink for K, K-feldspar or kaolinite could not dissolve. The comparison of the three codes with respect to mineral changes is given in Figure 5.2.

a) Calcite

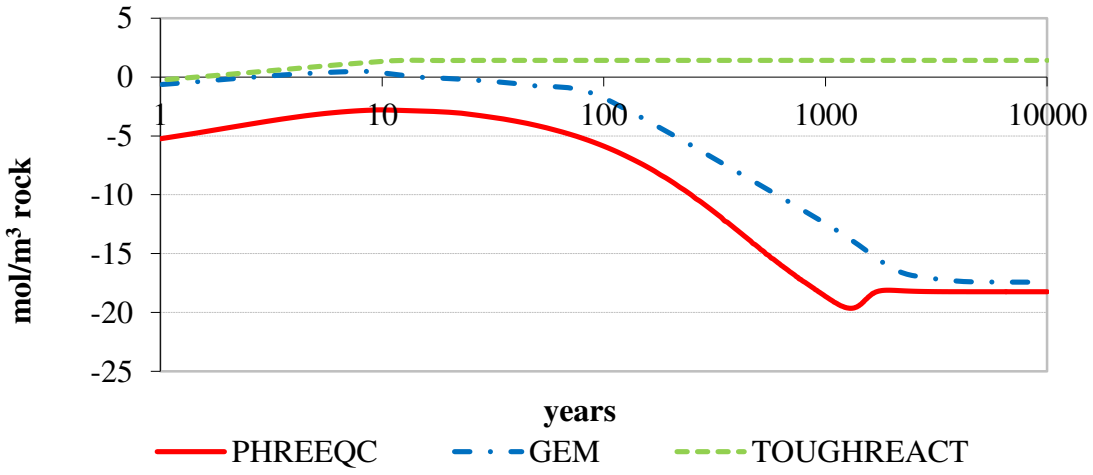

b) Chalcedony

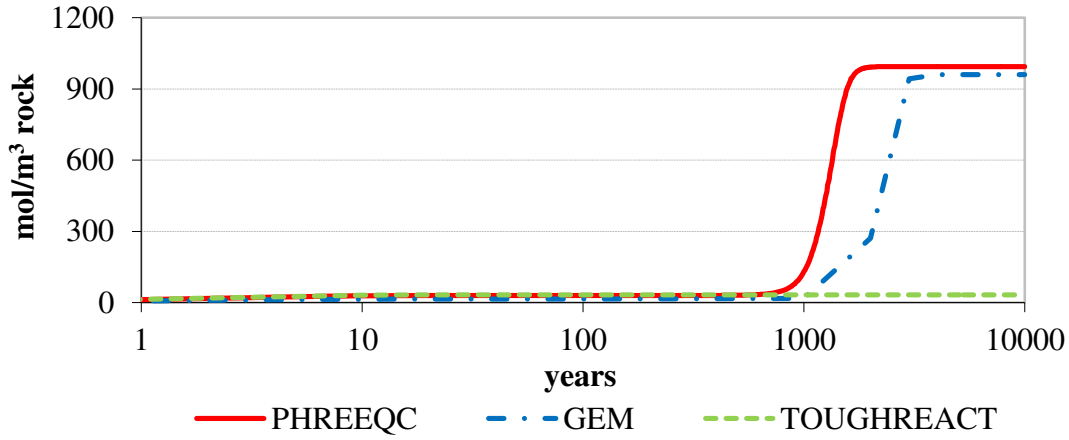

c) Dolomite

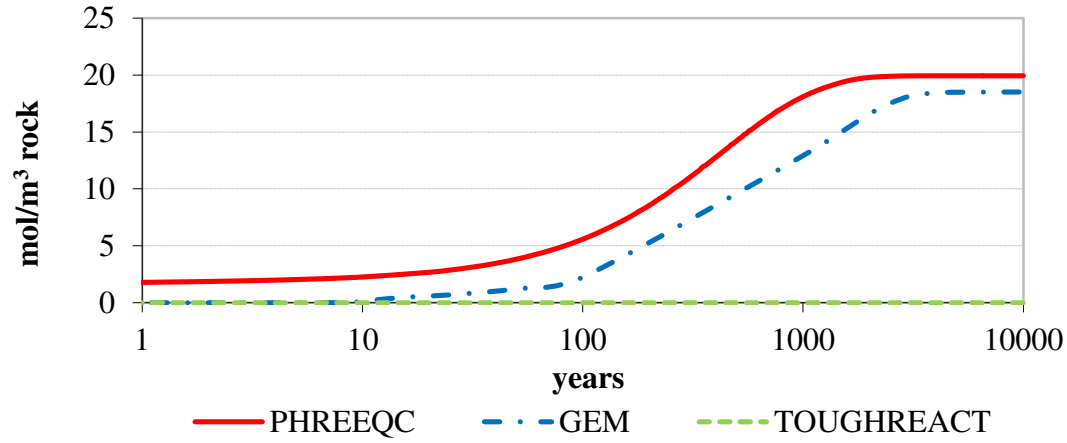

d) Illite

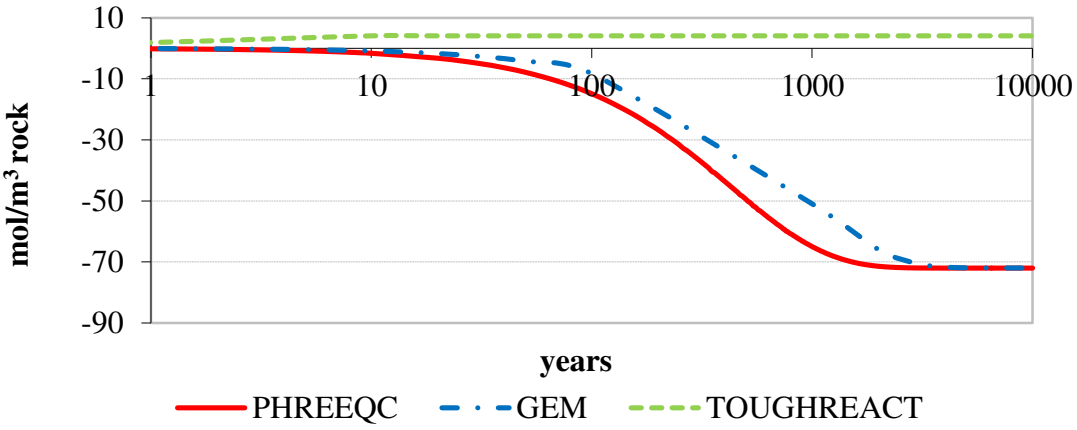

e) K-feldspar

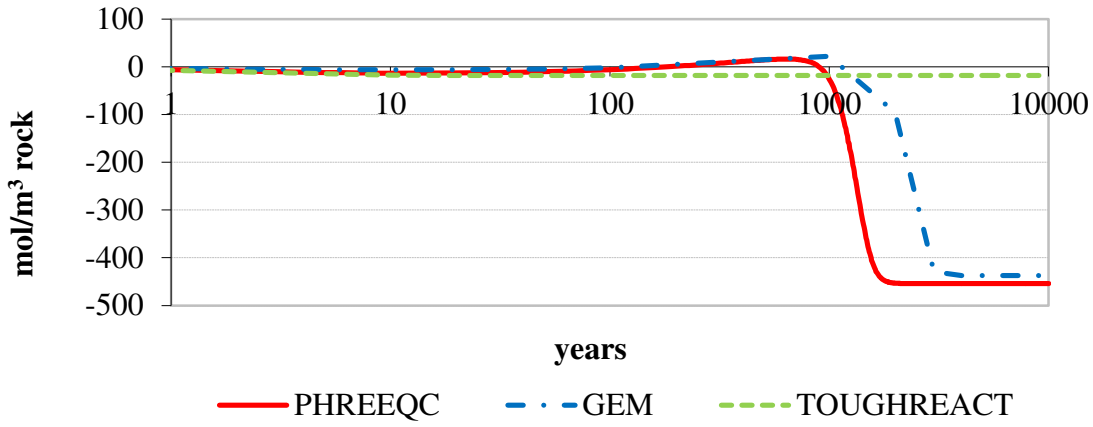

f) Kaolinite

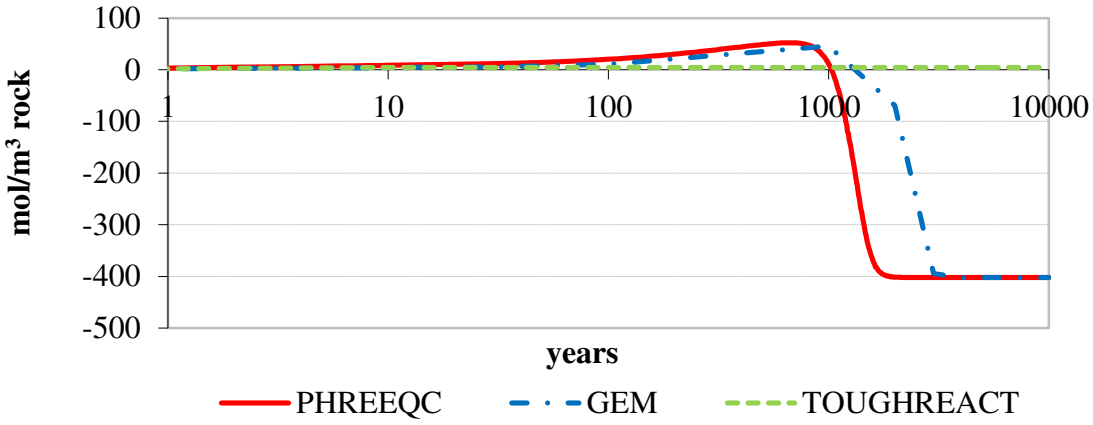

g) Muscovite

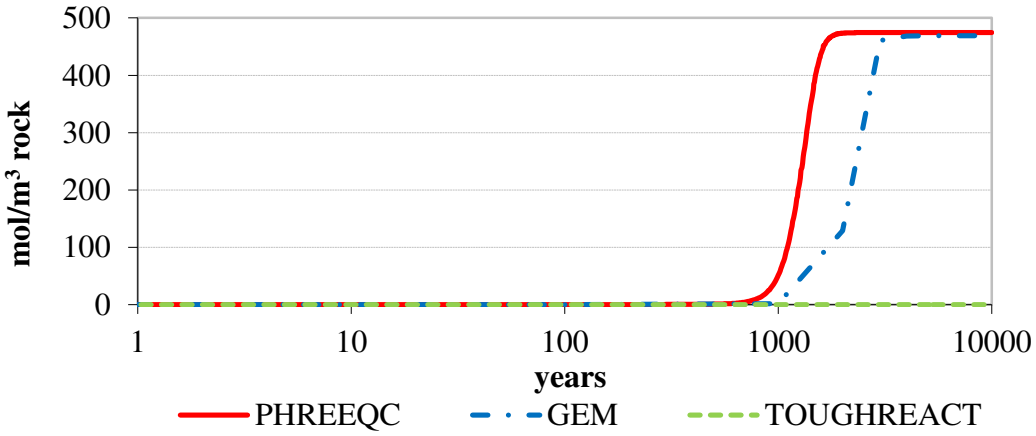

Figure 5.2 (a-g) Mineral changes in moles per m^3 of medium with time (positive values precipitation, negative values dissolution) for Oseberg rock type

5.3.7. The mineral reactions observed in the simulations in Forties type

In Forties rock type, initially the K-feldspar dissolution and the kaolinite precipitation is observed by PHREEQC and GEM:

2 K-feldspar + 2 CO_2 + H_2O = Kaolinite + 4 Chalcedony + 2 K^+ +2HCO_3^-

Then kaolinite started to dissolve with K-feldspar, and muscovite and chalcedony precipitated.

As in the case of Oseberg rock type, TOUGHREACT simulated a low level of reactivity with minor dissolution of feldspar, and precipitation of kaolinite and chalcedony. The comparison of the three codes with respect to mineral changes is shown in Figure 5.3.

a) Chalcedony

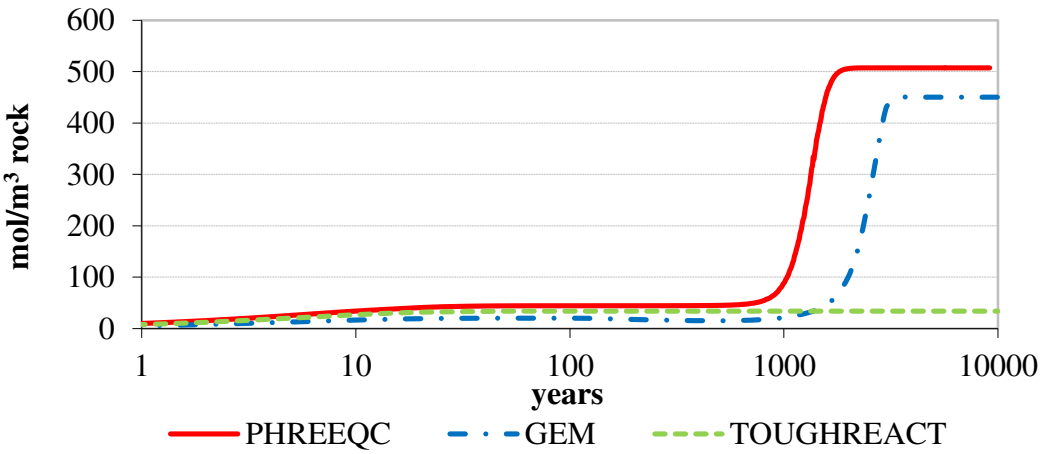

b) K-feldspar

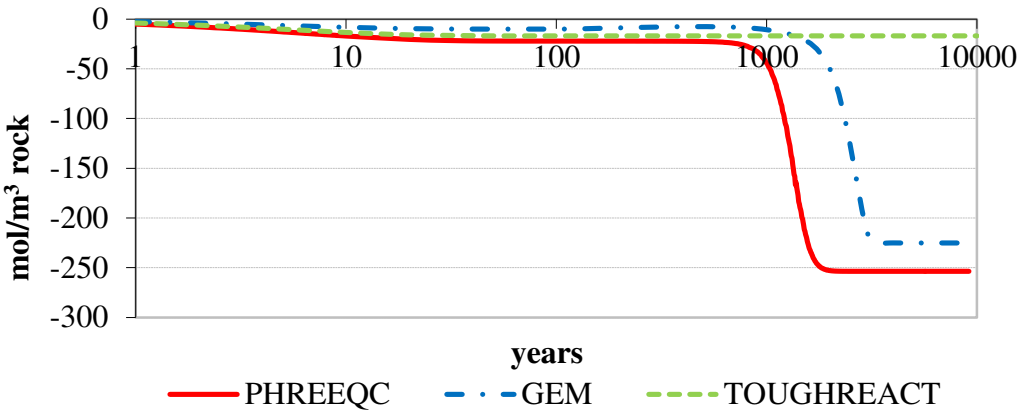

c) Kaolinite

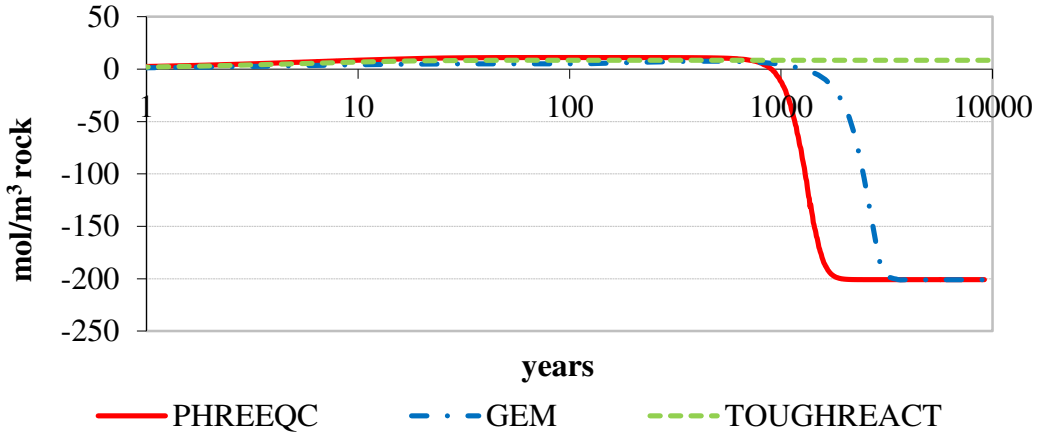

d) Muscovite

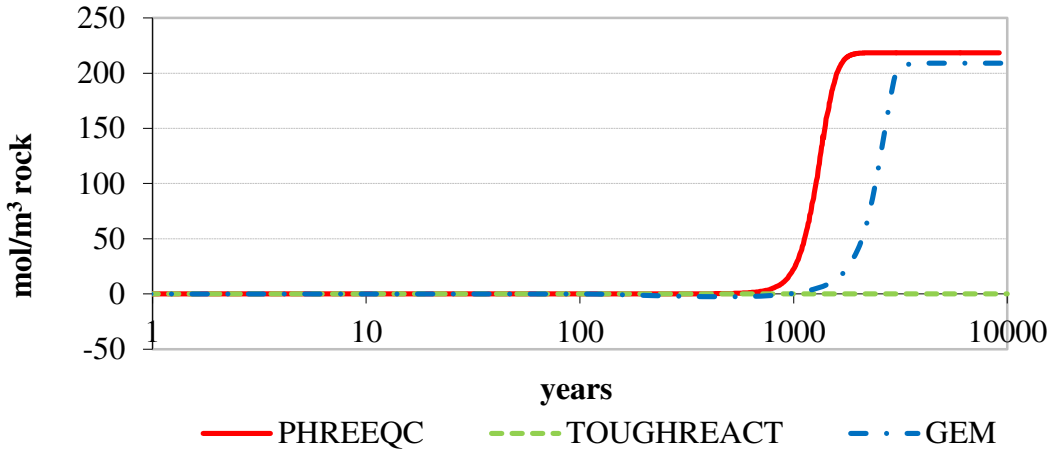

Figure 5.3 (a-d) Mineral changes in moles per m^3 of medium with time (positive values precipitation, negative values dissolution) for Forties rock type

In conclusion, there is fairly good agreement between PHREEQC and GEM in all three cases, whereas TOUGHREACT gave diverging results in the Oseberg and Forties models. The major reason for the low level of reactivity in TOUGHREACT is that the simulator predicted negative saturation index for muscovite. With no muscovite precipitation, and hence no sink for K^+, K-feldspar reached equilibrium with the brine and stopped dissolving.

In order to identify if the differences in the results are due to the differences in thermodynamic data, the simulations of the Oseberg rock type were re-run with the

same thermodynamic data by using the PHREEQC's equilibrium constants for aqueous and mineral reactions in the three codes. The simulation results are given in Figure 5.4. the different earlier TOUGHREACT results do appear to be primarily due to the different thermodynamic data it used. With the same equilibrium constants all three simulators predicted similar mineral precipitation and dissolution in the long run, but the way in which they reached equilibrium is still quite different.

a) Calcite

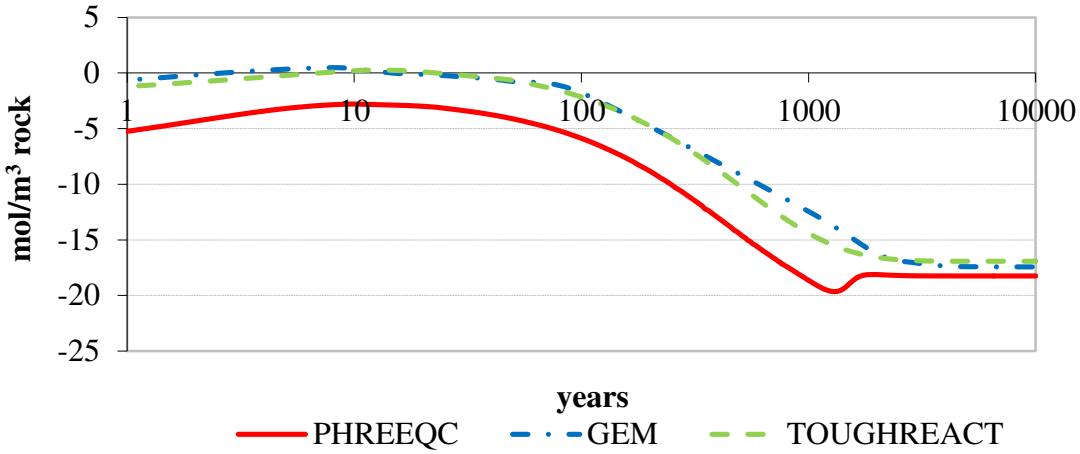

b) Chalcedony

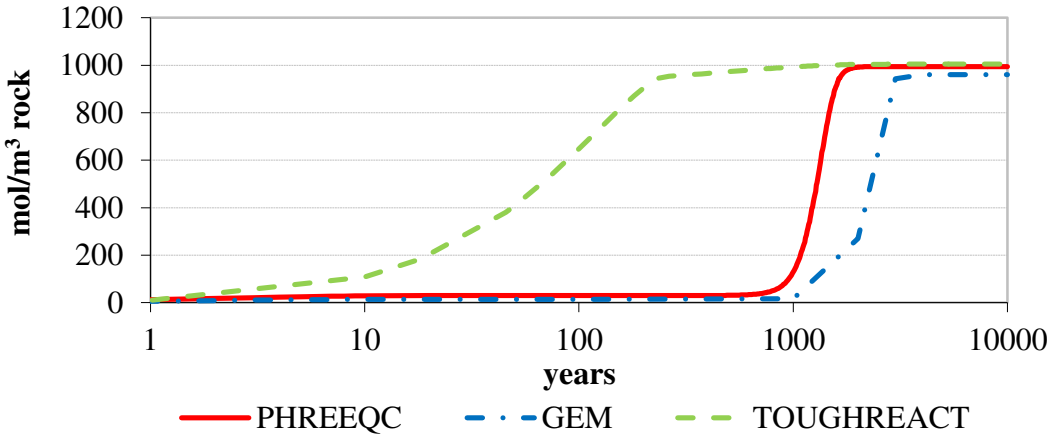

c) Dolomite

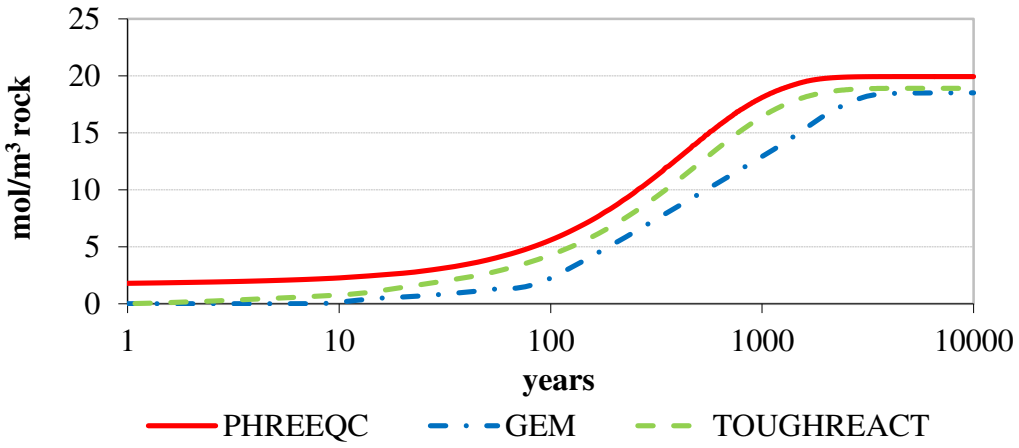

d) Illite

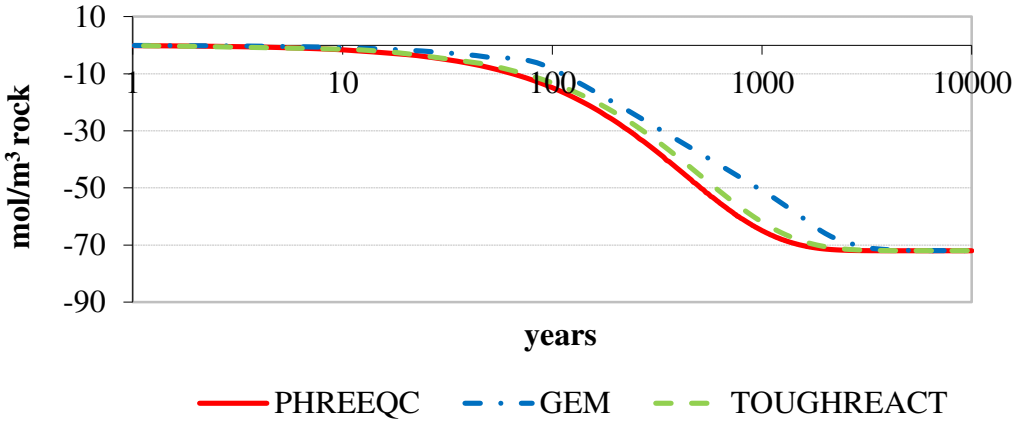

e) K-feldspar

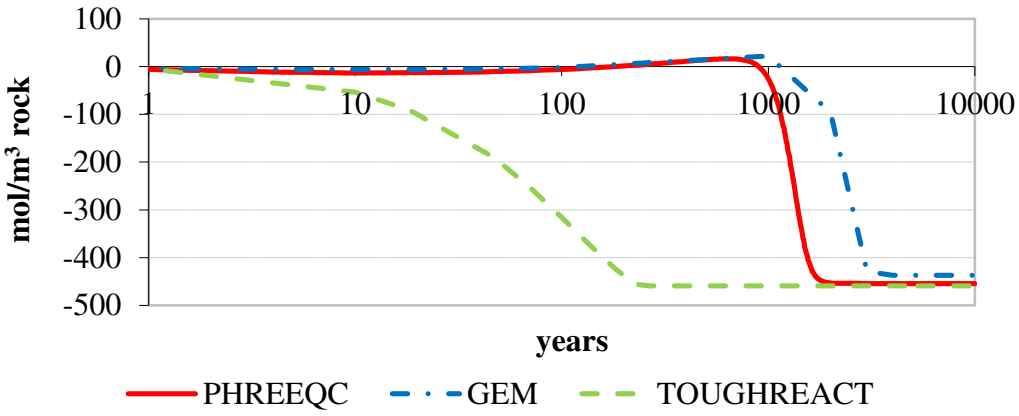

f) Kaolinite

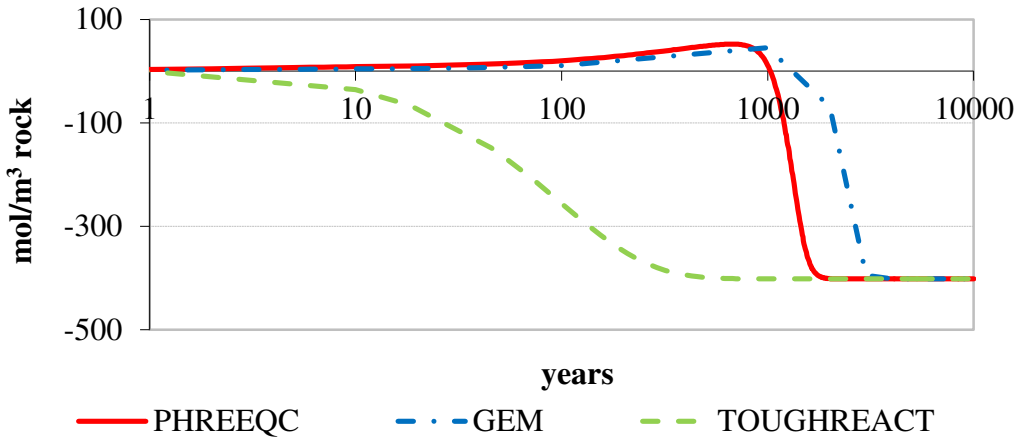

g) Muscovite

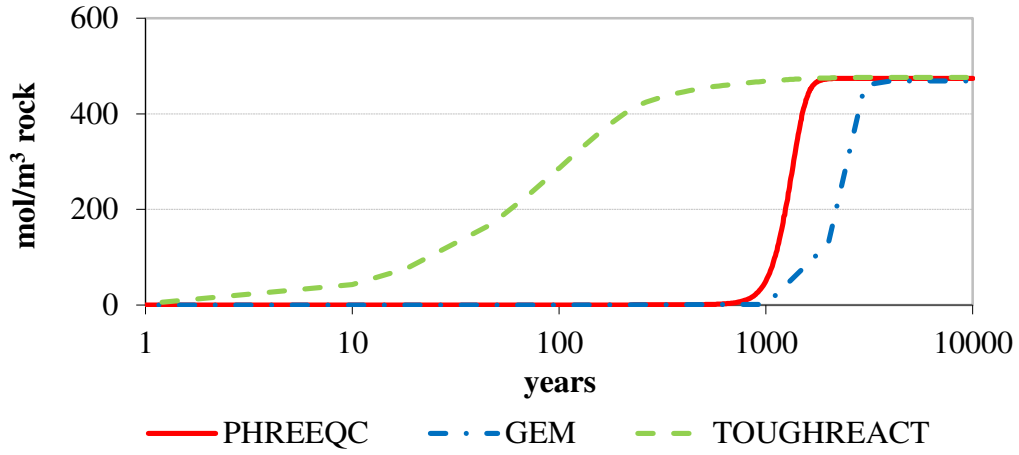

Figure 5.4 (a-g) Mineral changes in moles per m^3 of medium with time (positive values precipitation, negative values dissolution) for Oseberg rock type (Same log K values are used in all three codes.)

The differences are most likely due to the differences in the calculated activity coefficient and the activities. The direct comparison of the activities of the aqueous species for the initial brine of the Oseberg formation, given in Table 5.4, calculated by PHREEQC and TOUGHREACT are given in table 5.10. GEM does not output these values, hence they are not included.

Table 5.10 Comparison of the computed activities for the initial brine of Oseberg formation given in Table 3

	Activity (log molal except for H_2O)	
Species	PHREEQC	TOUGHREACT
H_2O	0.978	0.980
Al^{3+}	-14.74	-14.63
AlO_2^-	-7.19	-7.10
$Al(OH)_2^+$	-9.67	-9.31
$AlOH_2^+$	-11.78	-11.83
Ca^{2+}	-2.40	-2.59
$CaCl^+$	-3.20	-3.34
$CaHCO_3^+$	-3.85	-4.01
$CaCl_2$	-3.68	-3.76
$CaCO_3$	-5.19	-5.36
Cl^-	-0.43	-0.40
$CO_2(aq)$	-2.51	-2.49
CO_3^{2-}	-6.89	-6.90
H^+	-6.04	-6.04
HCO_3^-	-2.85	-2.85
K+	-2.65	-2.60
Mg^{2+}	-2.67	-2.96
$MgCl^+$	-2.94	-3.18
$MgCO_3$	-6.07	-6.33
$MgHCO_3^+$	-4.11	-4.37
Na^+	-0.44	-0.45
NaCl	-1.36	-1.32
$NaCO_3^-$	-7.90	-7.90
$NaHCO_3$	-3.71	-3.72
$NaHSiO_3$	-5.11	-5.09
SiO_2	-2.84	-2.84
OH^-	-6.21	-6.23

No field observation or laboratory data were available to confirm the simulation results, but these reactions were inferred from the diagenesis occurring in North Sea reservoirs (Bjorkum and Gjelsvik, 1988; Bjørlykke et al., 1992, 1995).

Among the three rock types studied, only one has some mineral trapping potential because of the chlorite content. Porosity did not evolve significantly throughout the simulations in any of the rock types with changes of -0.12% in Rannoch, 1.12% in Oseberg and 0.6% in Forties formation type. Although muscovite and chalcedony precipitation can have dramatic effects on permeability, and hence on the injectivity, due to the slow kinetics of these minerals, it can have only a positive effect on the enhancement of the confinement properties of the rock.

5.4 Conclusions

The objective of this study was to compare three numerical codes, PHREEQC, GEM and TOUGHREACT, from the point of view of geochemical modelling of CO_2 storage. The codes were applied to three target sandstone reservoirs in the North Sea. The equilibrium constants of the selected minerals, activity models, the solubility of CO_2, pH and evolution of the aqueous species and minerals in time were compared.

While large discrepancies in the calculated amount of dissolved CO_2 are found (Table 5.5), the pH values are in reasonably good agreement. The codes gave different results for the aqueous concentrations and the evolution of the mineral species. The discrepancies are mainly due to the differences in the thermodynamic databases and activity models. The simulations with the same equilibrium constants used in the three codes are in good agreement in the long run, but are still quite different before reaching equilibrium. Significant differences were found in the equilibrium constants used in their internal databases. This study shows how critical the selection of these data is. Hence the experience of the modeller is critical for the outcome of the modelling process. However, as was pointed out by Zhu and Anderson (2002) *"...judging the quality of thermodynamic data is a job for specialists, and even they often do not agree among themselves.*"

Reservoir engineers have a good understanding of multiphase flow in reservoirs, but they usually do not have extensive knowledge of geochemical modelling because

geochemical processes are not as important in petroleum reservoir simulations as in geological storage of CO_2 because of the considerable time perspective for storage. On the other hand, geochemists have good experience of these processes. Therefore, collaboration between reservoir engineers and geochemists is essential for accurate prediction of fluid rock interactions during CO_2 storage.

As the kinetic data are not well known and the thermodynamic data are uncertain, the results of the geochemical modelling should be treated as qualitative rather than quantitative. In order to verify the results, they need to be tested against experimental data and field observations. This is challenging because of the long timescales of the geochemical processes. However, the data from the early stages of CO_2 storage from field observations and experiments on heterogeneous rock samples are still valuable not only to evaluate the changes in injectivity but also to give insights in the trend of the geochemical processes. On the other hand, because of the high number of the parameters and the complexity of the processes involved in heterogeneous rocks and real brines, it is difficult to interpret the thermodynamic and kinetic data from these kinds of observations and specific experiments are needed to obtain the thermodynamic and kinetic data.

It could be easily argued that without transport processes batch modelling has limited application to the geochemical modelling of CO_2 storage, as injection of large quantities of CO_2 involves complex coupled physical and chemical processes. Although reactive transport modelling is more appropriate for proper modelling of these processes, batch modelling gives important insights into reaction paths and chemical processes in the aqueous phase, and it is a good starting point to build a reactive transport model.

5.5 References

Audigane, P., Oldenburg, C.M., van der Meer, B., Geel, K., Lions, J., Gaus, I., Robelin, C., Durst, P. and Xu, T., 2007, Geochemical modelling of the CO_2 injection into a methane gas reservoir at the K12-B field, North Sea, Special publication of AAPG on geological storage of CO_2.

Bazin, B., Brosse, É. and Sommer, F., 1997, Chemistry of oil-field brines in relation to diagenesis of reservoirs 1. Use of mineral stability fields to reconstruct in situ

water composition, Example of the Mahakam basin, Marine and Petroleum Geology, 14(5): 481-495.

Bjorkum, P.A. and Gjelsvik, N., 1988, An isochemical model for formation of authigenic kaolinite, K-feldspar and illite in sediments, Journal of Sedimentary Research, 58(3): 506-511.

Bjorlykke, K., Aagaard, P., Egeberg, P.K. and Simmons, S.P., 1995, Geochemical constraints from formation water analyses from the North Sea and the Gulf Coast Basins on quartz, feldspar and illite precipitation in reservoir rocks, Geological Society, London, Special Publications, 86(1): 33-50.

Bjorlykke, K., Nedkvitne, T., Ramm, M. and Saigal, G.C., 1992, Diagenetic processes in the Brent Group (Middle Jurassic) reservoirs of the North Sea: an overview, Geological Society, London, Special Publications, 61(1): 263-287.

Cantucci, B., Montegrossi, G., Vaselli, O., Tassi, F., Quattrocchi, F., Perkins, E.H., 2009, Geochemical modeling of CO_2 storage in deep reservoirs: The Weyburn Project (Canada) case study, Chemical Geology, 265(1-2): 181-197.

Duan, Z., Møller, N. and Weare, J.H., 1992a, An equation of state for the CH_4-CO_2-H_2O system: I. Pure systems from 0 to 1000°C and 0 to 8000 bar, Geochimica et Cosmochimica Acta, 56(7): 2605-2617.

Duan, Z., Møller, N. and Weare, J.H., 1992b, An equation of state for the CH_4-CO_2-H_2O system: II. Mixtures from 50 to 1000°C and 0 to 1000 bar, Geochimica et Cosmochimica Acta, 56(7): 2619-2631.

Gaus, I., Azaroual, M. and Czernichowski Lauriol, I., 2005, Reactive transport modelling of the impact of CO_2 injection on the clayey caprock at Sleipner (North Sea), Chemical Geology, 217(3-4): 319-337.

Helgeson, H.C., 1969, Thermodynamics of hydrothermal systems at elevated temperatures and pressures, Am J Sci, 267: 729-804

Helgeson, H.C., Kirkham, D.H. and Flowers, G.C., 1981, Theoretical prediction of the thermodynamic behavior of aqueous electrolytes by high pressures and temperatures; IV, Calculation of activity coefficients, osmotic coefficients, and

apparent molal and standard and relative partial molal properties to 600 degrees C and 5kb, Am J Sci, 281(10): 1249-1516.

Johnson, J.W., Nitao, J.J. and Knauss, K.G., 2004. Reactive transport modelling of CO_2 storage in saline aquifers to elucidate fundamental processes, trapping mechanisms and sequestration partitioning. Geological Society, London, Special Publications, 233(1): 107-128.

Kaszuba, J.P., Janecky, D.R. and Snow, M.G., 2005. Experimental evaluation of mixed fluid reactions between supercritical carbon dioxide and NaCl brine: Relevance to the integrity of a geologic carbon repository. Chemical Geology, 217(3-4): 277.

Kharaka, Y.K., Cole, D.R., Thordsen, J.J., Kakouros, E. and Nance, H.S., 2006. Gas-water-rock interactions in sedimentary basins: CO_2 sequestration in the Frio Formation, Texas, USA. Journal of Geochemical Exploration, 89(1-3): 183-186.

Steefel, C.I. and Lasaga, A.C., 1994, A coupled model for transport of multiple chemical species and kinetic precipitation/dissolution reactions with application to reactive flow in single phase hydrothermal systems, Am J Sci, 294(5): 529-592.

Svensson, U. and Dreybrodt, W., 1992, Dissolution kinetics of natural calcite minerals in CO_2-water systems approaching calcite equilibrium, Chemical Geology, 100(1-2): 129-145.

Thibeau, S., Nghiem, L. and Ohkuma, H., 2007, A Modeling Study of the Role of Selected Minerals in Enhancing CO_2 Mineralization During CO_2 Aquifer Storage, SPE Annual Technical Conference and Exhibition, Anaheim, California, USA, SPE 109739.

Wigand, M., Carey, J.W., Schütt, H., Spangenberg, E. and Erzinger, J., 2008, Geochemical effects of CO_2 sequestration in sandstones under simulated in situ conditions of deep saline aquifers, Applied Geochemistry, 23(9): 2735.

T.J. Wolery, 1992, EQ3NR, A computer program for geochemical aqueous speciation-solubility calculations: Theoretical manual, user's guide, and related

documentation (Version 7.0), Lawrence Livermore National Lab., Livermore, CA, USA.

Xu, T., Apps, J.A. and Pruess, K., 2005, Mineral sequestration of carbon dioxide in a sandstone-shale system, Chemical Geology, 217: 295-318.

Zhu, C. and Anderson, G., 2002, Environmental Applications of Geochemical Modeling, Cambridge University Press, Cambridge, New York.

CHAPTER 6

FULL FIELD REACTIVE TRANSPORT MODELLING: TRAPPING CAPACITY OF THE RANNOCH FORMATION

In the previous chapter modelling work was carried out using batch models to give insight into geochemical reactions and to prepare the geochemical data for reactive transport models. In this chapter reactive transport modelling of CO_2 storage in an aquifer is studied. The formation chosen for this propose is the Rannoch formation because it has the highest potential for CO_2 mineralization among the formations studied in the previous chapter. The main goal of the simulations is to identify the CO_2 trapping capacity of the aquifer in mineral forms.

6.1 Model Set Up

The first attempt at modelling was performed using GEM. However, there were difficulties due to convergence problems and long execution times. Hence, MoReS was used for the rest of the modelling. A comparison of simulation results carried out with both codes is given in Section 6.2.

6.1.1. Assumptions

The reservoir simulation model is based on the following assumptions:

- 100% CO_2 purity
- Isothermal conditions
- No flow boundaries.

6.1.2. Geological model and Reservoir Properties

As the aim of the modelling is to study the trapping capacity of the Rannoch formation and not a specific aquifer, a generic aquifer model representing the characteristics of the formation and the conditions prevalent in the UK Continental Shelf is used. The geological model of a tilted aquifer was created by Dr. Min Jin for CO_2 storage modelling using Petrel. The Petrel model was imported to GEM via Eclipse, and to MoReS via REDUCE++. The original model has a 200 m horizontal grid block size. Petrophysical properties of the Rannoch formation were assigned to the model. As reactive transport models are computationally expensive the model was upscaled to 1000m horizontal grid size (labelled as coarse grid model) in Petrel and then refined around the wellbore and the CO_2 plume (labelled as refined grid model) in GEM and MoReS. The discretization of the grid is shown in Figures 6.1 and 6.2.

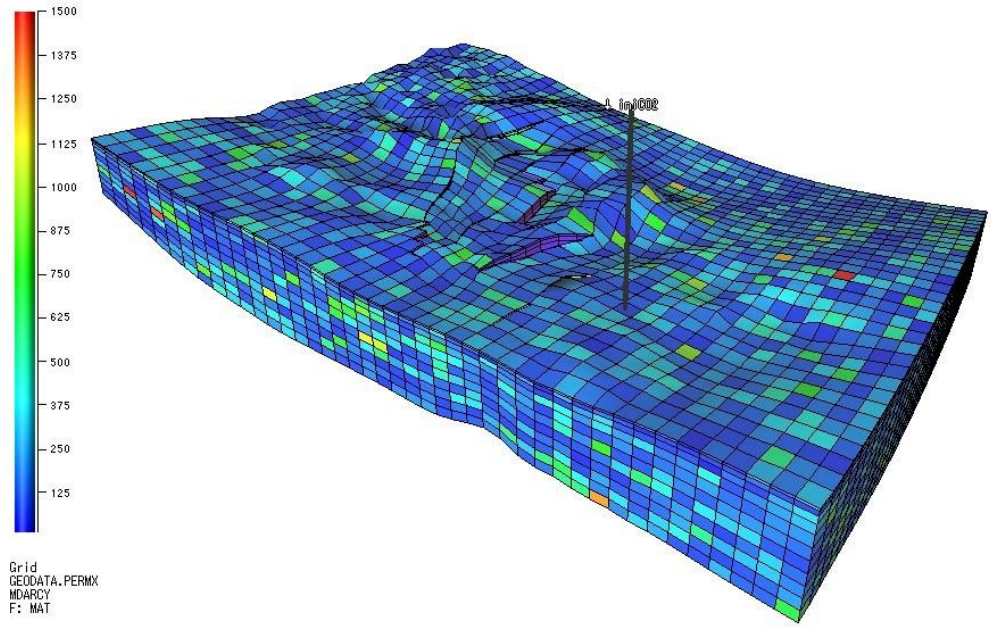

Figure 6.1 Coarse grid model (35*43*11grid blocks): permeability distribution

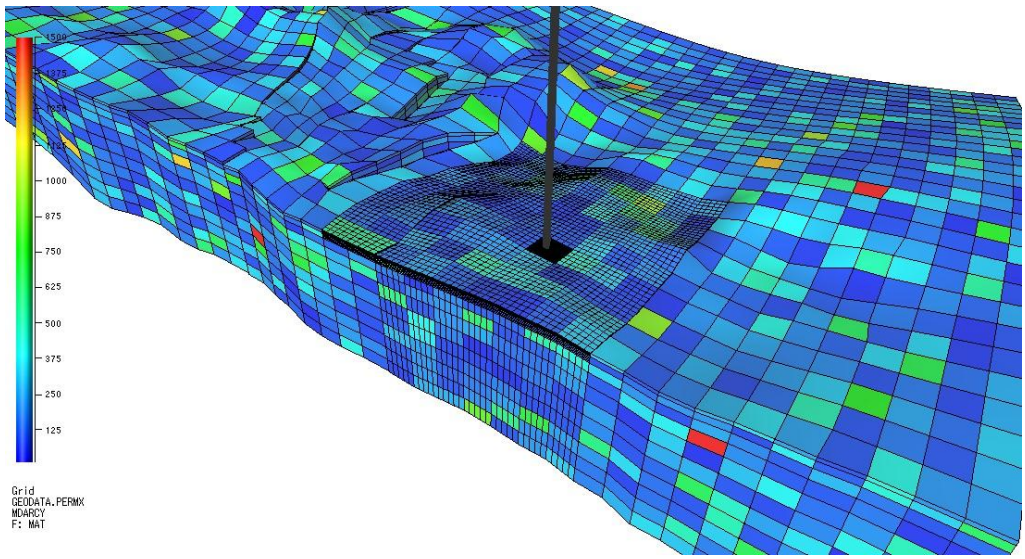

b)

Figure 6.2 Refined grid model: the upper two layers are refined around the CO_2 plume and the remaining layers are refined around the wellbore

The grid thickness is variable with thin top layers. The average depth of the formation is 2600 m. There are 11 faults in the model. The connectivity of the faults is set to zero. The grid properties are given in Table 6.1.

Table 6.1 Grid properties

Property	**3D Coarse**	**3D Refined**
Number of grid cells	15609	61634
Horizontal grid size (m)	1000	40-1000
Grid thickness (m)	4.86-51.79	0.67-51.79

The model has heterogeneous porosity and permeability distributions with average values 0.25 and 200mD respectively. The temperature and pressure of the aquifer at

2700 m depth is 92°C and 430 bar. A temperature gradient of 0.035°C /m and hydrostatic equilibrium[6] is assumed. Aquifer properties are summarized in Table 6.2.

Table 6.2 Aquifer properties

Property	**Value**
Temperature (°C)	92
Pressure (bar)	430
Reference depth (m)	2700
Porosity	0.250
Horizontal permeability (mD)	200
Vertical permeability (mD)	20

No measured relative permeability data were available so these data were taken from Bennion and Bachu (2008). The relative permeability model parameters are given in Table 6.3. The relative permeability model was created by Corey correlations for two-phase system. Both imbibition and drainage curves were defined to model gas relative permeability hysteresis in MoReS. In GEM it is not allowed to define both curves and hysteresis was modelled by using only the imbibition curve end point for the gas phase.

[6] The differences in calculation of pressures by the two codes lead to minor differences in pressure. GEM calculates the pressures from hydrostatic gradient and saturations. MoReS calculates the pressures only from hydrostatic gradient with the default phase as gas for a water-gas system if the phase is not specified.

Table 6.3 Relative permeability data: S_{wc} is critical water saturation, S_{rg} is residual gas saturation, k_{rw} and k_{rg} are relative permeability of water and gas respectively, and c_w and c_g are Corey water and gas exponent respectively

Curve	S_{wc}	S_{rg}	k_{rw}	k_{rg}	c_w	c_g
Drainage	0.423	0	1	0.2638	1.7	2.8
Imbibition	0.423	0.297	0.3646	0.2638	2.1	4

A single injection well is located down dip. A constant injection rate of $2.14*10^7$ Sm^3/day for a period of 15 years from bottom five layers is assumed. This injection rate corresponds to circa 15 Mt of CO_2 per year which is roughly equivalent to the emissions from an 1800 MW coal power plant. The injection was controlled by maximum bottomhole pressure (BHP) of 600 bar, which is less than the lithostatic pressure. However the set injection rate was achieved because the BHP never exceeded the maximum value. It should be noted that typical injection rates will be order of magnitude lower, not due to the risk of rock failure but due to pumping constraints, and thus these calculations would represent the highest flow velocities in the near well zone that are likely to be observed.

6.1.3. Fluid properties and geochemical data

Peng–Robinson equation of state was used to model the thermodynamic properties of the fluids. In GEM the Rowe–Chou correlation (Rowe and Chou, 1970) was used to calculate the aqueous phase density and the correlation of Kestin (1981) was used to calculate aqueous phase viscosity as a function of pressure, temperature and salinity. In MoReS the aqueous phase density was calculated with the model given by Garcia (2001) and the aqueous viscosity was calculated by an internal correlation.

The initial composition of the aqueous phase and minerals is the same as the Rannoch core sample model in Chapter 5. In MoReS the mineral reactions were modelled using a kinetics approach, with the exception of carbonates which were modelled using an equilibrium approach. In GEM all minerals were modelled using a kinetics approach.

6.2 Results and discussion

6.2.1. Coarse Grid Model Simulations

The base case of the simulations ran without considering the geochemical reactions in order to better identify the differences between GEM and MoReS. The duration of the simulated time was 600 years from the start of injection. The comparison is plotted in Figures 6.3 and 6.4.

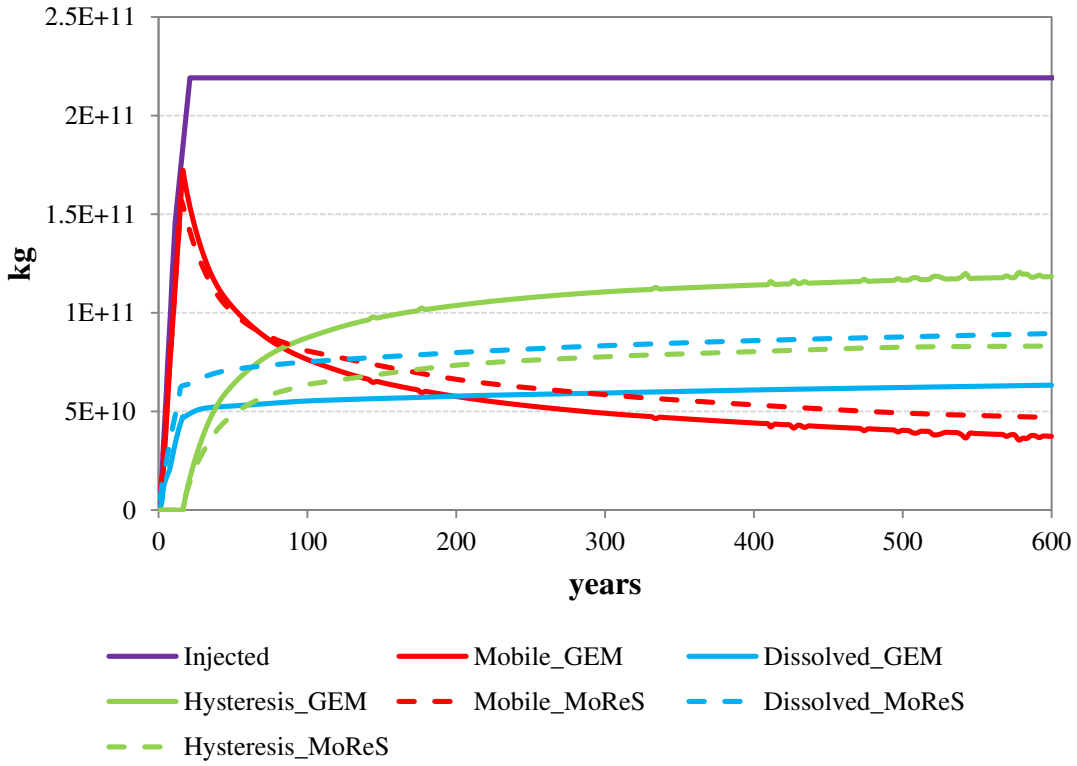

Figure 6.3 Evolution of CO_2 in different phases when geochemical reactions are not considered (continuous lines are GEM predictions, dashed lines are MoReS predictions)

The main difference between GEM and MoReS runs is the quantity of dissolved CO_2 and CO_2 trapped by hysteresis. Differences in residual trapping are due to differences in the calculations mentioned in Section 6.1. Differences in dissolved CO_2 are partly due to the differences in the residual trapping and partly due to the differences in modelling of CO_2 dissolution. Since less CO_2 is trapped by hysteresis more mobile CO_2 is available to migrate and dissolve. In MoReS dissolution of CO_2 is calculated using the PHREEQC module by reading the fugacity from the reservoir module. This causes

higher dissolution values with respect to GEM. The CO_2 plume flowed laterally about 4000 m at most from the injection well in the top layer. Most of the solubility and hysteresis trapping were observed in the first years although both of the trapping increased slowly during entire simulation period.

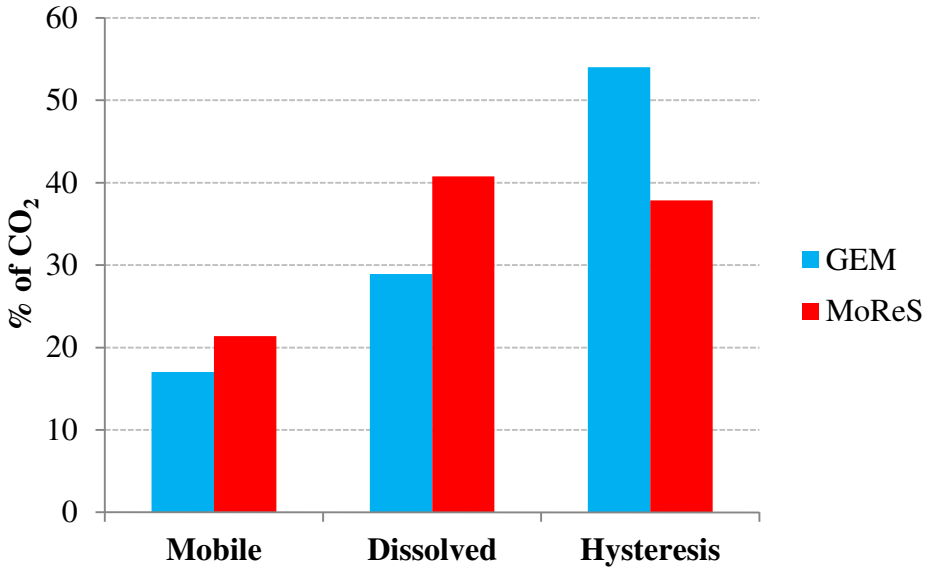

Figure 6.4 Distribution of CO_2 in different phases after 600 years when geochemical reactions are not considered: GEM and MoReS

Although there were no problems in running the 1D model in the previous chapter, GEM had great difficulty in running the 3D model with geochemical reactions. This was overcome only by reducing the kinetic rates of all minerals by two orders of magnitude. After the injection, CO_2 migrated to the upper layers and reached the top layer in 5 years. The CO_2 plume flowed laterally about 3500 m from the injection well in the top layer and 1500 m in other layers. After 200 years the system reached quasi-steady state. The distribution of the CO_2 in different phases is given in Figure 6.5. However the differences between the codes are small and the difference in mineralization between the two runs is about 3.5% as shown in Figure 6.6.

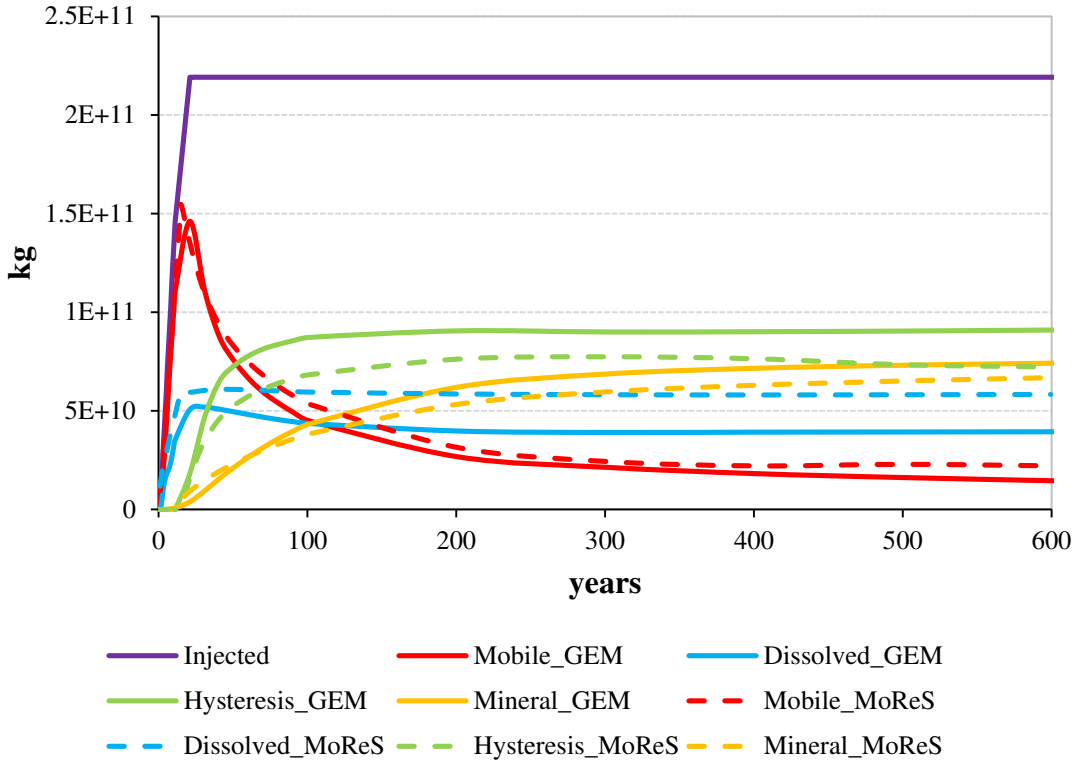

Figure 6.5 Evolution of CO_2 in different phases (continuous lines are GEM predictions, dashed lines are MoReS predictions)

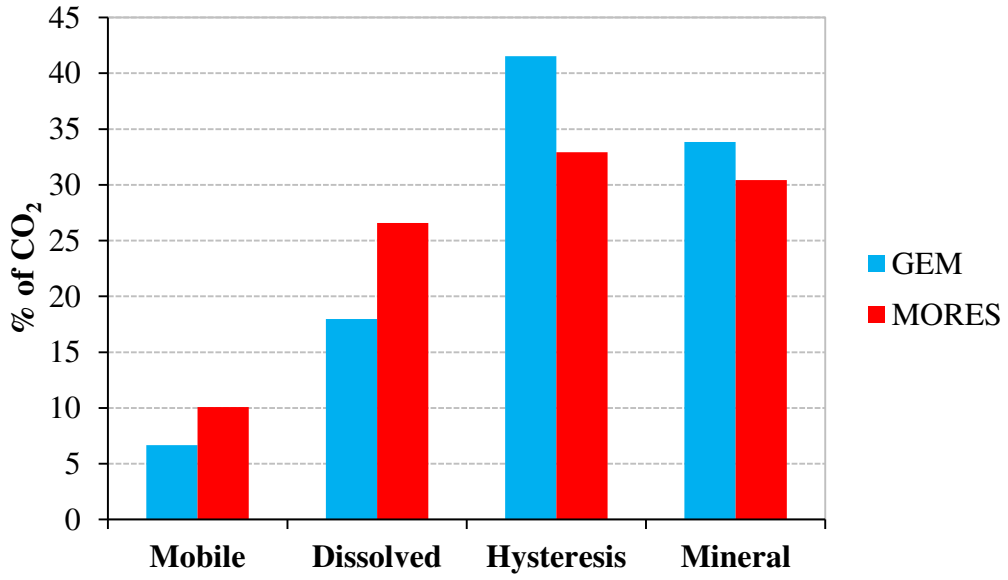

Figure 6.6 Distribution of CO_2 in different phases after 600 years: GEM and MoReS

The pH of the aquifer decreased from 6.48 to 4.7 inside the plume in the GEM simulation and from 6.33 to 4.47 in the MoReS simulation. The reduction of pH induced the dissolution of clinochlore and K-feldspar. Chalcedony and muscovite precipitated. CO_2 was mineralized as magnesite. Dolomite was not formed. The evolution of minerals with time is given on Figure 6.7. The change of porosity due to mineral reactions was negligible.

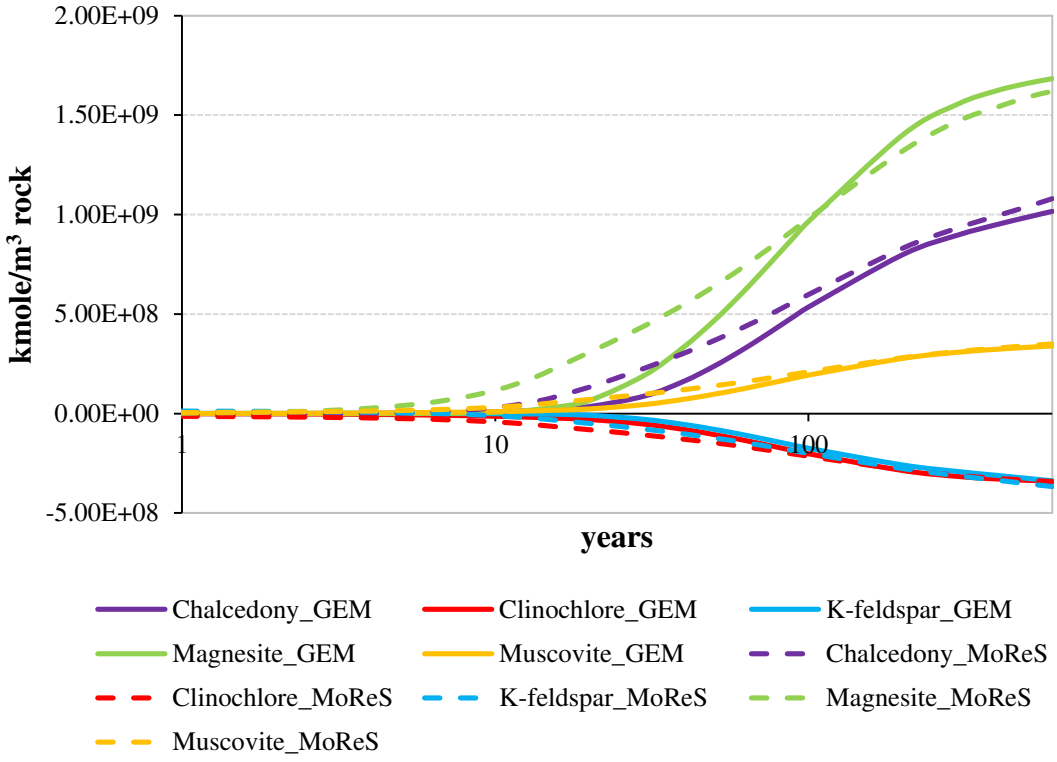

Figure 6.7 Mineral changes in moles per m³ of rock with time (+ values precipitation, - values dissolution). The x-axis is in log units to show short term changes.

6.2.2. Effect of kinetic rates

Since these simulations were performed with slower kinetic rates, simulations with the original kinetic rates were carried out using MoReS for comparison. It can be seen in Figures 6.8 and 6.9 that no significant difference was observed other than that the equilibrium was reached earlier and the graphs are translated on the x-axis. This can be explained by the combined effect of advection and kinetics. Since more free CO_2 is available with the slow kinetics, the CO2 plume flows and expose to the fresh grid

blocks. The overall effect at reservoir scale is faster mineralization. The model with faster kinetic rates reaches the same level of mineralization after 500 years.

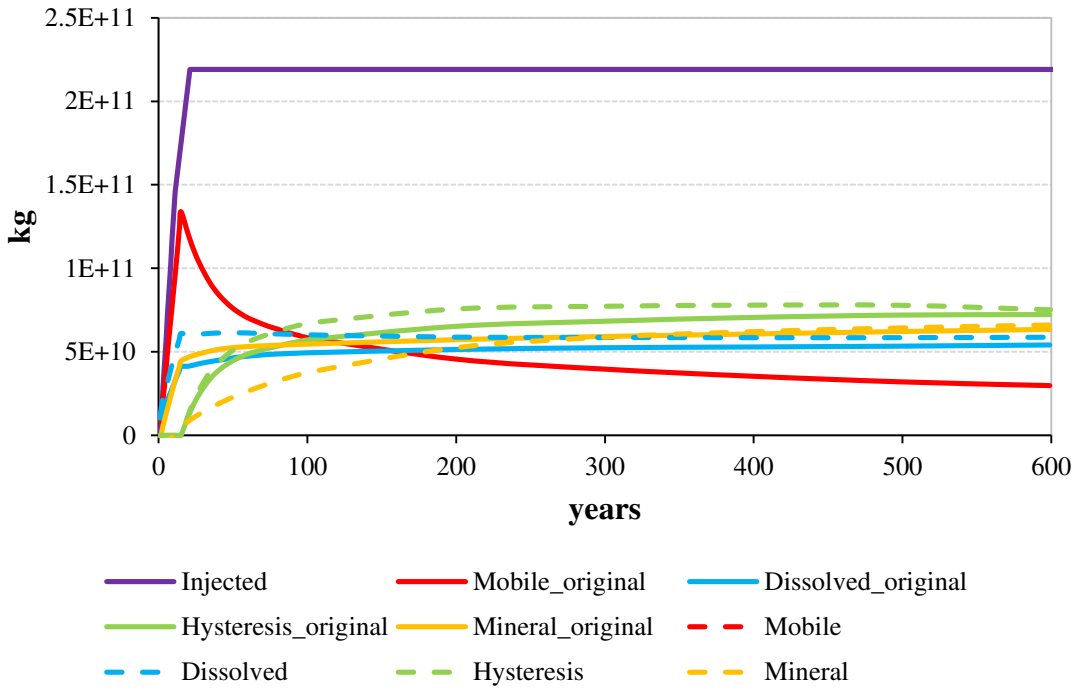

Figure 6.8 Evolution of CO_2 in different phases: comparison of run with original kinetic rates (continuous lines) and run with kinetic rates two orders of magnitude smaller (dashed lines)

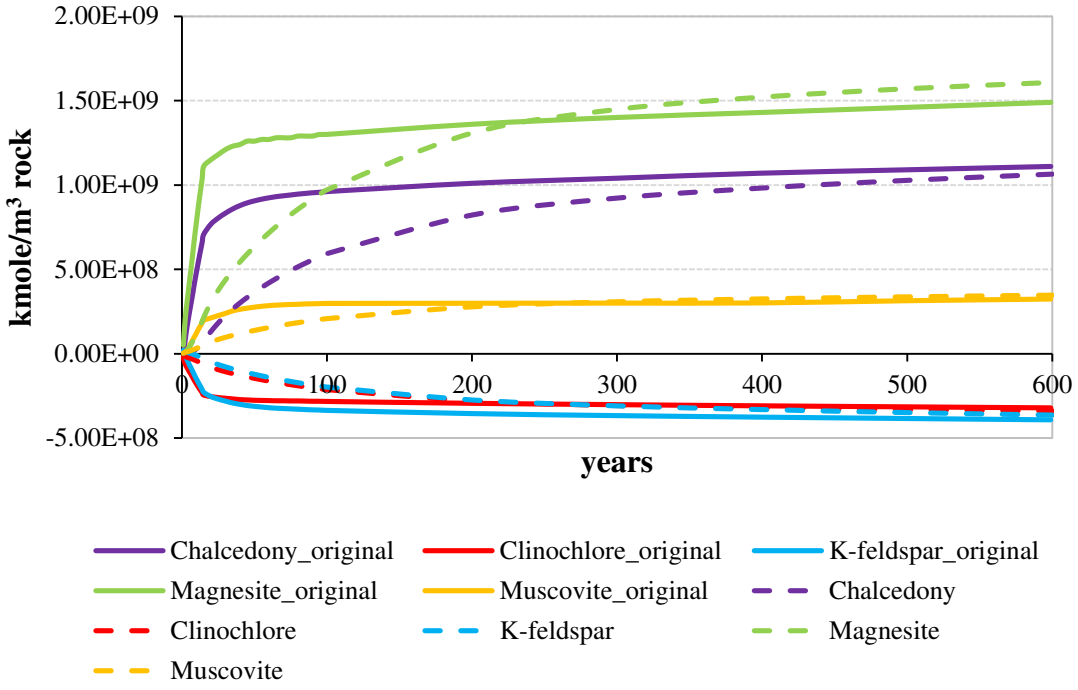

Figure 6.9 Mineral changes in moles per m^3 of rock with time (+ values precipitation, - values dissolution): comparison of run with original kinetic rates (continuous lines) and run with kinetic rates two orders of magnitude smaller (dashed lines)

6.2.3. Effect of grid resolution (Refined grid model)

The grid resolution in the coarse model does not adequately represent the CO_2 plume and buoyancy effects. The model was improved by application of local grid refinement and used for the rest of the simulations. MoReS was employed for the refined grid simulations. The gas saturation of the coarse grid model and refined grid model after 600 years is shown in Figures 6.10 and 6.11. It can be seen that more CO_2 accumulated in the upper part of the aquifer in the refined grid model. This is due to the lower mobility of the CO_2 plume with respect the coarser grid model and consequently less exposition to the fresh rock.

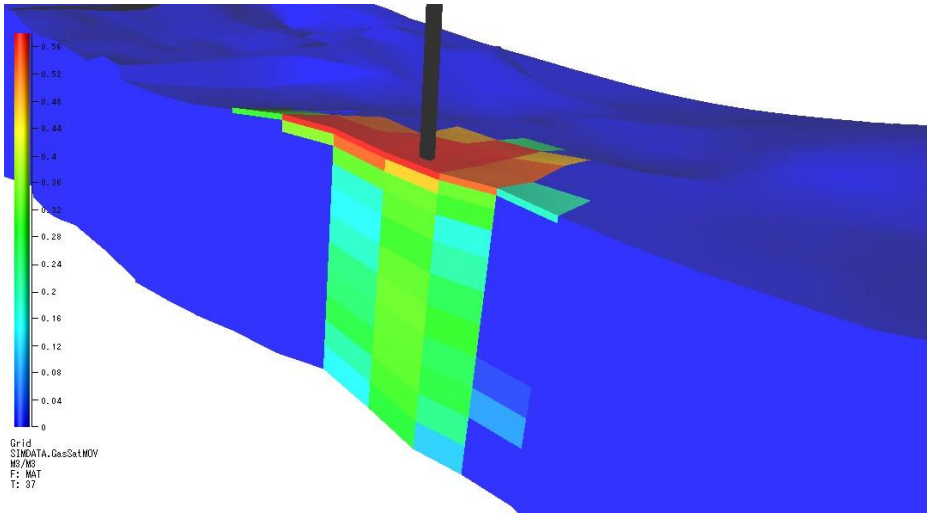

Figure 6.10 Coarse grid model: gas saturation after 600 years

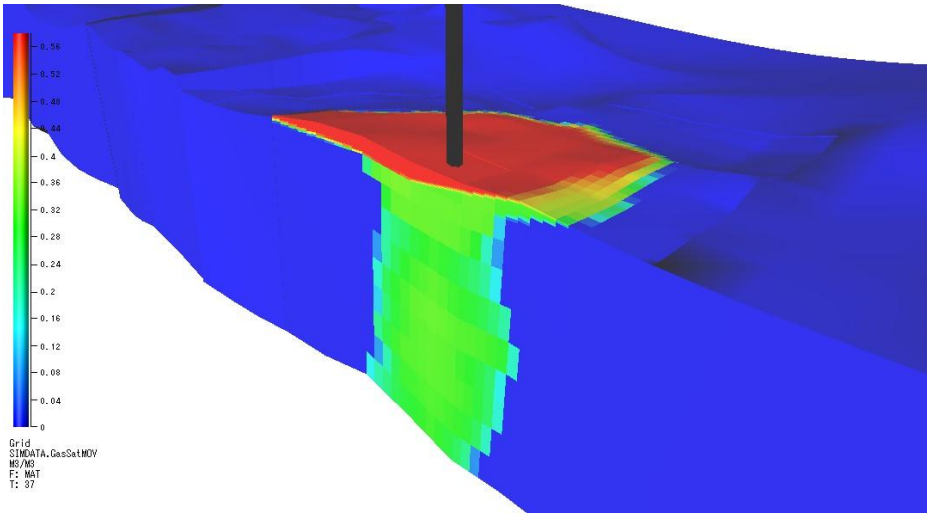

Figure 6.11 Refined grid model: gas saturation after 600 years

The grid resolution had a strong impact on the inventory of CO_2 (Figures 6.12 and 6.13). In the refined model more CO_2 was trapped by hysteresis because less CO_2 was dissolved and the movement of CO_2 towards the upper parts was enhanced due to buoyancy. Significantly less dissolution and precipitation of minerals were also observed with the refined grid (Figure 6.14).

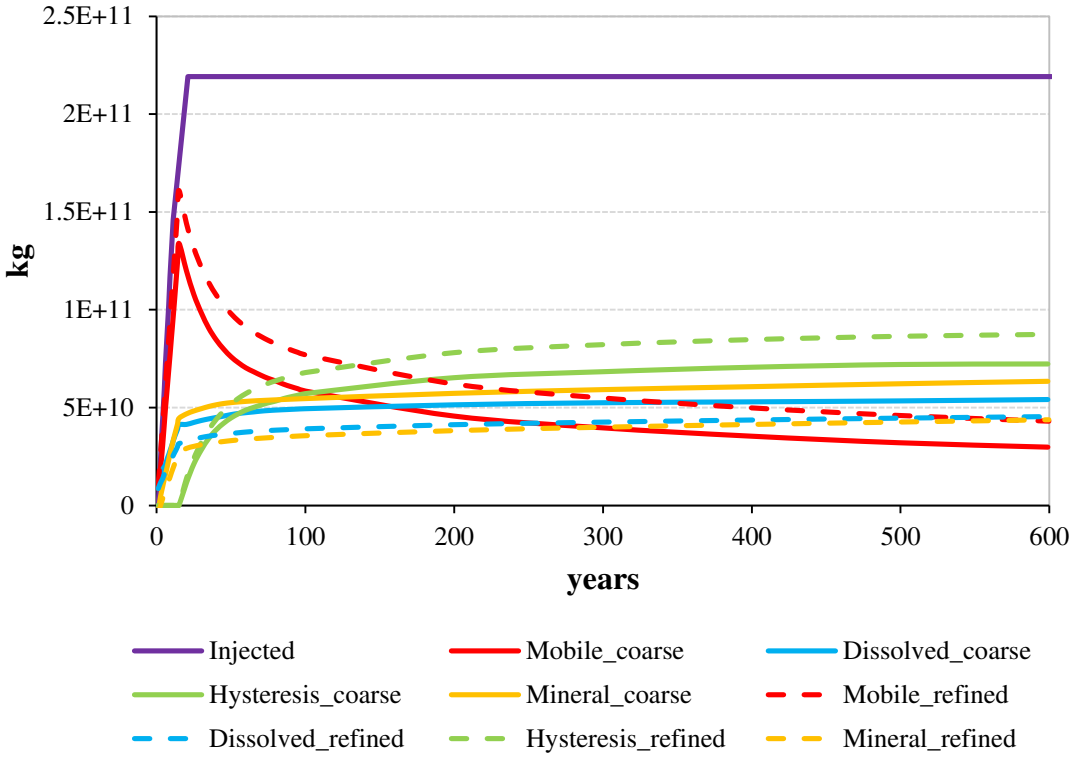

Figure 6.12 Evolution of CO_2 in different phases: comparison of coarse grid model (continuous lines) and refined grid model (dashed lines)

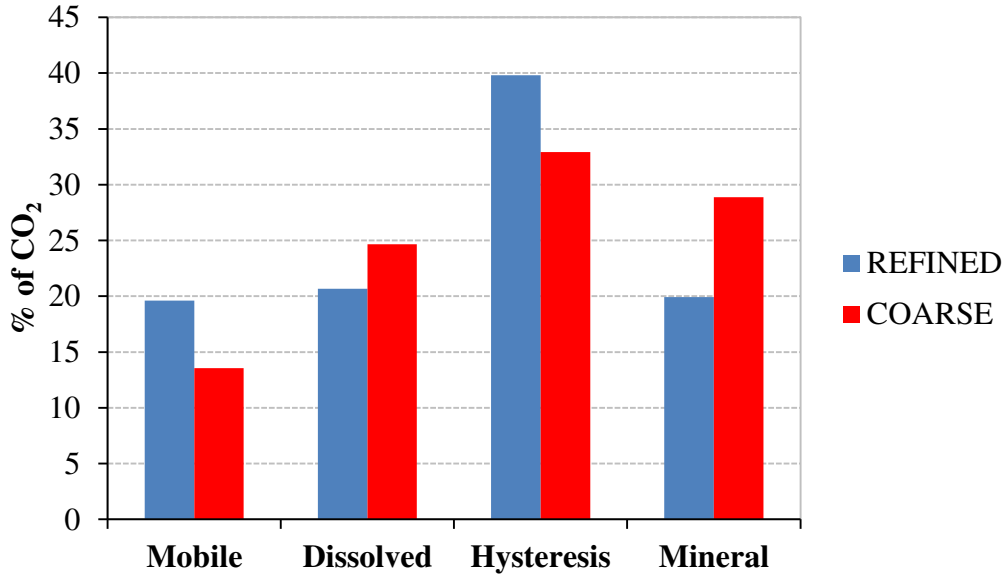

Figure 6.13 Distribution of CO_2 in different phases after 600 years: refined and coarse grid

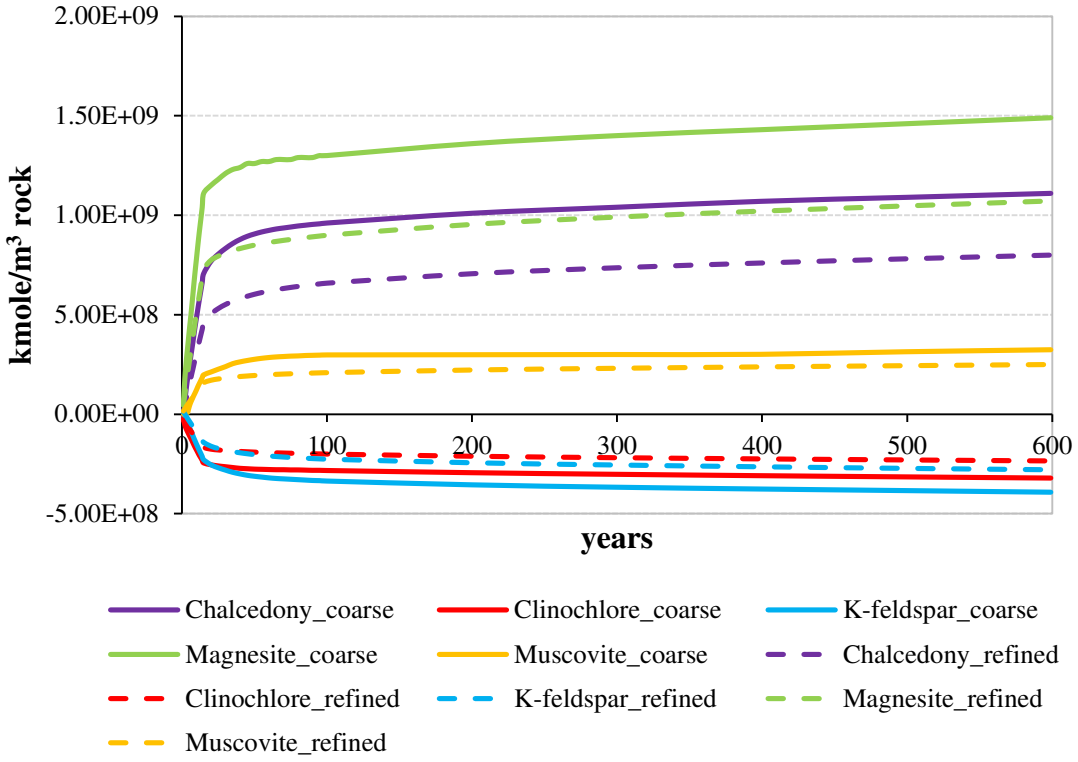

Figure 6.14 Mineral changes in moles per m^3 of rock with time (+ values precipitation, - values dissolution): comparison of coarse grid model (continuous lines) and refined grid model (dashed lines)

6.2.4. Effect of residual phase saturations

Since there were no measurements of relative permeability data for the formation, simulation without hysteresis modelling was carried out in order to compare the impact of hysteresis on CO_2 trapping. In the simulations without hysteresis modelling the residual gas saturation is zero and only the drainage relative permeability curve was used. The results revealed that hysteresis has a strong effect on the distribution of different CO_2 phases. If hysteresis effects were not taken into account, more CO_2 remained in the mobile phase after 1000 years (Figures 6.15 and 6.16). As there was more mobile CO_2, CO_2 migrated more in the reservoir and dissolved more (Figure 6.17). Consequently more mineralization was observed. The overall impact was comparable to the effect of a coarse grid.

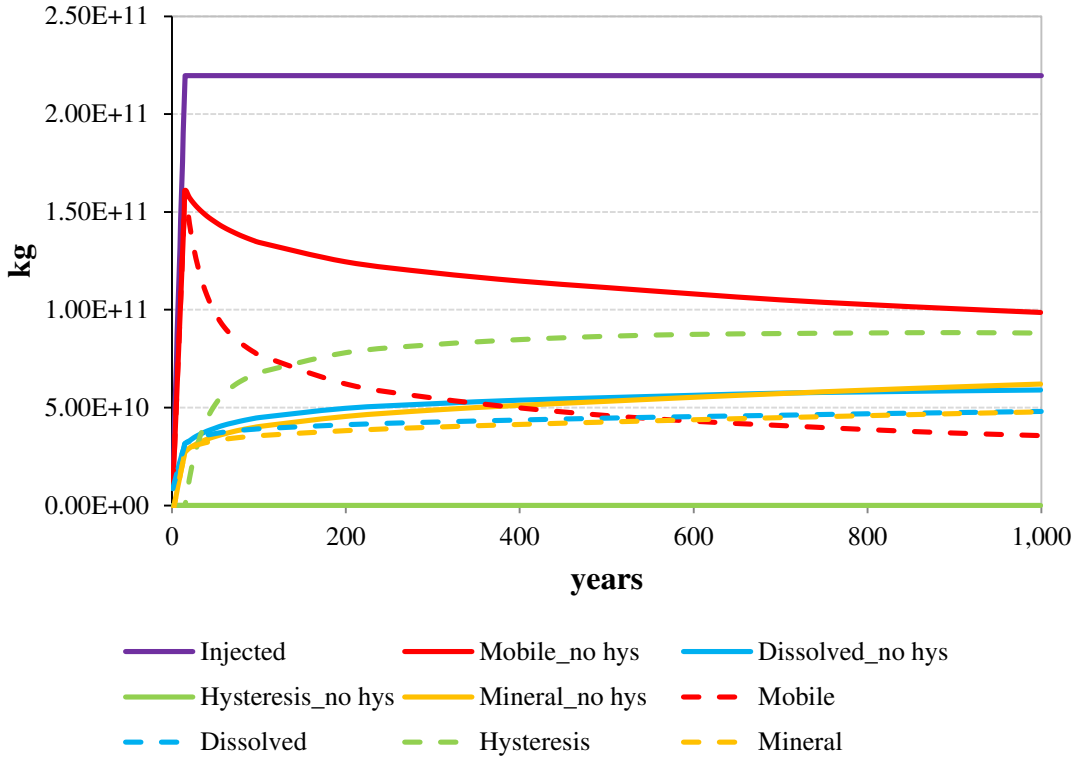

Figure 6.15 Evolution of CO_2 in different phases: comparison of simulations without hysteresis modelling (continuous lines) and with hysteresis modelling (dashed lines)

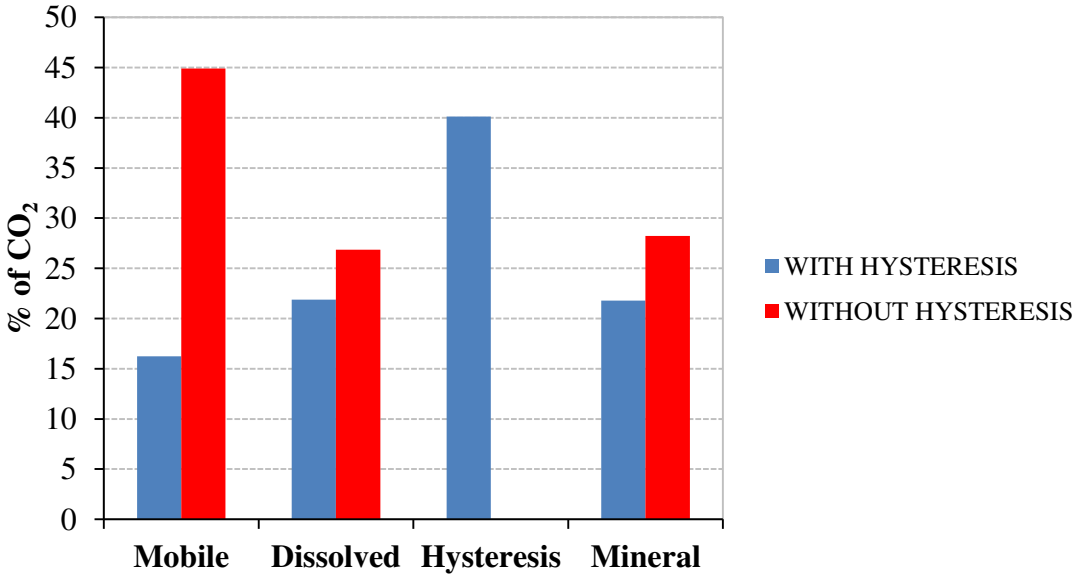

Figure 6.16 Distribution of CO_2 in different phases after 600 years: with and without hysteresis

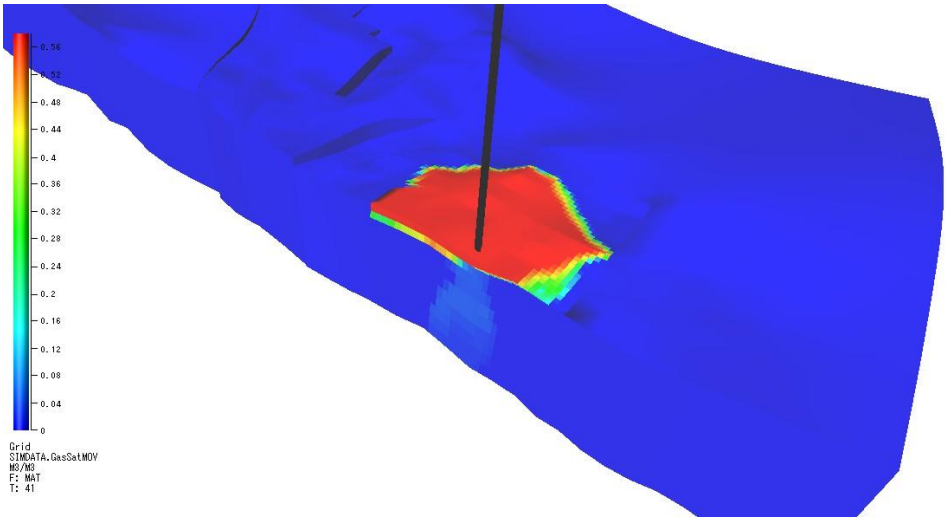

Figure 6.17 Refined grid model without hysteresis: gas saturation after 1000 years

6.2.5. Effect of reaction kinetics

The kinetics and thermodynamic equilibrium models were compared to identify whether thermodynamic equilibrium can be applied. The thermodynamic equilibrium approach gave identical results for the entire duration of the simulations (Figure 6.18). This is because the reaction kinetics are fast due to the high aquifer temperature and high activation energy of clinochlore. The kinetic parameters (reaction rate constants, activation energy and reactive surface areas of the minerals) have high uncertainty. The thermodynamic equilibrium modelling is favourable not only because it is less prone to uncertainty, but also kinetic calculations are computationally intensive for the simulators. The simulation times reduce dramatically with the equilibrium model. In this specific case, the simulation ran 3.75 times faster using the equilibrium approach. The CPU times for both runs are given in Table 6.4. Note that the refined grid model simulations were run using Linux clusters at Shell research laboratories, and the simulation times using an average PC are much longer.

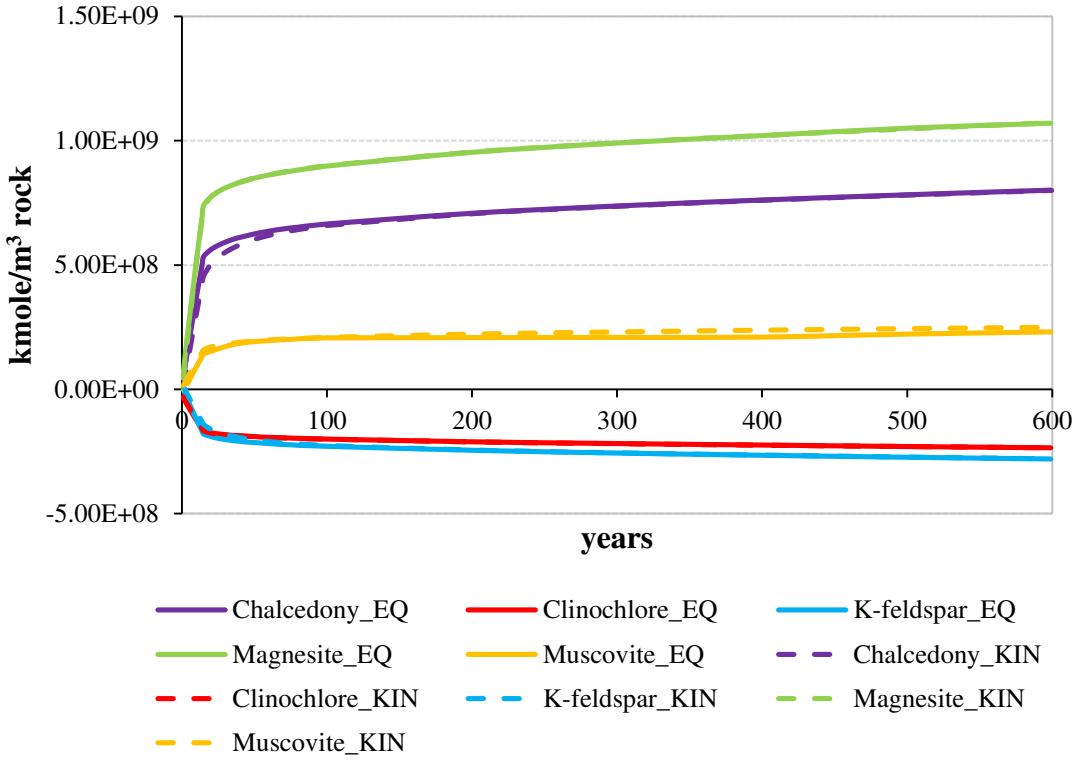

Figure 6.18 CO_2 inventory: Comparison of equilibrium and kinetics approaches

Table 6.4 CPU times for equilibrium and kinetic models

Model	CPU time for reactions (sec.)	Total CPU time (sec.)
Equilibrium	31870	58543
Kinetics	176588	219578

In Figure 6.19 the number of iterations for the grid block 23,30,1 (three blocks away from the injection well) is shown for the two approaches. As can be seen from the pH plot (Figure 6.20), the increase in iterations corresponds to CO_2 breakthrough. The number of iterations decreases substantially if the reaction rates are smaller.

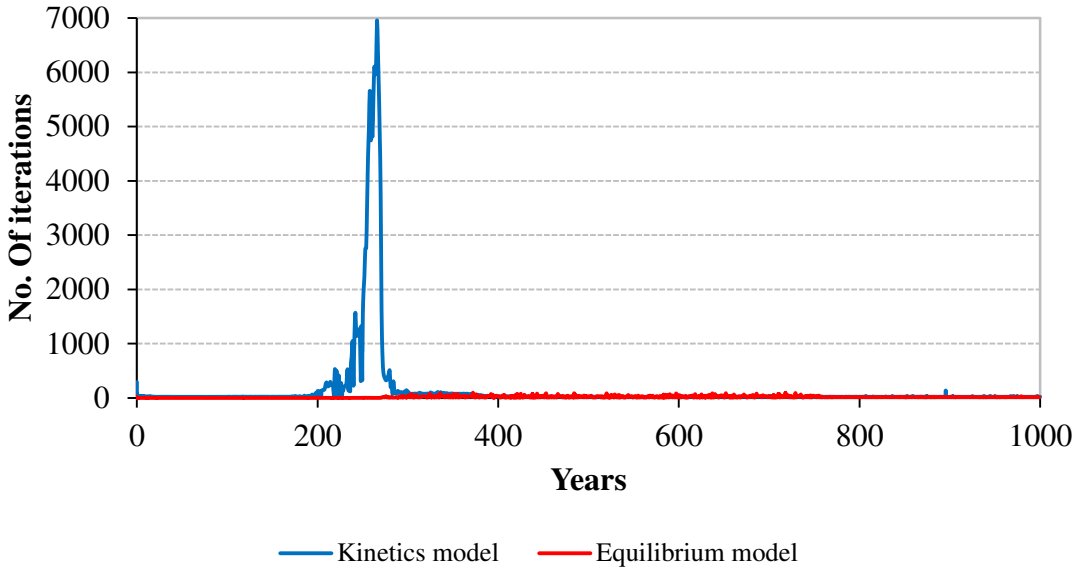

Figure 6.19 Comparison of the number of interactions needed to solve the geochemical reactions by equilibrium and kinetics approach for the grid block 23,30,1/3,3,1

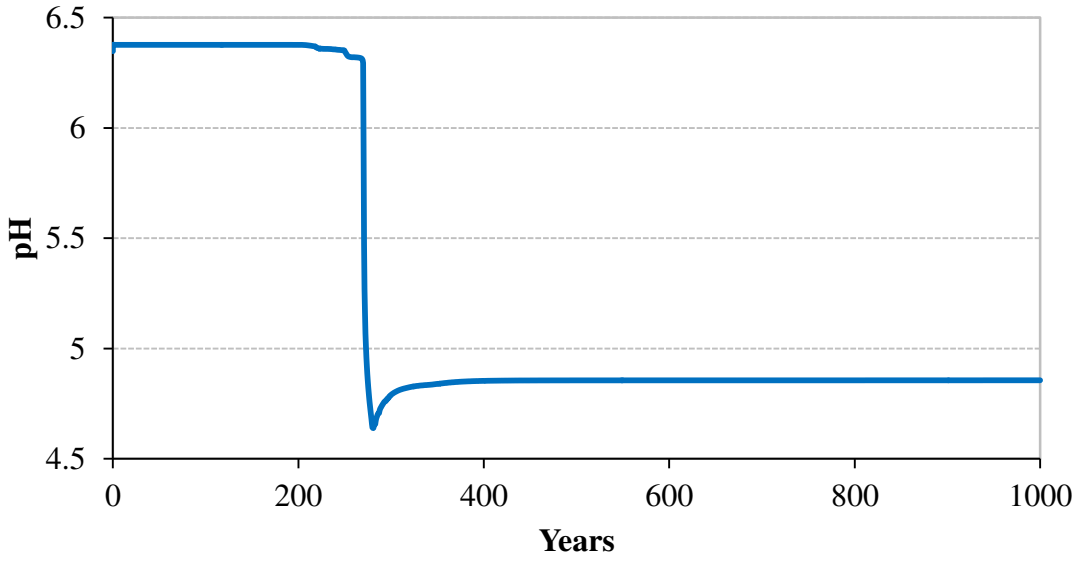

Figure 6.20 Evolution of pH in grid block 23,30,1/3,3,1 in the kinetics model

The two approaches were also compared for a system at 60°C. Although the differences between the two approaches start to become evident, in the long run the results are still the same due the depletion of the reactive minerals (Fig 6.21).

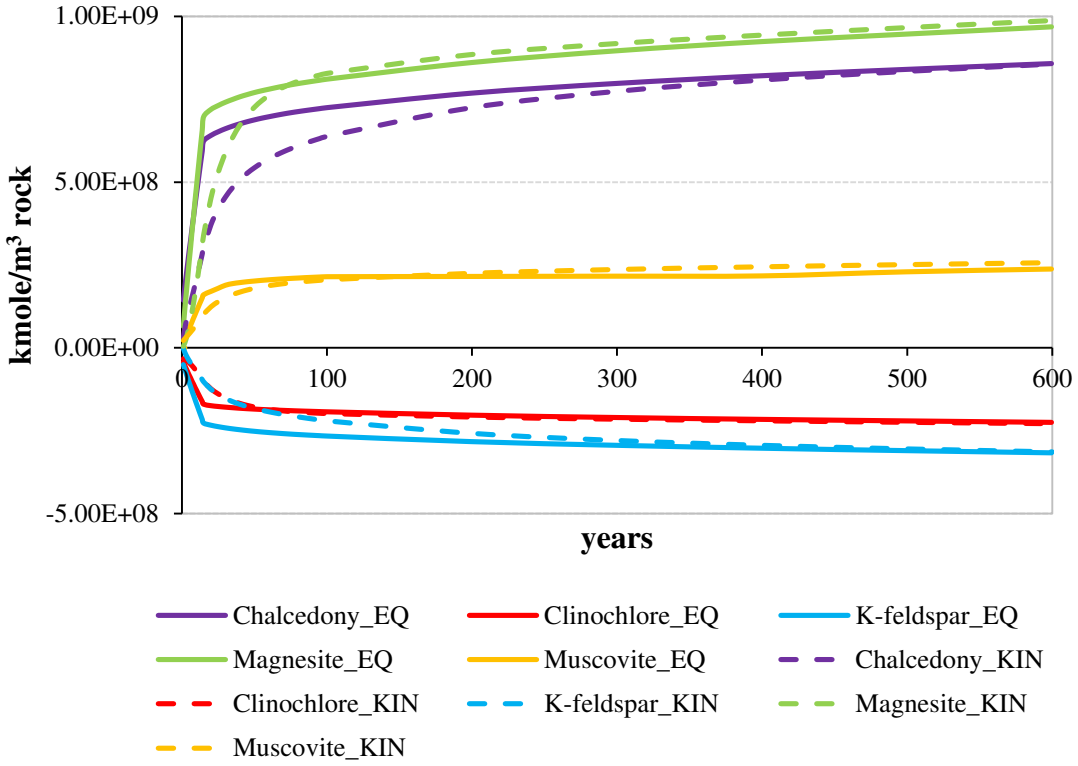

Figure 6.21 CO_2 inventory: Comparison of equilibrium and kinetic approaches at 60°C

It is also worth mentioning that in these models the initial rock contains very little clinochlore (1.5%). As a result it needs little time to be consumed, and after that the reaction rates have no effect. For example the change in clinochlore in grid block 25,30,1/3,3,1 is shown in Figure 6.22. The change of mineral abundance in the equilibrium model is sharp and it is independent of the quantity of mineral present. On the other hand, in the kinetics model the change is smooth and is dependent on the quantity of mineral present. The time needed to reach equilibrium depends on the initial amount of mineral and the availability of CO_2.

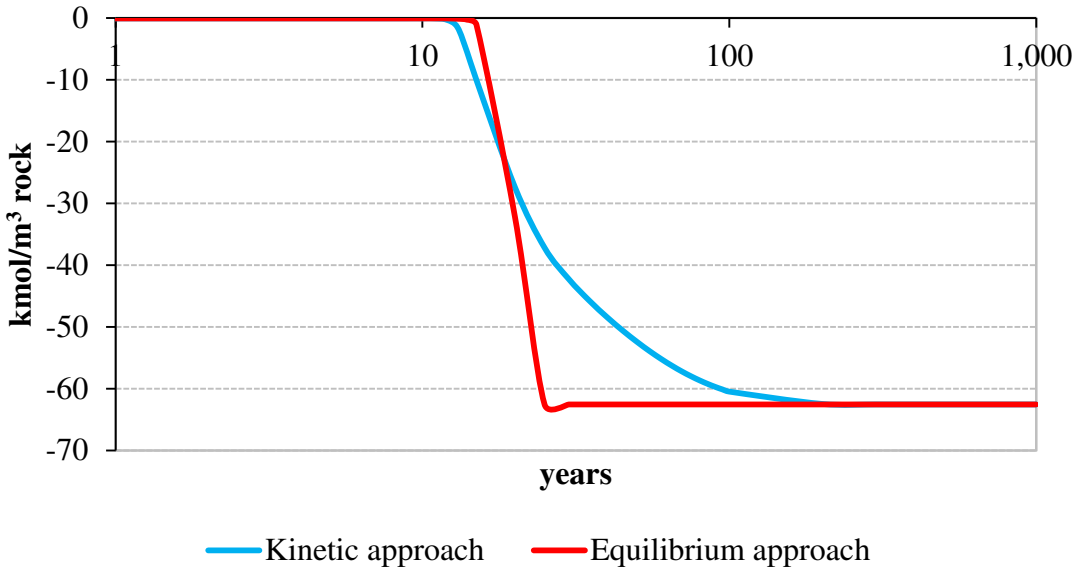

Figure 6.22 Change in abundance of clinochlore in grid block 25,30,1/3,3,1: Kinetics vs. equilibrium model

6.2.6. Effect of clinochlore fraction

The effect of the initial clinochlore content was explored. These sensitivity runs were carried out on a 2D slice of the 3D model where the injection well is located in order to reduce run times. The grid with the porosity distribution is illustrated in Figure 6.23. The initial volume fractions of 1.5, 3 and 5% of clinochlore were compared.

Simulation results indicated that increasing the volume fraction of clinochlore increased the mineral trapping capacity from 28.5% to 55%. This increase decreased the other forms of CO_2 in equal proportions (Figures 6.24 and 6.25).

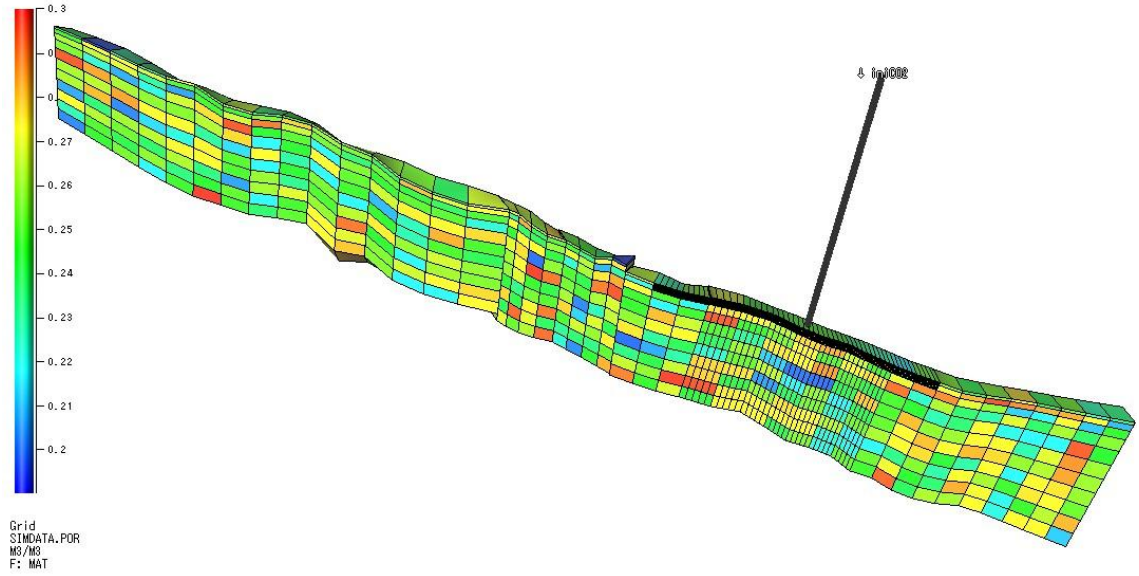

Figure 6.23 2D model: porosity distribution

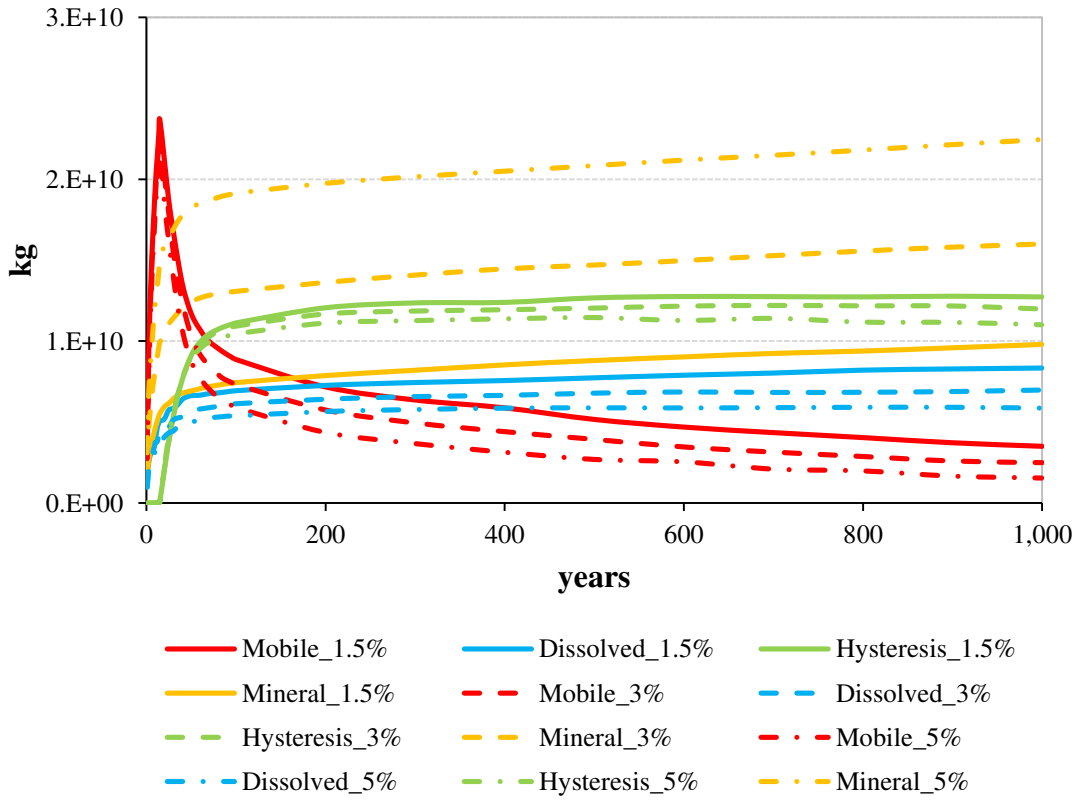

Figure 6.24 Evolution of CO_2 in different phases: comparison of simulations with 1.5%, 3% and 5% initial clinochlore content in the formation

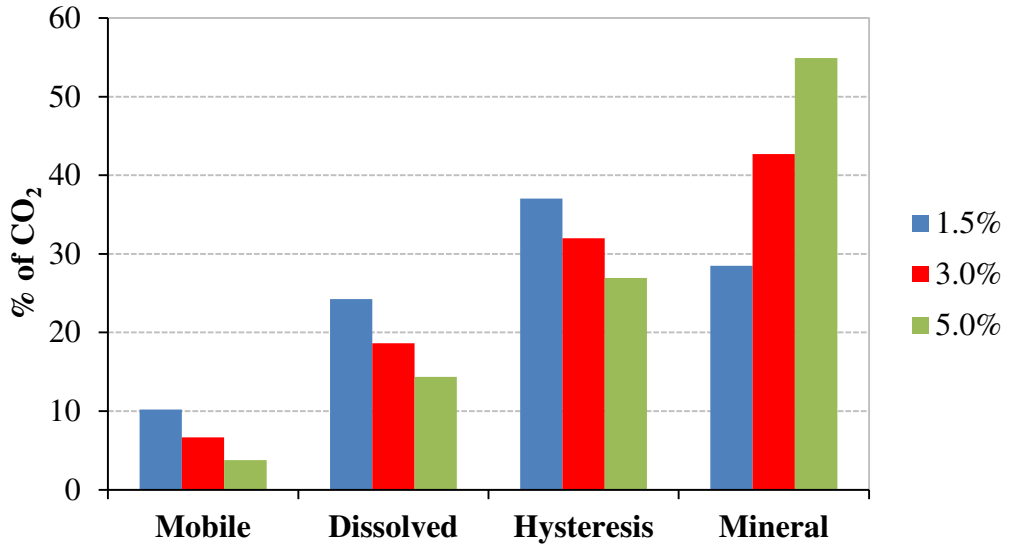

Figure 6.25 Distribution of CO_2 in different phases after 1000 years: 1.5, 3 and 5% initial clinochlore content

6.2.7. Effect of pressure on equilibrium constants

The activities of species are dependent on pressure. For aqueous reactions this can be negligible, but for mineral reactions this can be significant due to the compressibility of minerals (Millero, 1982). The equilibrium constants for the minerals at 460 bar were calculated with the SUPCRT code (Johnson et al., 1992). The equilibrium constants of the minerals as a function of the pressure are given in Table 6.4. For the pressure range of interest the variation of the equilibrium constants with pressure is small compared to the variation with temperature (Table 5.5). Hence no significant difference was observed in the simulations with the updated logK values.

Table 6.4 Equilibrium constants of minerals as a function of pressure, P

Mineral	**logK as a function of P(bar)**
Chalcedony	0.0001P - 2.91
Clinochlore-14A	0.0022P + 49.09
Dolomite-dis	0.0008P + 1.51
K-feldspar	0.001P – 1.61
Magnesite	0.0004P + 0.77
Muscovite	0.0018P + 5.15

6.3 Limitations

Reactive transport models have greater uncertainty compared to batch models due to the increasing number of parameters. The simulations presented in this chapter have uncertainties and approximations.

Since reactive transport modelling is computationally intensive large grid block size are used but the simulation results are sensitive to grid discretization.

The models are discretized in as much as grid blocks of 40*40 m in the horizontal directions and the properties of each block are average properties. Hence processes such as convective mixing and near well processes, which need more resolution, were not accounted for.

One of the major limitations of the simulations is the kinetic parameters. Reactive surface areas, rate constants and activation energies are highly uncertain. These data were taken from the literature, but the original sources of the data were also uncertain. Moreover, nucleation processes, which can delay the precipitation of minerals, were not considered. Hence temporal aspects are not more than informed guesses.

The composition of the formation was considered homogeneous throughout the aquifer, but local heterogeneities can exist and impact the simulation results.

6.4 Conclusions

Simulations presented in this chapter shows that with the current codes we can model the reactive transport of CO_2 storage at the reservoir scale. GEM and MoReS gave similar results. However, there are significant differences in numerical performance of the codes. At current state it is not feasible to use GEM for complex reservoir scale models and it needs further improvement.

Simulations revealed that the thermodynamic equilibrium model and the kinetics model gave the same results. This is case specific, and is true here due to the relatively high reservoir temperature and the very limited initial clinochlore content of the rock. Increasing or decreasing all kinetic rates only changes the time scale of the reactions.

Simulations also suggest that results are sensitive to the grid discretization, and coarser grids estimate more mineral trapping.

Results indicated that the mineral trapping is comparable to solubility trapping. Mineral trapping becomes the dominant mechanism with increase of clinochlore content only from 1.5% to 5% and more than half of the injected CO_2 can be trapped as magnesite.

Results of the simulations also reveal that the magnitude of mineralization is inversely proportional to the magnitude of hysteresis effects.

Simulations also suggest that the effect of pressure on equilibrium constants has no effect on the simulation results.

6.5 References

Garcia, J.E., 2001, Density of aqueous solutions of CO_2, Lawrence Berkeley National Laboratory Report, LBNL-49023.

Johnson, J.W., Oelkers, E.H., Helgeson, H.C., 1992, SUPCRT92: A software package for calculating the standard molal thermodynamic properties of minerals, gases, aqueous species, and reactions from 1 to 5000 bar and 0 to 1000°C, Computers & Geosciences, 18 (7): 899-947.

Kestin, J., Khalifa, H.E. and Correia, R.J., 1981, Tables of the Dynamic and Kinematic Viscosity of Aqueous NaCl Solutions in the Temperature Range 20-150°C and Pressure Range 0.1−35 MPa, *J. Phys. Chem. Ref. Data*, 10: 71-87.

Millero, F.J., 1982, The effect of pressure on the solubility of minerals in water and seawater, Geochimica et Cosmochimica Acta, 46(1): 11-22.

Rowe, A.M. and Chou, J.C.S., 1970, Pressure-Volume-Temperature-Concentration Relation of Aqueous NaCl Solutions, *J. Chem. Eng. Data*, 15: 61-66.

CHAPTER 7

CONCLUSIONS

Carbon capture and storage is a mitigation option for stabilizing greenhouse gases. However, there are concerns for the development of this technology. The main concern is the long term containment of CO_2. The questions that need to be answered are how much CO_2 can be trapped geochemically since mineral trapping is a permanent storage mechanism, and whether CO_2 injection can alter the caprock and wellbore due to the acidification of brine, and thus leak to the surface. The second concern is if CO_2 alters the formation around the wellbore due to the vaporisation of brine and the consequent salt precipitation, and thereby affects the injectivity. Geochemical modelling can partly answer these questions.

This thesis contributes to the development of reliable storage of CO_2 by

- a comprehensive review of previous research on CO_2 induced geochemical reactions (Chapter 2)
- the state of the art review of geochemical modelling of CO_2 storage and identification of the criteria for code selection (Chapter 3)
- evaluation of CO_2 solubility models (Chapter 4)

- benchmarking of numerical codes and identification of trapping capacities of potential North Sea formations (Chapter 5)
- application of the reservoir scale reactive transport modelling of the Rannoch formation and the exploration of the impact of parameters on model behaviour (Chapter 6).

Is there any evidence of CO_2 induced geochemical reactions?

The literature review provided evidence of CO_2 - brine - rock interactions from the previous modelling work, experiments and natural analogue studies. The review suggests that sandstone reservoirs that contain minerals which supply divalent cations by dissolution have greater potential for mineral trapping. The reactions observed are mainly dissolution of feldspars, mica and carbonates with secondary precipitation of carbonates, clays and silica. The review reveals that non-equilibrium conditions can occur over long time frames, but dissolution and precipitation of minerals can also occur within a short time scale. This indicates that the duration of the simulated time required can be very variable. The experimental studies show that the major limitation is the limited duration of the experiments compared to the time scales needed by some of the chemical reactions. The natural analogues give indications of the long term geochemical reactions, but there are difficulties in isolating the CO_2 associated processes due to the complexity of the natural systems and unknown reaction kinetics. Hence the modelling work is essential for the understanding of the long term geochemical reactions. [Chapter 2]

How do we model CO_2 - brine - rock interactions and what are the requirements?

Our goal is to understand and predict the geochemical reactions in the reservoir due to the injection of CO_2 by modelling. The modelling requirements and the criteria for the code selection are identified. There are three main processes that form the basis of geochemical modelling: thermodynamics, reaction kinetics, and flow and transport processes. If the accurate mineralogical and brine analysis, an accurate CO_2 solubility model, thermodynamic database and activity model are all available, then the geochemical equilibrium of the system can be characterized. However, equilibrium assumption is not always valid for minerals other than carbonates and kinetic rate

constants, reactive surface areas and reaction rate laws are required to incorporate reaction kinetics in geochemical models. Due to the complex interactions between flow, transport and chemical processes reactive transport modelling is more suitable to model CO_2 storage. Hence, in addition to the parameters above, site specific parameters such porosity, permeability, flow rate, EOS, pressure and temperature gradients are required. None of the codes used in this study meet all the criteria identified for code selection in Chapter 3. However MoReS is the best choice as it incorporates the advantages of both PHREEQC and GEM; however this code has very limited availability. [Chapter 3]

Can we model CO_2 solubility accurately?

The modelling of CO_2 solubility in brine is important not only for the storage capacity evaluations, but also because the main driver of the geochemical reactions is the acidification of the brine due to the dissociation of the dissolved CO_2. It is demonstrated that accurate CO_2 solubility models are important for the accurate predictions of trapping capacity. CO_2 solubility is a function of temperature, pressure and salinity of the brine. A single EOS that can predict the phase behaviour of CO_2 and brine does not exist. CO_2 solubility is modelled by mixed models that use EOS for the gas phase and the Henry's constants or activity models for the aqueous phase. A number of EOS were evaluated for the calculation of CO_2 fugacity and several solubility models were compared over 50-100°C, 100-500 bar and 0-5M salinity. The comparison indicates that Soave-Redlich-Kwong EOS and Spycher and Reed EOS are not suitable for CO_2 fugacity calculations. Peng-Robinson EOS is the recommended EOS due to its simplicity and relative accuracy. It is demonstrated that the fugacity correction has the greatest impact on the accuracy of the CO_2 calculations compared to salting-out and the pressure dependence of Henry's constants. CO_2 solubility varies significantly between the models. Close attention needs to be paid when primarily geochemical codes are used since these codes overestimate the CO_2 solubility and their thermodynamic data should be tuned. However, none of the models were tested at pressures over 200 bars because no CO_2 solubility data is available; hence some level of uncertainty is present in all models. [Chapter 4]

The modelling studies reviewed in literature are mostly simplified batch or 1D models that rarely take into account the flow and transport. The review also revealed that there are very few studies on North Sea formations and no comparison of the geochemical codes (Chapter 2). This thesis not only tried to extend the modelling to full reservoir scale but also compared the geochemical calculations of North Sea sandstone formations by the most frequently used numerical codes.

Do the geochemical codes give the same answers?

Rannoch, Oseberg and Forties formation core samples were used to compare the three numerical codes, PHREEQC, GEM and TOUGHREACT. As the objective of the comparison is the geochemical calculations, transport effects were not considered. The equilibrium constants of the selected minerals, activity models, dissolved CO_2, pH and evolution of the mineral phases were compared. The main reaction pathways were also identified. Simulations demonstrate that only Rannoch formation has mineral trapping potential due the chlorite content. Although there were large discrepancies in the calculated amount of dissolved CO_2, the codes showed reasonably good agreement on pH calculations. While PHREEQC and GEM were in good agreement on the evolution of the minerals, TOUGHREACT gave different results on Oseberg and Forties samples. The discrepancies are mainly due to the thermodynamic databases and activity models. The use of the same equilibrium constants in the three codes only gave good agreement in the long run, but the simulations were quite different before reaching equilibrium. [Chapter 5]

Will CO_2 be trapped in the Rannoch formation and what matters?

Full field reactive transport modelling of Rannoch formation was performed. MoReS, for the first time, was successfully applied to model reactive transport of CO_2 injection into an aquifer. It is found that it may not be feasible to use GEM for complex full field models due to the convergence problems. Although MoReS and GEM perform similarly when geochemical calculations are not considered, when these calculations are included MoReS outperforms GEM. However, the comparison of the simulation results of GEM and MoReS showed reasonably good agreement. Simulations revealed that the thermodynamic model and the kinetics model gave the same results for the entire duration of the simulations due the relatively high reservoir temperature and the very

small initial chlorite content. It was demonstrated that the grid resolution and relative permeability hysteresis have strong impact on the inventory of CO_2. While a coarser grid results in estimates of more mineral trapping, the magnitude of mineralization is inversely proportional to the magnitude of hysteresis effects. It is also shown that the simulations are very sensitive to the initial mineral fraction of the reactive minerals. Increasing the chlorite content from 1.5% to 5% increases the mineral trapping capacity from 28% to 55%. [Chapter 6]

Primary conclusions

Geochemical modelling is an intrinsic part of feasibility studies of CO_2 storage, and should not be ignored. The CO_2-brine-rock reactions are evident from the previous modelling work, experiments and natural analogue studies. Depending on the mineralogical composition of the reservoir, mineral trapping can be the dominant trapping mechanism.

Current codes can model geochemical reactions with acceptable simplifications. The choice of simulator is not critical for the model predictions. The parameters and input information used in the models are far more critical. It was demonstrated how thermodynamic data and activity models can affect the modelling results. It was also found that the models are sensitive to mineral composition, grid discretization, permeability models, and kinetic parameters.

Although geochemical modelling is quantitative, the model results are mainly qualitative. This is due to two major difficulties. Firstly, information on geochemical parameters and reservoir properties is usually not available. Secondly, geochemical processes are often not well understood. Although it is very challenging to overcome these difficulties due to the long temporal scales of geochemical reactions, the heterogeneity of the subsurface and the complexity of the processes, the difficulties can be partly overcome by new experiments, field tests and measurements.

It is demonstrated that accurate CO_2 solubility models are important for the accurate prediction of trapping capacity. Geochemical codes overestimate the CO_2 solubility and their thermodynamic data should be tuned. Fortunately, the impact of inaccuracy of CO_2 solubility is small in mineral trapping calculations.

Although the physical reality is objective, conceptualization of the models is subjective. User errors are also almost inevitable. Hence the human factor influences the model outcomes.

Batch models are useful to understand CO_2-brine-rock interactions. 3D models, on the other hand, give more information on the applicability of CO_2 storage at reservoir scale. The drawbacks of reactive transport modelling include the high data requirements, and longer times spent for both building and running the models.

7.1 Future work

The models reported in this thesis could be improved in the future by tackling the limitations of the models stated above.

In this study modelling work focused on trapping capacity estimations. Investigation of other aspects, i.e. caprock integrity, well integrity and near well processes deserves future study for the comprehensive evaluation for the feasibility of CO_2 storage.

Groundwater flow was not considered, but its impact may be significant due to the further spreading of CO_2 in the aquifer.

The CO_2 stream depends on the capture system and can contain impurities such as O_2, SO_2, H_2S and N_2. The impact of these impurities on the CO_2 stream is rarely studied, and investigation of the impurities is needed to understand their role in geochemical processes.

The main limitation of geochemical modelling is the lack of geological and geochemical data and poor understanding of geochemical processes. Production of reliable data is essential for the reliability of the models.

The solubility models are not tested at high pressure and salinity. Hence experimental data on CO_2-brine systems at conditions relevant to CO_2 storage are required.

Among the three codes used in this study, GEM needs critical improvements. Changing the coupling solution methods and extending thermodynamic equilibrium modelling to the minerals would be beneficial. Extending thermodynamic equilibrium modelling to minerals is also useful for the initialization of the models without needing an external geochemical code. GEM models the geochemical reactions by inputting the aqueous

species in the beginning. This is a major limitation, because the reactions paths and the relevant aqueous species are unknown prior to the simulations, and they can change throughout the simulation period. Hence, handling the aqueous species as in PHREEQC would improve GEM significantly. GEM has an inflexible internal thermodynamic database which is difficult to read and modify. A flexible database structure could also improve the code. The Pitzer model also needs to be implemented.

The main limitation of PHREEQC is that it treats CO_2 as an ideal gas. Hence the implementation of a CO_2 solubility model is necessary.

In MoReS, CO_2 solubility data in the thermodynamic database needs to be tuned, or a new solubility model needs to be implemented in PHREEQC as stated in the previous paragraph. MoReS is very flexible compared to other codes, but writing monitors is time consuming and difficult for researchers with no familiarity of scripting language. Templates at least for the basic outputs, such as mineral abundance changes and CO_2 inventory, would be helpful.

APPENDIX A

Parameters for equation 4.14:

a_1	8.99288497e-2
a_2	-4.94783127e-1
a_3	4.77922245e-2
a_4	1.03808883e-2
a_5	-2.82516861e-2
a_6	9.49887563e-2
a_7	5.20600880e-4
a_8	-2.93540971e-4
a_9	-1.77265112e-3
a_{10}	-2.51101973e-5
a_{11}	8.93353441e-5
a_{12}	7.88998563e-5
a_{13}	-1.66727022e-2
a_{14}	1.39800000e+0
a_{15}	2.96000000e-2

Parameters for equation 4.17:

T-P coefficient	$\mu_{CO_2}^{l0} / RT$	λ_{CO_2-Na}	$\zeta_{CO_2-Na-Cl}$
c_1	28.9447706	-1.411370585	3.36389723e-4
c_2	-0.0354581768	6.07632013e-4	-1.98298980e-5
c_3	-4770.67077	97.5347708	
c_4	1.02782768e-5		
c_5	33.8126098		
c_6	9.04037140e-3		
c_7	-1.14934031e-3		
c_8	-0.307405726	-0.0237622469	2.12220830e-3
c_9	-0.0907301486	0.0170656236	-5.24873303e-3
c_{10}	9.32713393e-4		
c_{11}		1.41335834e-5	

Parameters for equation 4.18:

b_1	-38.640844
b_2	5.8948420
b_3	59.876516
b_4	26.654627
b_5	10.637097